Global Modeling and Assimilation Office 2008 Research Highlights

NASA Goddard Space Flight Center ★ May 17, 2009

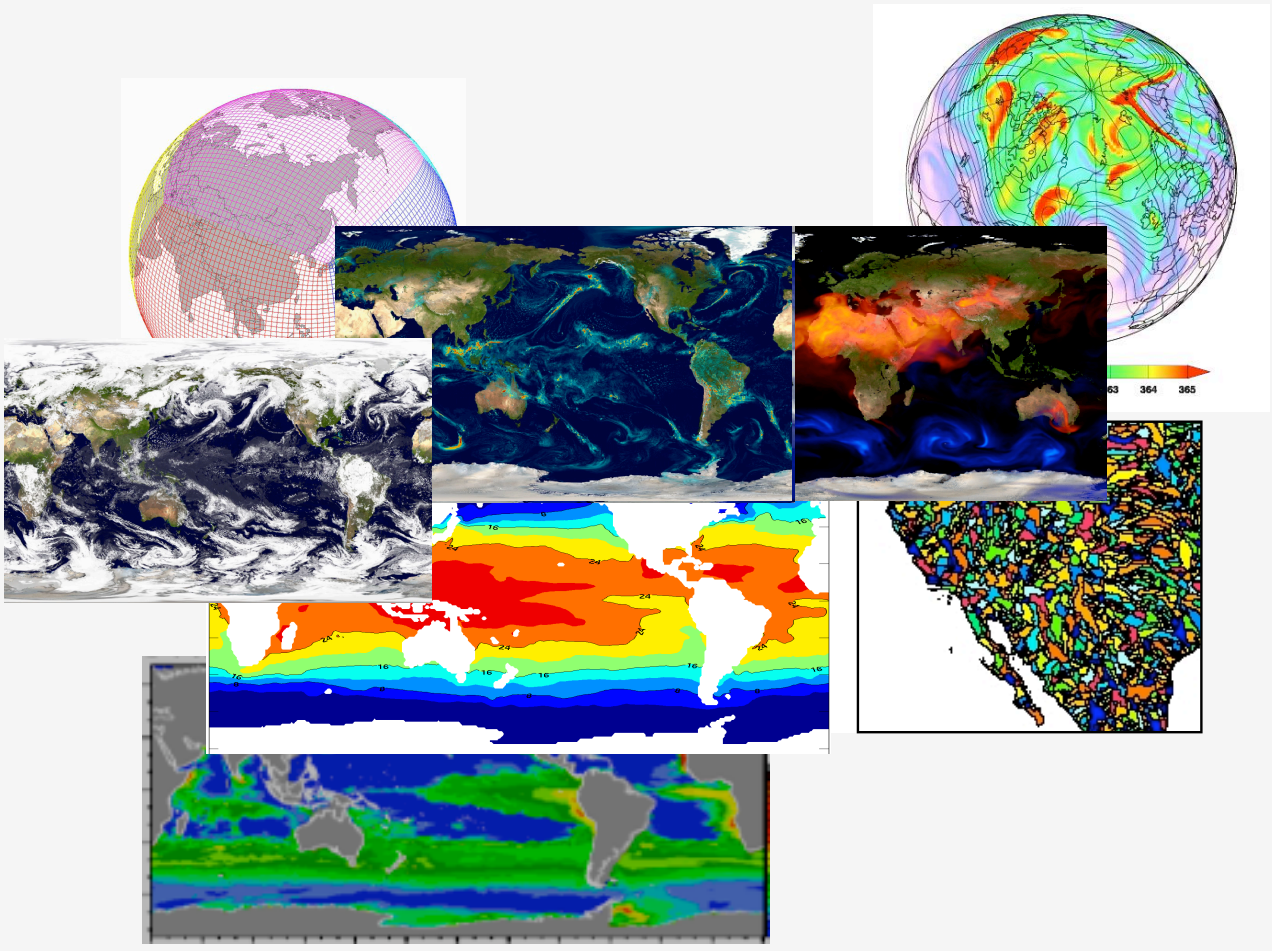

Table of Contents

Four-Dimensional Variational Atmospheric Data Assimilation

Ricardo Todling, Yannick Trémolet (ECMWF), Ronald M. Errico, Ronald Gelaro, Wei Gu, Jing Guo, Jong Kim, Hui-Chun Liu, Meta Sienkiewicz, and Banglin Zhang

Project Goals and Objectives: This project aims at replacing the current three-dimensional variational Goddard Earth Observing System (GEOS) atmospheric data assimilation system (ADAS) with a four-dimensional variational system with the purpose to better utilize modern observing systems such as satellites that provide nearly time-continuous information within the assimilation time window.

Project Description: A prototype strong-constraint incremental four-dimensional variational (4DVAR) atmospheric assimilation system is now available at the GMAO. Remaining details are presently being worked out to turn this prototype system into a fully mature data assimilation system with the objective of upgrading the present GEOS-5 ADAS.

The prototype system can be exercised as either the original 3DVAR or as the new 4DVAR. A low-resolution configuration of this system has been used to compare results between these two assimilation methodologies.

Results: An illustration of the status of present development of the strong constraint 4DVAR is given here by showing snapshots from a 2-degree experiment conducted over January 2006. The figure below displays zonally averaged monthly means temperature (left panels) and zonal wind (right panels) for the 6-hour 4DVAR (top panels), for 3DVAR (middle panels), and for their corresponding differences (bottom panels). In general the differences are not very large and serve as a sanity check for the prototype 4DVAR. Close examination shows a slightly cold 4DVAR atmosphere at the low-level mid- to high-latitudes. The 4DVAR zonal winds show a strong westerly bias in the tropical low- and high-troposphere, with some mixed biases along jet level in the mid-latitudes of the Southern Hemispheres. An independent comparison has shown the 3DVAR system, used in this preliminary study, to have an easterly bias of the same magnitude as seen in Figure 1, therefore suggesting the 4DVAR results to be an improvement in the right direction (not shown).

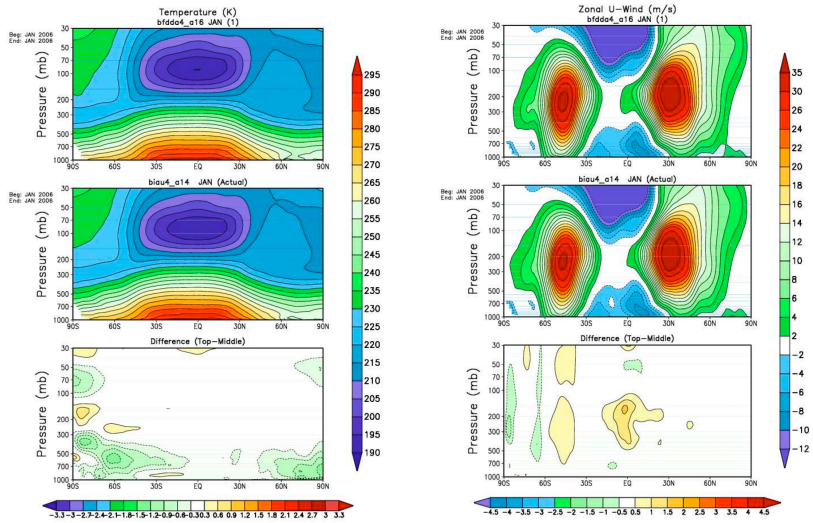

Figure 1: Zonally averaged January 2006 monthly mean for temperature (left-hand panels) and zonal winds (right-hand panels) with the GEOS-5 6-hr 4DVAR (top panels), the GEOS-5 3DVAR (middle panels), and their corresponding differences (bottom panels).

An expected benefit from 4DVAR, due to its enhanced ability to extract information from high-temporally distributed observations, is its improved predictive skills. In Figure 2 we display anomaly correlation plots of the 500 hPa geopotential height field in the Northern Hemisphere (NH; left) and the Southern Hemisphere (SH; right) Extra-Tropics using the prototype system. Curves for the 3DVAR, the 6-hour 4DVAR, and also the 12-hour 4DVAR are shown in the figure. All forecasts are issued at 2-degrees to be consistent with their corresponding underlying assimilation schemes. As such, we remark that the 3DVAR skills shown here are not representative of what is normally obtained with a full-resolution version of the GEOS-5 DAS, but are suitable to the present comparison. The prototype 4DVAR system shows improved results over 3DVAR in both hemispheres. The 12-hour 4DVAR shows neutral results over the 6-hour 4DVAR in the NH, but a clear improvement in the SH. Though preliminary, these results are consistent with similar comparisons found elsewhere. They illustrate the benefits of taking the dynamics as a constraint to the minimization problem of variational assimilation, and consequently making better use of the observations within the assimilation time window. There is also noticeable benefit from increasing the assimilation time window beyond 6-hours to allow more observations to participate in the minimization.

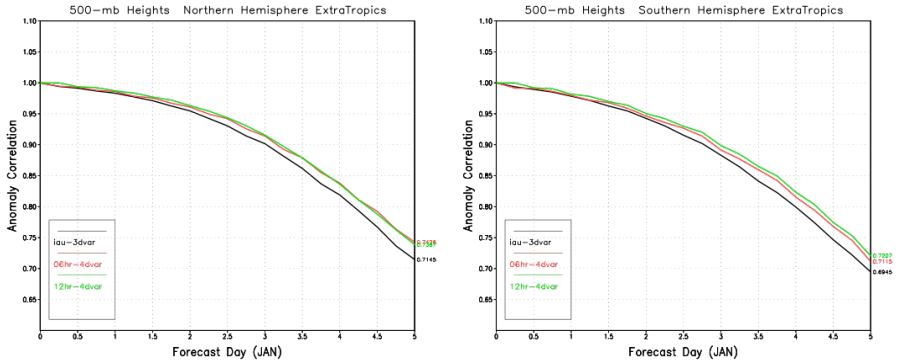

Figure 2: Anomaly correlations of the 500 hPa geopotential heights in the Northern (left) and Southern (right) Hemispheres Extra-Tropics. GEOS-5 3DVAR results in black, prototype GEOS-5 6-hour 4DVAR in red, and prototype GEOS-5 12-hour 4DVAR in green.

Much remains to be done in the GMAO strong constraint 4DVAR. At the present stage of development the tangent linear model (TLM) and adjoint model (ADM) of the finite-volume dynamical core pose a computational limitation to the prototype 4DVAR, due to their MPI implementations. We plan to upgrade the TLM and ADM to be compatible with a more recent version of the forward nonlinear cubed-sphere dynamical core being added to the GEOS-5 atmospheric model, and therefore not suffer from the present MPI limitation. We also plan to account for moist convective processes in the simplified physics used in the 4DVAR TLM and ADM codes. And furthermore, we plan to examine the interplay between the digital filter initialization with the GSI background error covariance balance constraint.

The path to gradually develop the strong constraint GEOS ADAS 4DVAR system is arduous but clear: it will follow the steps taken by the various successful 4DVAR systems operational around the world. When the implementations and evaluations planned above are complete, we will re-tune the background error covariance. The goal soon after will be to have 4DVAR running in near real-time along side with the GEOS-5 ADAS 3DVAR operational system.

The challenge is in the long term, when the focus will turn to develop a weak-constraint 4DVAR system that accounts for model errors and allows for extension of the assimilation beyond the typical 12-hour time window.

Observing System Simulation Experiments

Ronald M. Errico, Runhua Yang, Meta Sienkiewicz, Ronald Gelaro, Ricardo Todling, and Hui-Chun Liu

Project Goals: The goal of this project is to develop, validate, and apply a capability to conduct observing system simulation experiments (OSSEs) at the GMAO. These will be used to estimate the expected impacts of competing instruments or design options regarding errors in climate analysis or numerical weather prediction. They will also be used for characterizing analysis and background errors statistics and assessing and improving data assimilation algorithms.

Project Description: Future satellite missions are often promoted by claims of their estimated impacts on improving the quality of data assimilation products. These estimates are best produced by conducting OSSEs. Although their results can be over-interpreted, only they can account for all the already existing observations and the interpolation or extrapolation of information in time.

Since analyses produced by data assimilation are, by design, the best estimates of global atmospheric states consistent with specified background and observation error characteristics, it is very difficult to also estimate statistics of their errors. In an OSSE context, however, a state of truth is provided in the form of a nature run (NR). If the NR and OSSE are sufficiently realistic, some important characteristics of analysis uncertainty can be estimated. This should lead to better tuning of assimilation system algorithms and background statistics and better design and interpretation of ensemble techniques.

For either of these two purposes, it is imperative that a baseline OSSE be well validated. The OSSE should faithfully reproduce many metrics used to assess observations and data assimilation systems when similar existing observation types are considered. Without such validation, many past OSSEs have been discounted.

During 2008, we developed our first generation software for simulating observations and their errors for most data types currently assimilated at the GMAO. The NR was provided by ECMWF at 3-hour and 1/3° resolution as part of an international "Joint OSSE" effort. Since many users are already requesting our products, we have expedited their development by utilizing a few simplifications. We have also built in flexibility to account for possible deficiencies in some unexplored characteristics of the NR. The software has undergone rigorous testing and its products have been validated, so far, by assimilating data for the month of January 2006 (after a prior month spin-up).

Results: By design, the numbers of observations accepted by the GSI quality control algorithm for both OSSE and real data assimilations are similar. Notably fewer microwave observations are assimilated in the OSSE because, absent a good model of surface emissivity error over land and ice, the simulations by the current software simply exclude such affected channels. The OSSE also has slightly fewer infrared observations excluded due to cloud contamination.

One important statistic to duplicate in the OSSE is the temporal standard deviation of analysis increments since this is a measure of the aggregate innovations (updates due to new observations during each assimilation period). Figure 1 displays an example result for the v wind component for both OSSE and real assimilations. At best poorly validated in earlier OSSEs, here the agreement is

quite remarkable.

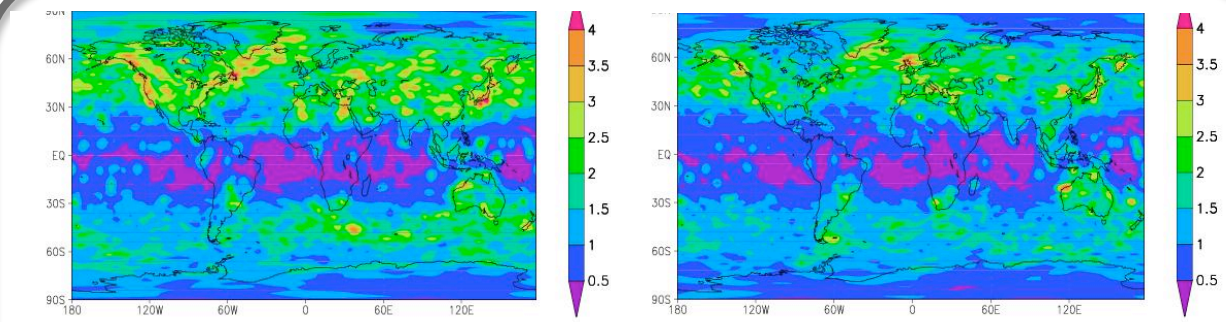

Figure 1: Temporal standard deviation of analysis increment for v wind for OSSE (left) and real (right) assimilations.

The best past OSSE validation efforts usually included a few data denial comparisons (i.e., observing system experiments) performed in OSSE and real contexts. Here instead, we have used the adjoint estimation of observation impacts on 24-hour forecast skill measured in terms of the global total energy norm applied to the differences between forecast and verifying analysis fields. As an example, such results are presented here in Figure 2 for both OSSE and real data assimilations for indicated observation types. The agreement between OSSE and real results is again remarkable.

The OSSE does show greater reduction of forecast error by satellite winds. .

Other usual data assimilation metrics were also compared for OSSE and real assimilations (not shown). In particular, means and variances of innovations for individual instrument types compared very well.

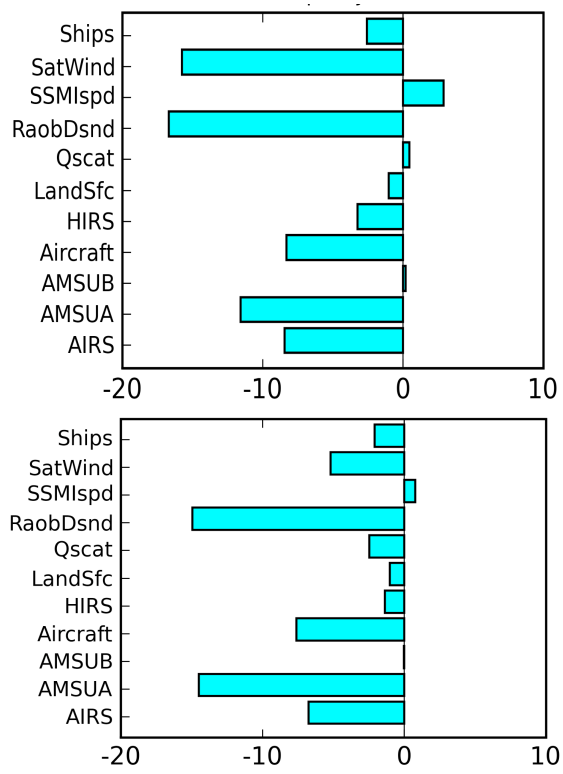

Figure 2: Mean change in E-norm of the 24-hour forecast error due to assimilating the indicated observation types at 0 UTC for OSSE (top) and real (bottom) assimilations.

The next step is to perform a similar validation for a boreal summer month. If results compare as well as for January, we will then release our first generation software as well as the baseline set of simulated observation for the entire NR period. The second-generation software will correct known deficiencies such as assignments of locations and error of cloud track winds, the simulated ascent and reporting for rawindsondes, microwave emissivity over land and ice, and specification of clouds for infrared transmission.

URL: http://gmao.gsfc.nasa.gov/projects/osse

Observation Impact Studies Using Adjoint Tools

Ronald Gelaro, Yanqiu Zhu, Ricardo Todling, Ronald Errico and Yannick Trémolet (ECMWF)

Project Goals: The project goal is to develop accurate and efficient tools for assessing the impact of observations on analyses and forecasts produced by the Goddard Earth Observing System (GEOS) atmospheric data assimilation system. Such tools will help monitor system performance, design intelligent data selection strategies and possibly identify future observing system needs.

Project Description: Modern atmospheric data assimilation systems (DAS) routinely ingest millions of observations to produce initial conditions for weather and climate forecasts. The number and diversity of observations, combined with the complexity of the algorithms required to assimilate them effectively, make it difficult to determine the impact of individual observations or observation types on the quality of the forecast. However, many of the required components of the DAS, particularly the adjoint (transposed) forms of certain operators, can serve a dual purpose as powerful diagnostic tools in this regard, obtained as a shared development cost. With the complete adjoint of a data assimilation system, the impact of any or all assimilated observations on measures of forecast skill can be estimated accurately and efficiently. The approach allows aggregation of results in terms of individual data types, channels locations, etc., all computed with a single execution of the system.

The GMAO has developed the adjoint of the GEOS DAS, which includes adjoint versions of the GEOS general circulation model (GCM) and the Gridpoint Statistical Interpolation (GSI) analysis scheme. The adjoint system can be easily invoked as an option in either the current 3D variational (3DVAR) or future 4D variational (4DVAR) GEOS DAS configurations. The adjoint system will be used to examine the impacts of hyper-spectral satellite instruments such as the Atmospheric Infrared Sounder (AIRS) and to conduct routine monitoring of the entire observing system.

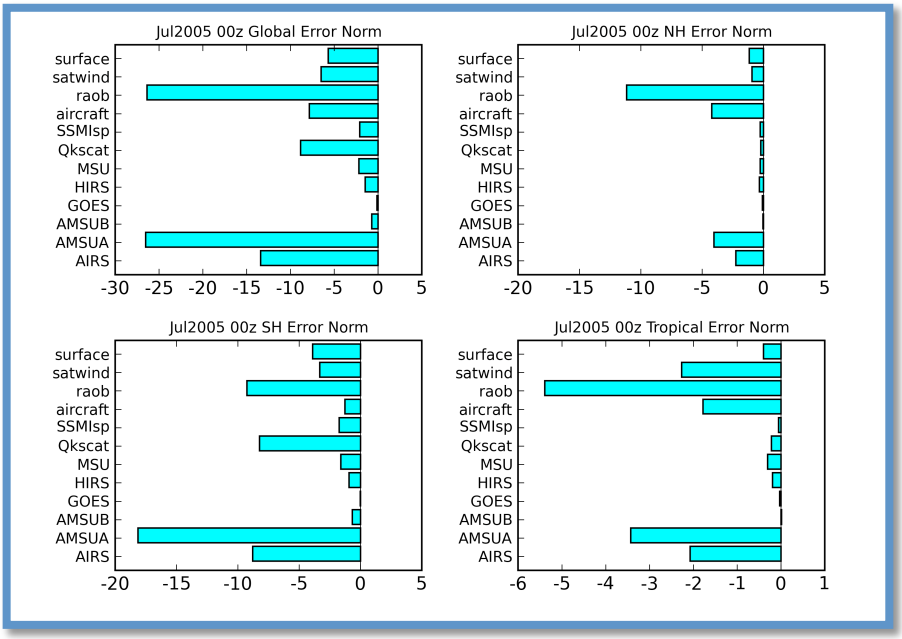

Figure 1: Accumulated impact of various observing systems assimilated at 00 UTC on GEOS-5 24-h forecasts during July 2005. Results are shown for verification regions over the globe (upper left), Northern Hemisphere (upper right), Southern Hemisphere (lower left) and tropics (lower right). The units are J/kg.

Results: The adjoint of the current GEOS-5 DAS has been used to examine observation impacts in several experiments, in preparation for its operational implementation. Figure 1 shows the accumulated impacts of the major observing systems assimilated in GEOS-5 on 24-hr forecasts during July 2005. The results show the contribution of each observing system to the overall reduction of an energy-based measure of forecast error that combines wind, temperature and surface pressure from the surface to ~ 130 hPa. Negative values indicate that an observation type has improved the 24-h forecast. The individual panels show the impact of observations on forecast skill measured over the globe, Northern Hemisphere (NH), Southern Hemisphere (SH) and tropics, respectively. The verification states are the GEOS-5 analyses valid at the same time as the 24-h forecasts. It can be seen that all observing systems shown have an accumulated beneficial impact on the forecast, although the magnitudes vary significantly by region. Rawinsondes (raob) and AMSU-A radiances (amsua) have the largest impact globally, with smaller, but significant, impacts from AIRS, aircraft observations and satellite winds. Rawinsondes have the largest impact in the NH while AMSU-A has the largest impact in the SH. In the tropics, the relative impacts of the various observing systems are similar to the impacts globally, but smaller in magnitude.

The same results allow examination of the impacts of individual AIRS channels on the forecast, as shown in Figure 2. We note that it would require roughly 200 separate assimilation experiments to produce such a figure using a traditional data denial approach. While most of the AIRS channels assimilated improve the forecast, some indeed degrade the forecast (positive values), especially ones in the channel index range 160–200. These channels are most sensitive to atmospheric water vapor, the assimilation of which remains a challenging and only partially solved problem at present. These results do not necessarily imply that the observations themselves are of poor quality; it is likely that deficiencies in the current methodology used to assimilate these observations also contribute to the results. Further investigation is underway.

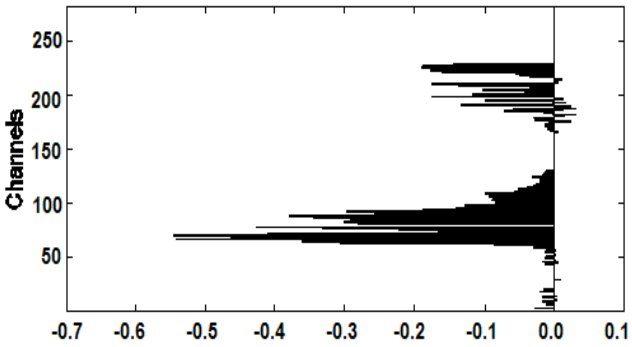

Figure 2: Accumulated impact of individual AIRS channels assimilated at 00 UTC on GEOS-5 24-h forecasts during July 2005 based on the global verification region. The units are J/kg.

This GEOS-5 adjoint DAS will be run as a regular part of the GMAO's operational job stream. Observation impacts in the GMAO's prototype 4DVAR system will be examined to help evaluate its performance and optimize the benefits of new observation types.

URL: http://geos5.org/wiki/index.php?title=Main_Page

Publications:

Gelaro, R. and Y. Zhu, 2009: Examination of observation impacts derived form observing system experiments (OSEs) and adjoint models. *Tellus*, **61A**, 179–193.

Zhu, Y. and R. Gelaro, 2008: Observation sensitivity calculations using the adjoint of the Gridpoint Statistical Interpolation (GSI) analysis system. *Mon. Wea. Rev.*, **136**. 335–351.

Gelaro, R., Y. Zhu and R. M. Errico, 2007: Examination of various-order adjoint-based approximations of observation impact. *Meteorologische Zeitschrift,* **16**, 685–692.

Validation of GEOS-5 Temperature Analyses in the Upper Troposphere, Stratosphere and Mesosphere

Emily Hui-Chun Liu

Project Goals and Objectives: The goal of this project is to estimate the temperature biases in GEOS-5 analyses in the upper troposphere, stratosphere, and mesosphere.

Project Description: The GEOS-5 Data Assimilation System provides meteorological analyses of temperature, moisture, and winds. Among all the state variables, temperature is probably the most important. It is not only critical in the minimization process of estimating the optimal analysis state but is also fundamental to many diagnostic variables such as clouds and saturation water vapor mixing ratio over ice or water.

In this project, the biases of GEOS-5 temperature analyses in the upper troposphere, stratosphere, and mesosphere are assessed for the current GEOS-5 operational run (d520_fp) and for MERRA (Modern Era Retrospective-analysis for Research and Applications) stream-I. This assessment uses the retrieved temperature profiles from Aura/MLS (Microwave Limb Sounder) and from the LIMS (Limb Infrared Monitor of the Stratosphere) instrument on board the Nimbus-7 satellite. MLS provides detailed temperature structure from the upper troposphere (316 hPa) up to the mesosphere (0.001 hPa) with 3.5-14 km vertical resolution. LIMS is also a limb-sounding instrument but used infrared emissions. LIMS was operational for about seven months from 25 October to 28 May, 1978, providing vertical profiles of temperature from the upper troposphere to the mesosphere. The retrieved temperatures from MLS and LIMS are not part of the observing system in GEOS-5, and thus can provide an independent evaluation on GEOS-5 temperature biases.

To obtain statistical significance in the validation, two sets of one-month statistics were performed in February and August 2008, respectively, for the GEOS-5 operational d520_fp run. For each month, the retrieved MLS temperatures were collocated spatially and temporally with GEOS-5 analyses. Approximately 95,000 collocated data were found and used in the monthly statistics. Figure 1 shows an example of the horizontal coverage of MLS in a 24-hour (in gray) and 6-hour (in red) window. The GEOS-5 temperature analyses were mapped vertically from the model's eta coordinate to the MLS pressure levels so that the biases can be obtained directly at each MLS pressure.

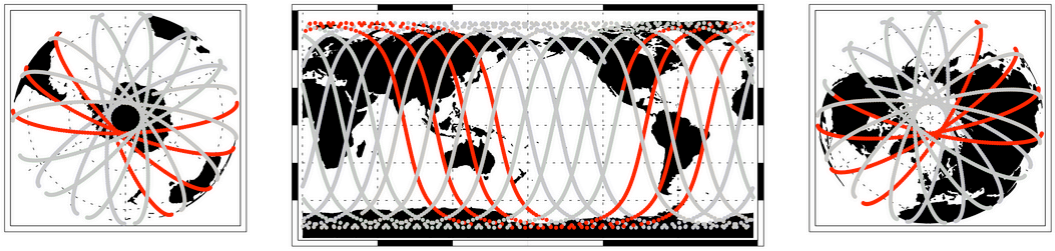

Figure 1: An example of horizontal coverage of MLS data in a 24-hour (orbits in gray) and a 6-hour (orbits in red) window are shown. Three views, centered at the South Pole, the equatorial Pacific Ocean, and the North Pole, are shown.

The MERRA stream-I spin-up started in 1978. The satellite radiance data from TOVS (TIROS Operational Vertical Sounder) system on board of TIROS-N were assimilated from December 1978. The SSU (Stratospheric Sounding Unit) in the TOVS system is the major constraint for stratospheric temperature in this period. In this initial validation of MERRA, we compared individual GEOS-5 temperature profile at locations covered by TIRO-N orbits with the collocated LIMS retrieved temperature profiles. The monthly statistics will be assessed in the future.

Results: The estimated biases for GEOS-5 d520_fp temperature analyses are presented in Figures 2 and 3 for February and August, respectively, in six different geographical locations. The discussions are divided into three vertical regions: the upper troposphere (from 316 hPa to 100 hPa), the stratosphere (from 100 hPa to 1 hPa), and the mesosphere (above 1 hPa). In the stratosphere, the temperature biases of GEOS-5 analyses at all MLS levels are less than 1 K except at 1 hPa where the biases can be as large as 5 K. This large bias near the stratopause is caused by biases in the forecast model since there are no direct analysis constraints from observations around this level. In the current GEOS-5 observing system, the observations such as AMSU-A channel 14 can provide constraints up to 2 hPa. There are essentially no direct constraints from observations above 2 hPa except the tails of the weighting functions extended from the center altitudes by different instrumentation. For the same reason, the temperature biases of GEOS-5 in the mesosphere show large discrepancies compared to the retrieved temperatures from MLS. In the mesosphere, the temperature biases are considerably higher than those in the stratosphere, with the largest around 20 K at the winter pole (Figure 3f). In this region the gravity wave drag model undoubtedly contributes to the large temperature bias. In the upper troposphere, the temperature biases are in general less than 1 K except around 200 hPa, where a 2.5 K difference, on average, is found between GEOS-5 and MLS. The systematically colder temperature of GEOS-5 could be attributed to the systematic errors in the GEOS-5 and the bias in cloud screening in the processing of retrieving temperatures from MLS. The source of this bias can be further investigated by using additional observational data such as temperatures from Rawinsondes.

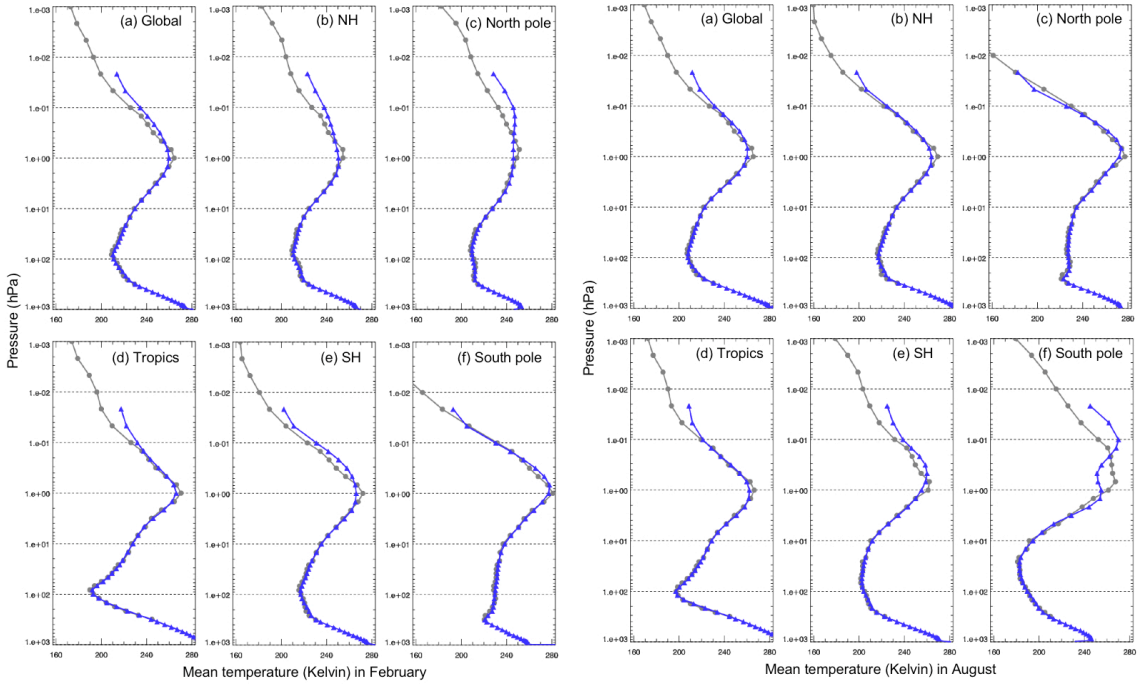

Figures 2 (left) and 3 (right): Monthly mean temperature profiles for the retrieved temperatures from MLS (grey) and the GEOS-5 temperature analyses (blue). The mean temperature profiles from MLS and GEOS-5 analysis are compared in 6 different regions: (a) Global, (b) Northern Hemisphere, (c) North Pole region, (d) Tropics, (e) Southern hemisphere, (f) South Pole region. Figure 2 shows February and Figure 3 August 2008.

The result of GEOS-5 temperature biases for MERRA stream-I run is preliminary. For this initial assessment, we compare individual GEOS-5 temperature profiles with collocated temperatures retrieved from LIMS along the SSU tracks (Figure4a). Examples of such comparisons are shown in Figures 4b-c at two locations. The GEOS temperatures show good agreement with LIMS in the stratosphere up to 5 hPa. The SSU instrument should provide information up to 2 hPa, however, the channel 3 from SSU in this period was not performing well (too noisy) so it was not assimilated in MERRA. The GEOS-5 temperatures show larger biases in upper stratosphere as expected due to the absence of SSU channel 3 in the assimilations. The comparison of temperatures in the upper troposphere should be ignored because the quality control to eliminate cloud-contaminated data from LIMS was not applied due to the lack of information. This issue needs to be revisited for the final assessment of the temperature biases for MERRA.

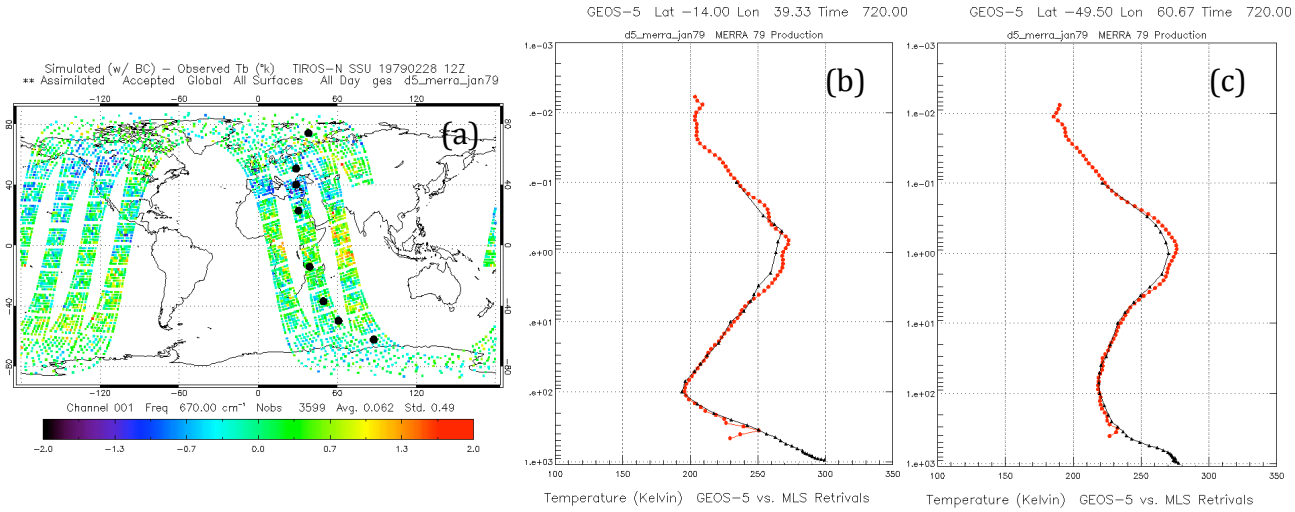

Figure 4: Validation of temperature analyses for MERRA stream-I with temperatures retrieved from LIMS. (a) Locations of GEOS-5 analyses along the SSU orbit analyzed. (b) Comparison of GEOS-5 temperature profile with collocated LIMS temperature retrievals at 14°S, 39°E. (c) Same as b, but for 49.5° S, 61°E.

We plan next to undertake a similar validation for MERRA temperature analyses using retrieved temperatures from LIMS (1978-1979), HALOE (Halogen Occultation Experiment; 1991-2005), HIRDLS (High resolution Dynamics Limb Sounder; 2005-2008), and UASR-MLS (Upper Atmosphere research satellite; 1991-1999), and MLS (2004-2008).

Publications:

Liu, H.C., 2008: Impacts of variational bias correction on GEOS-5 temperature analyses and assimilation of AIRS 15 micron CO_2 channels. *EOS Trans. AGU,* **89**(53), Fall Meet. Suppl., Abstract A53F-0340.

Impacts of Variational Bias Correction on GEOS-5 Temperature Analyses in the Stratosphere

Emily Hui-Chun Liu

Project Objectives: The objective of this project is to show that it is beneficial to turn off variational bias correction for observations in regions where data types are rare, measurements are sparse and the background information is not reliable.

Project Description: Satellite instruments, like any other measurement system, are imperfect and prone to error. Biases in the observation, if uncorrected, can systematically damage the data assimilation scheme, and ultimately the quality of the forecasting system. For an optimal analysis, the systematic observational biases need to be removed as much as possible prior to assimilation. In GEOS-5, the variational bias correction scheme (VarBC) developed at NCEP (Derber and Wu, 1998) is currently used for satellite radiances. The VarBC updates the bias inside the assimilation system by finding corrections that minimize the radiance departures while simultaneously improving the fit to other observed data types inside the analysis. Thus, observations are adjusted together with the analysis control variables, taking all available information into account. The advantage of VarBC is that the bias estimate is adaptive and consistent with all components in the analysis. In practice, it is difficult to separate the observation bias from the systematic errors in the background in regions where observations are sparse and background fields are biased. In such cases, the VarBC does not work well and the analysis tends to include systematic errors from the forecast model. One region where this is likely to happen is the mid-to-upper stratosphere and mesosphere where the observations are sparse and background fields are biased. As an example, GEOS-5 temperatures biases range from 5-20 K at these altitudes around the winter pole. The only constraint from observations on the temperature analysis at these altitudes is the AMSU-A channel 14, the highest peaking channel for this instrument.

Our objective is to investigate whether turning VarBC off for AMSU-A channel 14 would be beneficial to temperature analyses in the stratosphere. Retrieved temperatures from the Microwave Limb Sounding (MLS) on board Aura are used as the validation metric to assess the impact of VarBC on GEOS-5 temperatures. To obtain a statistically significant validation, one month of MLS data were collocated spatially and temporally with GEOS-5 analyses. Approximately 95,000 collocations were found and used in the monthly statistics.

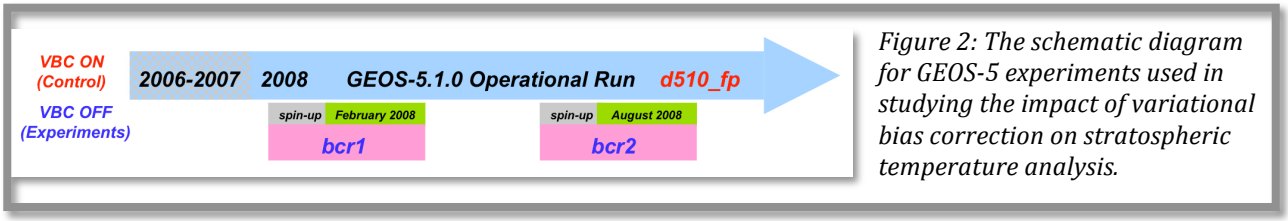

Figure 2: The schematic diagram for GEOS-5 experiments used in studying the impact of variational bias correction on stratospheric temperature analysis.

To assess the impact of VarBC on temperatures in the stratosphere and above, we compare two experiments, d510-fp and bcr2 from two versions of GEOS-5 operational system, GEOS-5.1.0 and GEOS-5.2.0 (MERRA), respectively. The GEOS-5.1.0 version invokes the VarBC for AMSU-A channel 14; while the GEOS-5.2.0 version does not (Figure 1). The impacts of VarBC on temperature can be observed by taking the temperature differences between experiments 510_fp and bcr2. (Figure2).

The impact of VarBC is concentrated around and above 10 hPa. This is expected since the influence of AMSU-A channel 14 is in this region. Our goal is to investigate whether these impacts would be positive on the GEOS-5 temperature analyses.

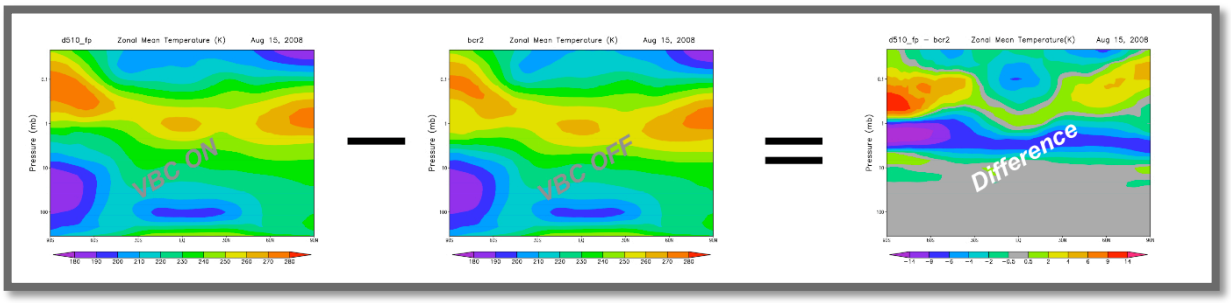

Figure 2: The vertical cross section of the temperature analyses and temperature differences between experiments d510_fp with VarBC on and bcr2 with VarBC off (d510_fp – bcr2 = difference).

Results: The results of the validation for the VarBC impacts on GEOS-5 temperature analyses using MLS are shown in Figure 3. The validations were done for 6 different geographical regions and results are plotted for each region in Figure 3 from A to F. The GEOS-5 temperature analyses generally agree well with MLS up to 10 hPa for both experiments. At pressure levels lower than 1 hPa, discrepancies between GEOS-5 analyses and MLS are large. The differences can be as large as 20 K in the Polar Regions in the winter hemisphere. This is mainly due to the lack of direct constraints from observations at these altitudes. In the mid and upper stratosphere between 10 and 1 hPa, turning off the bias correction for AMSU-A channel 14 efficiently removed most of the temperature biases. For all six regions investigated, the temperature biases were drastically reduced around 2 hPa where the weighting function of AMSU-A channel 14 peaks. In fact, the temperature analyses in the entire mid and upper stratosphere were largely improved when the VarBC is not used for this channel. In the d510_fp run (VarBC on), the VarBC introduces systematic background errors into the bias estimation for AMSU-A channel 14 and this, in turn, has a detrimental impact on the temperature analysis from this channel.

More evidence of positive impacts from turning off VarBC for AMSU-A channel 14 can be seen from the time series of the analyzed minus observed (AN-OB), the background minus observed (FG-OB), and the total bias correction of brightness temperatures for AMSU-A channels 12-14 (Figure 4). The fit of GEOS-5 background and analysis temperatures to these AMSU-A observations is improved for experiment bcr2 (VarBC off), and the amount of the bias correction found by the analysis for channel 13 is also greatly reduced. In addition, the fit of the GEOS-5 temperature analyses from experiment bcr2 to some of the high-peaking stratospheric channels from AIRS instrument is improved significantly. The AIRS channels from 73 to 86 peaking in the mid and upper stratosphere are not assimilated in either d520_fp and bcr2 experiments. Therefore, the AN-OB of brightness temperatures for these passive AIRS channels can be used as a validation metric. Figure 5 shows the histograms of the AN-OB of two highest peaking channels from AIRS (channels 74 and 75) for experiment d510_fp (orange) and bcr2 (blue), respectively. The distributions of the histograms for experiment d510_fp (Figure 5A and 5B) exhibit clear cold biases in GEOS-5 temperature analyses, while the histograms for experiment bcr2 (Figure 5C and 5D) show a greatly improved fit of GEOS-5 temperature analyses to AIRS observations. The cold biases in most of the stratosphere are reduced significantly by turning the VarBC off for AMSU-A channel 14.

Publications:

Liu, H. C., 2008: Impacts of variational bias correction on GEOS-5 temperature analyses and assimilation of AIRS 15 micron CO_2 channels. *EOS Trans. AGU,* **89(**53), Fall Meet. Suppl., Abstract A53F-0340.

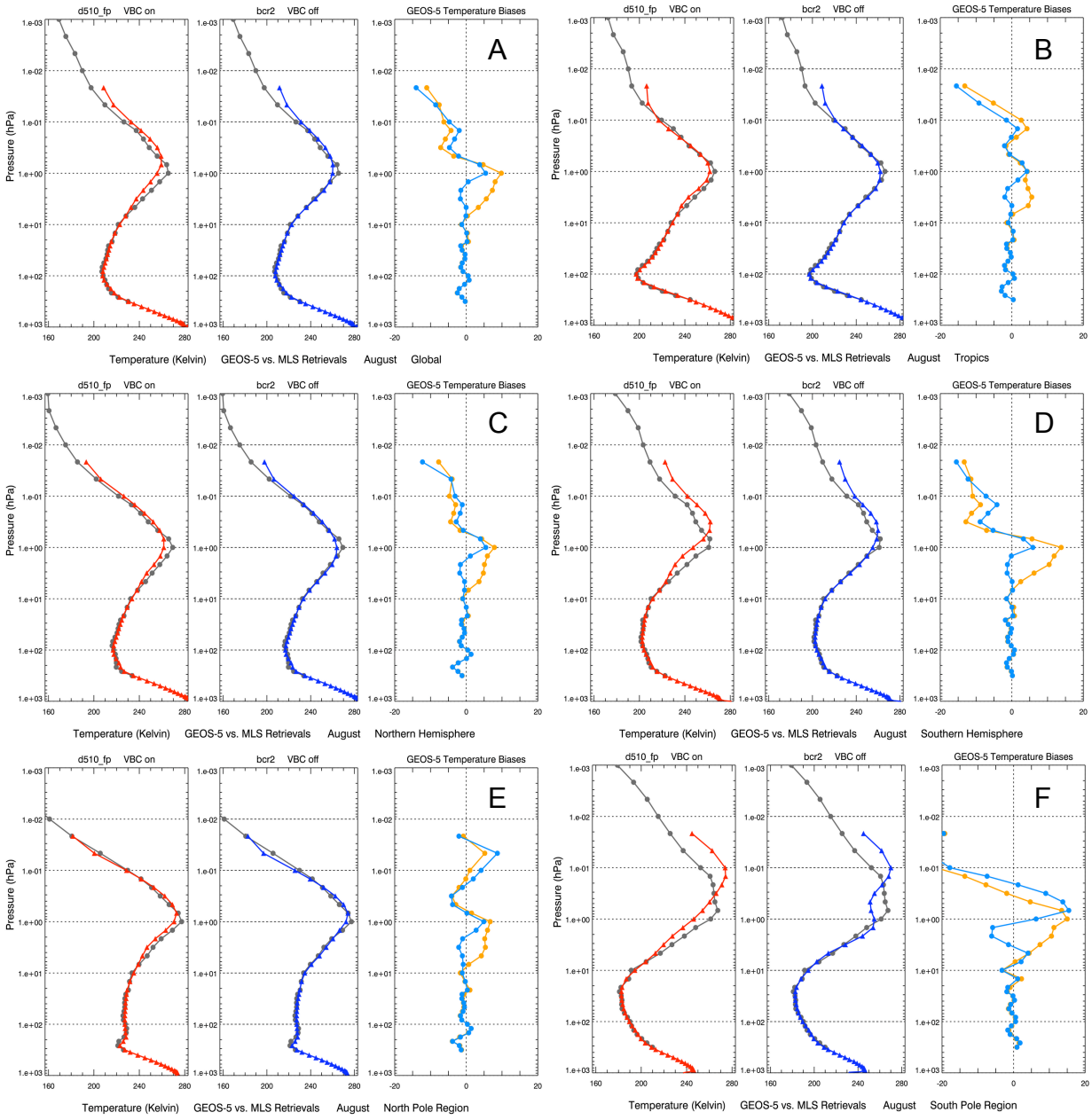

Figure 3: Subplots A to F are temperature statistics including monthly mean and biases against retrievals from MLS for 6 different geographical regions: global, tropics, Northern Hemisphere, Southern Hemisphere, North Pole, and South Pole regions. In each subplot, monthly mean temperatures for retrieved MLS (gray), GEOS-5 d510_fp (red), and GEOS-5 bcr2 (blue) are shown in the left two panels. The GEOS-5 monthly mean temperature biases calculated from retrieved MLS are shown in the third panel on the right for the d510_fp experiment (orange) and bcr2 experiment (cyan), respectively.

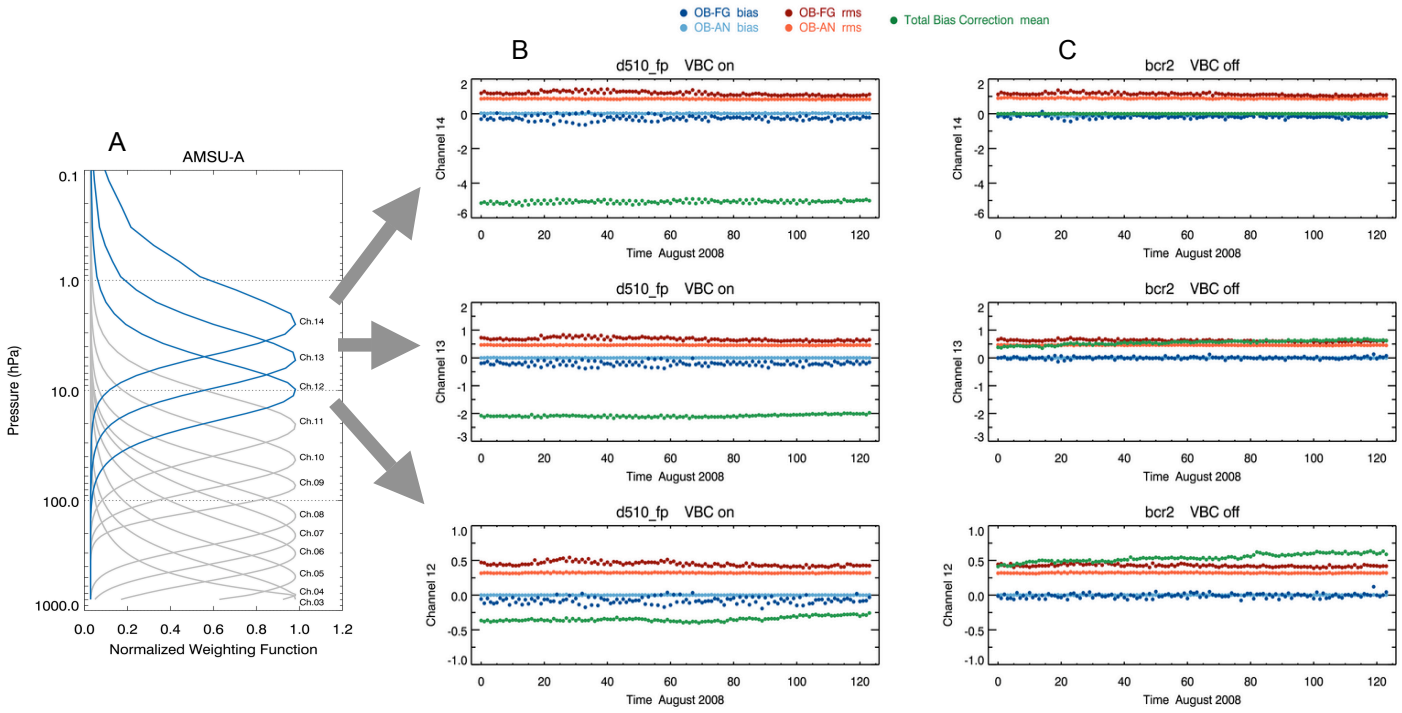

Figure 4: (A) Weighting functions of AMSU-A channels. (B) Time series of AMSU-A channels 12-14 departure statistics (FG-OB and AN-OB) and total bias correction for GEOS-5 d510_fp experiment. (C) Time series of AMSU-A channels 12-14 departure statistics (FG-OB and AN-OB) and total bias correction for GEOS-5 bcr2 experiment.

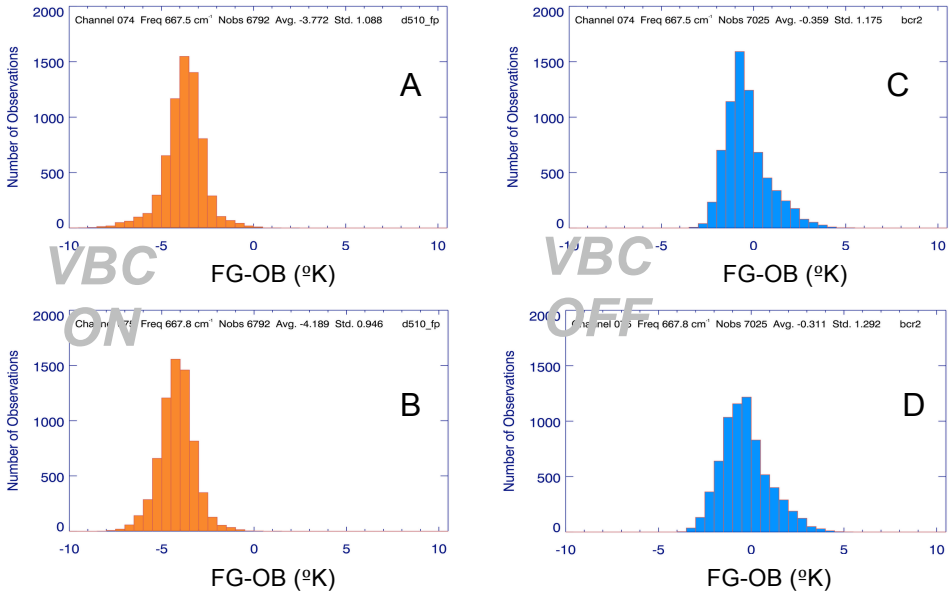

Figure 5: Histograms of departure statistics (FG-OB) for AIRS channels and 75. Subplots A and B (orange) are histograms for GEOS-5 d510_fp experiment, Subplots C and D (blue) are histograms for GEOS-5 bcr2 experiment.

Ensemble-based Data Assimilation of Precipitation Observations

Sara Zhang and Arthur Hou, in collaboration with Dusanka Zupanski and Milija Zupanski (CIRA, Colorado State University) and Wei-Kuo Tao, Roger Shih andd Toshihisa Matsui (Code 613.1)

Project Objectives: Our objective is to develop an ensemble-based data assimilation system to assimilate precipitation observations to produce high-resolution (~ 2 km) dynamic precipitation analysis for hydrological applications and climate studies in support of the Global Precipitation Measurement (GPM) Mission.

Project Description: Precipitation process plays key role in the global and regional hydrological cycles. Assimilation of precipitation observations into weather prediction models posts special challenges: the observation operator involves nonlinear and coupled physical processes, and cloud-resolving scales are needed to simulate realistic cloud and precipitation sensitive radiance comparable with satellite data. An ensemble-based data assimilation system has been developed to meet these challenges and enhance scientific applications of the Global Precipitation Measurement (GPM) Mission led by NASA and JAXA. The NASA Unified Weather Research Forecast (WRF) model is used to provide forecasts and propagate background error information. The model domain can be configured as nested grid and the analyses are carried out in multiple domains and the interactions between multi-resolution increments occur during ensemble model integrations. The NASA Unified WRF model employs the sophisticated cloud-resolving microphysics schemes of the Goddard Cumulus Ensemble (GCE) model. The Goddard Satellite Data Simulation Unit (SDSU) is also incorporated into the observation operator for assimilation of cloud/precipitation sensitive radiance. The observation system uses NCEP operational conventional data and clear-sky satellite radiance data, and is capable of assimilating cloud/precipitation data from microwave radiometers and radars. The system uses a maximum likelihood ensemble filter (MLEF) developed at the Colorado State University, which combines ensemble-based forecast error covariance propagation and the maximum likelihood estimate to obtain optimal analysis solution.

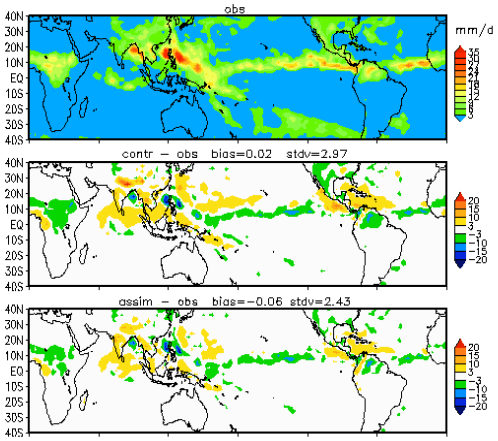

Figure 1: Global monthly-averaged precipitation for August 2005. (a) SSM/I, TMI, AMSR-E and AMSU retrievals (verification data); Difference between the verification data and the analysis (b) not using precipitation observations and (c) using precipitation observations from SSM/I and TMI.

Results: The ensemble assimilation algorithm (MLEF) uses an ensemble of nonlinear forward model simulations to link the model space and observed space, obviating the need for a tangent linear model and its adjoint for nonlinear cloud and precipitation processes. This methodology has been used successfully to assimilate moisture and temperature data in a NASA-GEOS5 column model (Zupanski et al, 2007) and to assimilate SSM/I and TMI precipitation data in the full GEOS-5

global AGCM. Ensemble experiments assimilating global satellite precipitation data have shown that the algorithm is effective in extracting information from observations to reduce errors in global precipitation analysis (Figure 1). At the current development stage, the regional MLEF-WRF system has been tested with a mesoscale 28 km resolution over the ocean surface, and a high-resolution nested grid configuration (9 km and 3 km) over land. The initialization for the regional WRF forecasts and the boundary conditions are provided by operational global analyses from NCEP. The perturbations for the ensemble members are generated from the flow-dependent error covariance estimated from the ensemble assimilation system. The observations are assimilated every 3 hours, the analyses and short–time forecasts are produced at 3-hour intervals as well. The mesoscale assimilation experiment showed improvements in cyclone location and intensity (Figure 2), and the high-resolution assimilation experiment over land captured the flow-dependency of the ensemble-estimated forecast error covariance (Figure 3).

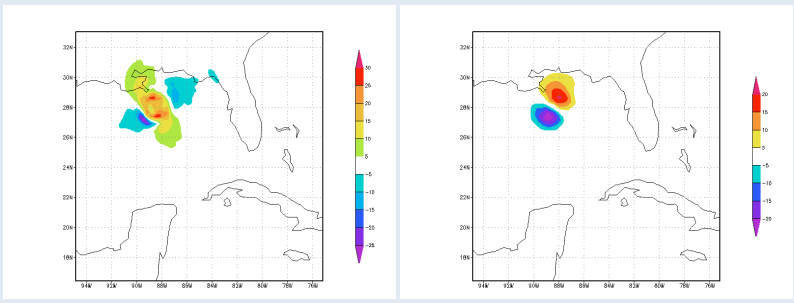

Figure 2: Hurricane Katrina forecast differences, valid at 00Z, 29 August 2005, calculated between the experiments with and without assimilation of conventional observations in the region. The differences are shown after a 3-day data assimilation for (a) v-wind at 550 hPa (ms^{-1}) and (b) surface pressure (hPa).

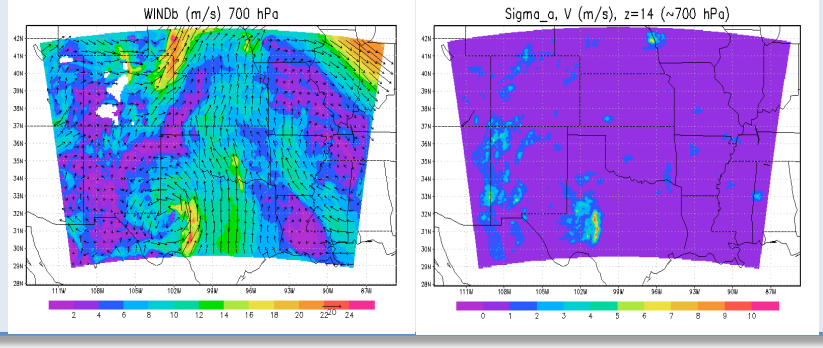

Figure 3: Storm Erin in Texas, 00Z, 18 August, 2007. Left panel: background forecast 700 hPa wind. Right panel: Ensemble-estimated background forecast error standard deviation of 700hPa meridional wind at that time.

We will continue the development and testing to build a robust MLEF-based ensemble data assimilation system capable of using all-weather radiance observations. The near-term goals include the development of an online bias correction for cloud/precipitation- sensitive radiance data, determining an adequate ensemble size and its impact to the spread of ensemble forecast errors, optimizing observation error statistics, and the implementation of an error covariance localization scheme.

References:

Zupanksi, M., 2004: Maximum likelihood ensemble filter: theoretical aspects. *Mon. Wea. Rev.*, **133**, 1710-1726.

Zupanski, D., A.Y. Hou, S.Q. Zhang, M. Zupanski, C. D. Kummerow and S. Cheung, 2007: Application of information theory in ensemble data assimilation. *Q. J. R. Meteorol. Soc.*, **133**, 1533-1545.

Toward an Energetically Consistent Data Assimilation System

Stephen Cohn

Project Goal and Objectives: The goal of this effort is to design and develop a logical successor to the GMAO 4D-Var atmospheric data assimilation system, based on the principle of energetic consistency. The short-term objectives are (i) to diagnose the extent to which the 4D-Var system fails to satisfy this principle; (ii) to implement and test an energetically consistent formulation of the model error term for the 4D-Var system; and (iii) to demonstrate proof-of-concept that energetic consistency can be used in a practical way as the central design principle for a system that could ultimately replace the 4D-Var system.

Project Description: Four-dimensional variational (4DVar) assimilation was first suggested in the mid-1980's and first implemented operationally in 1997 at ECMWF. Since then, 4DVar has become recognized as the state-of-the-art method for atmospheric data assimilation. Despite years of effort, both in the research community and the weather prediction centers, no alternative approach has yet been demonstrated to be superior to 4DVar in an operational environment. Concerted efforts have been made to implement two alternative approaches operationally, each of which on paper is supposed to be superior to 4DVar. The reduced-rank Kalman Filter (RRKF) approach developed at ECMWF was ultimately abandoned after a sustained effort, because it resulted in forecast skill scores indistinguishable from those of the 4DVar system. The ensemble Kalman Filter (EnKF) system developed at the Canadian Meteorological Center (CMC) became operational there in 2005 after a roughly ten-year effort. However, it is used only as part of the CMC ensemble prediction system, because to date it has not yielded improvement over the CMC 4DVar system.

The usual reasons that have been offered for the failure of these alternative approaches to surpass 4D-Var are essentially computational: calculation of the analysis error covariance (RRKF), and limited ensemble size (EnKF). If these reasons tell the whole story, then the natural conclusion to be drawn is that data assimilation is a mature field, with the primary remaining gains to come from more computer power, more and better observations, and higher-resolution models that more fully encompass the components of the Earth system, and with only minor gains to be expected from improvements in the data assimilation methods themselves.

These reasons are not scientifically satisfying, for they do not explain why three methods that look so different on paper, and are indeed very different in terms of algorithmic implementation, yield such remarkably similar results. From the point of view of estimation theory, however, these methods are far more alike than not. All are Bayesian estimation methods, all assume that every uncertain input is Gaussian distributed, all evolve just two moments (the estimated state and its covariance), under a linearity assumption for the covariance evolution, and all are based on finite-dimensional theory.

This project began with the premise that there must be a simple and physical, as opposed to computational, explanation underlying these failures. Such an explanation has been found, and a path forward has been identified.

Results: If the state variables are taken to be the natural energy variables, then the total energy, E_t, of the state at time t is simply $E_t = \|\mathbf{s}_t\|^2$, where $\mathbf{s}$ is the vector of state variables, and the norm is a global quadratic integral in the continuum case and a global quadratic sum in the spatially

discrete case. If there is uncertainty present, then under appropriate probabilistic assumptions, the statement of energy conservation $E_t = E_{t_0}$ for the nonlinear dynamics becomes

$$\left\|\bar{\mathbf{s}}_t\right\|^2 + \mathrm{tr}\,\mathsf{P}_t = \left\|\bar{\mathbf{s}}_{t_0}\right\|^2 + \mathrm{tr}\,\mathsf{P}_{t_0},$$

where $\bar{\mathbf{s}}$ is the mean state (state estimate) and P is the covariance operator; tr$\mathsf{P}$ is the global integral of the variance field in the continuum case and a global sum of the variances in the discrete case. This simple, exact relationship between the state estimate and its covariance is called the principle of energetic consistency.

It is shown in Cohn (2009) that for conservative continuum dynamics, the principle does not hold under an assumption that sources of uncertainty are Gaussian-distributed, but it always holds for an enormous class of non-Gaussian distributions. The reason that the Gaussian distribution is specifically excluded, essentially, is that it requires an assumption that there are states, plenty of them in fact, that have total energy larger than any given amount.

It is shown further that, for data assimilation schemes that evolve just the first two moments, the principle of energetic consistency for the energy variables cannot hold in general unless the state variables are in fact taken to be the energy variables. The reason for this is again elementary: knowing the first two moments in one set of state variables does not imply knowledge of any moments in another set of variables.

In simplest terms, these results imply that none of the three data assimilation methods discussed above, as currently formulated, can possibly converge toward the solution of a properly posed continuum estimation problem, either as resolution is increased, or as the rank is increased, or as the number of ensemble members is increased, or as the number of observations is increased. This is in stark contrast to numerical methods for modeling the hydrodynamics, for which convergence is guaranteed as resolution is increased.

It is conjectured that the strikingly similar performance of 4DVar, the RRKF, and the EnKF is no coincidence: all have hit the same wall of non-convergence. It is shown in Cohn (2008) that, by including the so-called nonlinear bias term in the equation for the state estimate, which itself depends on the evolving covariance, satisfaction of the principle of energetic consistency is guaranteed for the energy variables in the discrete case, for the same class of non-Gaussian probability distributions identified for the continuum case.

The effort in the coming year will (i) demonstrate the extent to which the GMAO 4DVar system fails to satisfy the principle of energetic consistency, (ii) formulate and begin implementing a model error parameterization for the 4DVar system to force satisfaction, and (iii) settle the early design decisions involved in implementing the approach of Cohn (2008), by carrying out a preliminary implementation for the shallow-water version of the dynamical core.

Publications:

Cohn, S. E., 2008: Energetic consistency and coupling of the mean and covariance dynamics. Pp. 443-478 in *Handbook of Numerical Analysis, Vol. XIV* (P. G. Ciarlet, ed.), *Special Volume: Computational Methods for the Atmosphere and the Oceans*, R. M. Temam and J. J. Tribbia (guest eds.), Elsevier.

Cohn, S. E., 2009: The principle of energetic consistency: Application to the shallow-water equations and to ensemble methods. Chapter in *Data Assimilation: Making Sense of Observations*, W. Lahoz, B. Khattatov and R. Menard (eds.), Springer.

An Adaptive Ensemble Kalman Filter for Land Data Assimilation

Rolf Reichle and Christian Keppenne, in collaboration with Wade Crow (USDA)

Project Goals: The input error parameters required by data assimilation systems are a source of uncertainty in the ensuing analysis. Errors in their specification may be alleviated with an adaptive filtering approach as we developed for the GEOS-5 land data assimilation system.

Project Description: Data assimilation products are sensitive to input observation and model error variances. With very poor input error parameters, assimilation analyses may be worse than model estimates without assimilation. To examine this issue, a suite of experiments was conducted with the GEOS-5 Land Data Assimilation System (G5-LDAS) using synthetic surface soil moisture observations. Each assimilation experiment has a unique set of input error parameters that leads to a unique pair of scalars: the (space and time) average forecast error variance (P_0) and the input observation error variance (R_0) for surface soil moisture. We can thus plot 2D surfaces of filter performance as a function of $\sqrt{P_0}$ and $\sqrt{R_0}$. The figure to the left shows one such surface using the RMSE of surface soil moisture estimates from a non-adaptive assimilation over the entire Red-Arkansas domain as the performance measure.

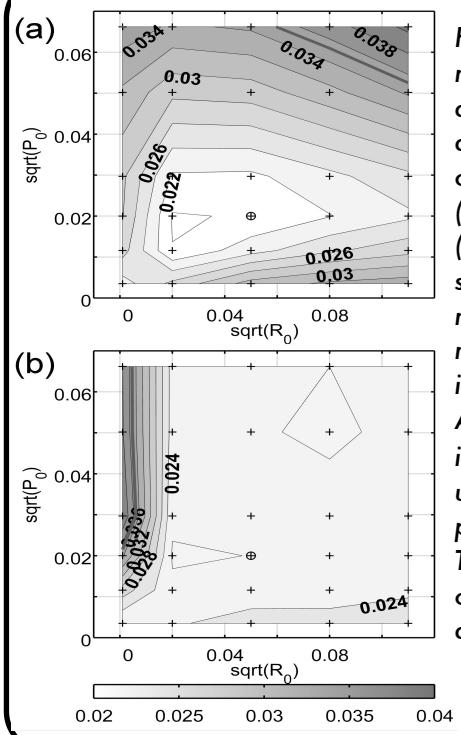

Figure 1: MSE of surface soil moisture for the (a) non-adaptive and (b) adaptive assimilation system as a function of input error parameters: (ordinate) forecast and (abscissa) observation error standard deviation. Units are m^3m^{-3}. Each + indicates the result of a 19-year assimilation integration over the Red-Arkansas domain. The ⊕ indicates the experiment that uses the true input error parameters for the assimilation. Thick gray lines indicate RMSE of the open loop (no assimilation) integration.

The estimation error in surface soil moisture is smallest near the experiment that uses the true error inputs. The minimum estimation error is around 0.02 m^3m^{-3}, down from the open loop (no assimilation) value of 0.035 m^3m^{-3}. The estimation error increases as the input errors deviate from their true values. The figure also indicates where the estimation error surface intersects the open loop error. For grossly overestimated error variances, the assimilation estimates of surface soil moisture are in fact worse than the open loop estimates. Ultimately, the success of the assimilation (measured through independent validation) suggests whether the selected input error parameters are acceptable.

Results: Adaptive filtering methods can assist with the estimation of input error parameters. The central idea behind adaptive filtering is that internal diagnostics of the assimilation system should be consistent with the values that are expected from input parameters provided to the data assimilation system. The most commonly used diagnostics for adaptive filtering are based on the observation-minus-forecast residuals or innovations (computed here as $v_t \equiv E\{y_{t,i} - H_t\, x_{t,i}^-\}$, where $E\{\cdot\}$ is the ensemble mean operator). For a linear system operating under optimal conditions, the

lagged innovations covariance is

(1) $E[v_t\, v_{t-k}^T] = \delta_{k,0}\,(H_t\, P_t\, H_t^T + R_t)$

where $E[\cdot]$ is the expectation operator and $\delta_{k,0}$ is the Kronecker delta. Equation (1) implies that the innovations sequence is uncorrelated in time and that its covariance is equal to the sum of the forecast error covariance $H_t\, P_t\, H_t^T$ (in observation space) and the observation error covariance R_t. Now recall that the forecast error covariance P depends on the model error covariance Q. If the innovations show less spread than expected, the input error covariances (Q and/or R) are too large, and vice versa. Such information can be used for adaptive tuning of Q and/or R.

Alternative diagnostics are based on the analysis departures $w_t \equiv E\{y_{t,i} - H_t\, x_{t,i}^+\}$ and the (observation space) analysis increments $u_t \equiv E\{H_t(x_{t,i}^+ - x_{t,i}^-)\}$. For linear systems under optimal conditions we have

(2) $E[u_t\, v_t^T] = H_t\, P_t\, H_t^T$

(3) $E[w_t\, v_t^T] = R_t$

Equations (2) and (3) suggest a simple way of estimating Q and R separately by tuning the input error parameters so that the output diagnostics on the left-hand-side of (2) and (3) match the right-hand-side error covariances. This approach is employed in the G5-LDAS as summarized in the flow diagram to the right.

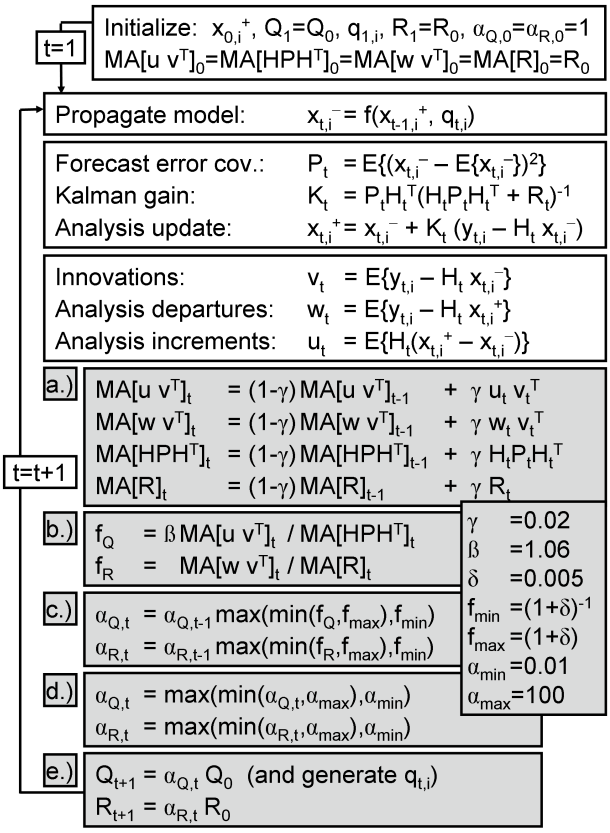

An example of the benefits of the adaptive module is given in Figure 1. The adaptive estimation of input error parameters leads to improved estimates of surface soil moisture regardless of *initial* error estimates, except for the case of severe underestimation of the input observation error variance. The poor performance in this special case is due to technicalities in the implementation and can easily be avoided in applications.

The adaptive filtering module will be used for estimation of retrieval error parameters of NASA satellite products (such as surface soil moisture from AMSR-E) and for the development of a SMAP Level 4 soil moisture assimilation product.

Publications:

Reichle, R. H., W. T. Crow, and C. L. Keppenne, 2008: An adaptive ensemble Kalman filter for soil moisture data assimilation, *Wat. Resour. Res.*, **44**, W03423, doi:10.1029/2007WR006357.

Crow, W. T. and R. H. Reichle, 2008: Comparison of adaptive filtering techniques for land surface data assimilation, *Wat. Resourc. Res.*, **44**, W08423, doi:10.1029/2008WR006883.

Reichle, R. H., and co-authors, 2008: Recent Advances in Land Data Assimilation at the NASA Global Modeling and Assimilation Office, *In: Data Assimilation for Atmospheric Oceanic and Hydrologic Applications*, Springer Verlag DOI: 10.1007/978-3-540-71056-1, Chapter 21.

Contribution of Soil Moisture Retrievals to Land Assimilation Products

Rolf Reichle, Randy Koster and Sarith Mahanama, in collaboration with Wade Crow (USDA) and Hatim Sharif (University of Texas)

Project Objectives: Satellite retrievals of surface soil moisture are subject to errors and cannot provide complete space-time coverage. Data assimilation systems merge available retrievals with information from land surface models and antecedent meteorological data, information that is spatio-temporally complete but likewise uncertain. For the design of new satellite missions it is critical to understand just how uncertain retrievals can be and still be useful. We conducted synthetic data assimilation experiments to determine the contribution of retrievals to the skill of land assimilation products as a function of retrieval and land model skill.

Project Description: A common approach to estimating soil moisture is to drive a land surface model (LSM) with observed meteorological forcing. The LSM integrates the forcing and produce estimates of soil moisture and other land surface fields. Indirect measurements (retrievals) of surface soil moisture can be obtained from satellites. Both the model and the satellite estimates are subject to errors. Data assimilation systems propagate the surface retrieval information into deeper soil layers, giving otherwise unobtainable information (e.g. root zone soil moisture) needed for applications such as weather and climate forecasts. Data assimilation systems are thus an invaluable part of any satellite-based soil moisture measurement mission.

Consider a mission assimilation product for which there is a target accuracy requirement. For a given level of model skill, a specific level of retrieval skill would be needed to bring the assimilation product to the target accuracy. Knowledge of such retrieval skill requirements is directly relevant to the planning of the L-band (1.4 GHz) Soil Moisture Active-Passive (SMAP) mission (projected launch in 2013). In this project, we developed a Data Assimilation-Observing System Simulation Experiment (DA-OSSE) that measures the contribution of surface soil moisture retrievals to the skill of the assimilation estimates (of surface and root zone soil moisture and evapotranspiration) as a function of the errors in the satellite retrievals and in the LSM.

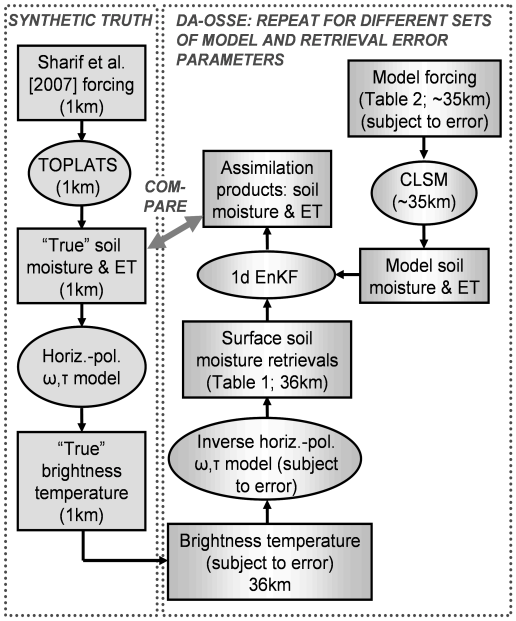

Figure 1: Flow diagram of the DA-OSSE.

Results: We conducted 96 assimilation experiments with synthetic observations (see Figure 1). Each experiment is a unique combination of a retrieval dataset (with a certain level of skill, measured in terms of R) and a model scenario (with its own level of skill). We can thus plot 2D surfaces of skill in the assimilation products as a function of retrieval and model skill.

Figure 2 shows skill *improvement* through data assimilation, defined as the skill of the assimilation product minus the skill of the model estimates (without assimilation). Specifically, for a given level of accuracy in the stand-alone model product, the figure shows how much information can be added to the *root zone* soil moisture product through assimilation of satellite retrievals of *surface* soil moisture with a given uncertainty. Note that the skill of the root

zone soil moisture assimilation product always exceeds that of the model. As expected, the improvements in R through assimilation increase with increasing retrieval skill and decrease with increasing model skill. Perhaps most important is that even retrievals of low quality contribute some information to the assimilation product, particularly if model skill is modest.

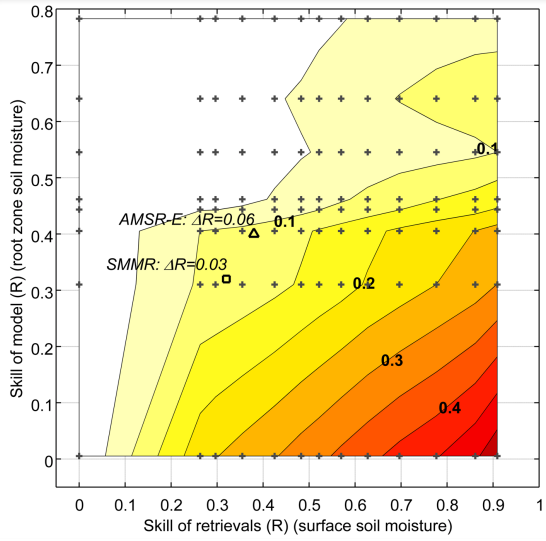

Figure 2: Skill improvement (ΔR) through assimilation for root zone soil moisture as a function of (ordinate) model and (abscissa) retrieval skill. Skill improvement is defined as skill of assimilation product minus skill of model estimates. Each plus sign indicates the result of one 19-year assimilation integration over the Red-Arkansas domain. Also shown are results for (triangle) AMSR-E and (square) SMMR.

We can compare previously published skill levels with these results. For 23 locations across the U.S. having *in situ* observations for validation, Reichle et al. [2007] report average R values of 0.38, 0.40, and 0.46 for AMSR-E retrievals, model root zone estimates, and the root zone assimilation product, respectively. From the figure we expect that for retrievals with R=0.38 and a model with R=0.40, the skill improvement through assimilation would be about R=0.1, which is roughly consistent with the AMSR-E result (indicated by Δ). The actual root zone improvements through assimilation of AMSR-E observations fall somewhat short of those suggested by the OSSE. Possible explanations include (i) the imperfect translation of information from the surface layer to the root zone in the data assimilation system and (ii) the fact that the *in situ* data used for validation of the AMSR-E result are themselves far from perfect (unlike the perfectly known truth of the synthetic experiments). The figure also includes the Reichle et al. [2007] results for assimilating retrievals from the Scanning Multichannel Microwave Radiometer (SMMR). Note that R values for SMMR results are based on monthly mean data, and that the validating *in situ* data for the AMSR-E and SMMR results are not within the geographical domain of our synthetic experiment.

This general framework to quantify the information added to land assimilation products by satellite retrievals of surface soil moisture will be used to provide comprehensive error budget analyses for SMAP data assimilation products.

Publications:

Reichle, R. H., W. T. Crow, R. D. Koster, H. Sharif, and S. P. P. Mahanama, 2008: Contribution of soil moisture retrievals to land data assimilation products, *Geophys. Res. Lett.*, **35**, L01404, doi:10.1029/2007GL031986.

Reichle, R. H., R. D. Koster, P. Liu, S. P. P. Mahanama, E. G. Njoku, and M. Owe, 2007: Comparison and assimilation of global soil moisture retrievals from AMSR-E and SMMR, *J. Geophys. Res.,* **112**, D09108, doi:10.1029/2006JD008033.

An Ocean Ensemble Kalman Filter for Initialization of Seasonal Forecasts

Christian Keppenne, Michele Rienecker, Atanas Trayanov, Robin Kovach and Jelena Marshak

Project Goals and Objectives: To (1) develop algorithms and error covariance models that allow us to optimize the ensemble Kalman filter performance for small-size ensembles and (2) initialize ensembles of coupled seasonal-to-interannual forecasts by assimilating ocean observations into an ensemble of coupled models using an ensemble Kalman filter.

Project Description: A skillful coupled model forecast requires one to effectively minimize initialization shocks. We are addressing this by directly assimilating the observations into the coupled model instead of applying the assimilation to a free-running ocean model prior to coupling.

Because the ensemble Kalman filter (EnKF) evolves an ensemble of model states, it is ideally suited to initialize ensemble forecasts. Our first generation coupled forecasting system was configured such that most ensemble members are initialized by mean of a conventional optimal interpolation analysis applied to the free running ocean model. The application of the EnKF to the free-running ocean model did not originally contribute to the production forecast initialization and only contributes one ensemble member in the current system.

We are in the process of completely reformulating our seasonal forecasting system using GEOS-5 for our second-generation system. The new system is based on the application of an "augmented" EnKF to the GEOS-5 coupled atmosphere-ocean general circulation model (AOGCM). The augmented EnKF assimilates ocean observations and the offline GMAO atmospheric analysis is used to constrain the atmospheric states of the coupled ensemble. The augmented EnKF estimates background error covariances from the current condition of an ensemble of continuous model integration streams and from high-pass filtered past (time-lagged) instances of these same streams. This procedure allows us to artificially increase the ensemble size beyond the limits imposed by current memory and time constraints. The flow-dependent background-error covariance estimates so obtained are augmented with steady-state (i.e., not flow-dependent) covariance information obtained from a static ensemble of estimated model-error and from bred perturbations.

Results: Figure 1 illustrates the coupled assimilation procedure in the case of a one-day ocean assimilation interval. The coupled analysis cycle involves a "replay" of the GMAO atmospheric analysis. **(1)** Following an ocean analysis at 03Z, the AGCM component of each coupled ensemble member is advanced to 06Z (thin black line) where **(2)** the corresponding background (red circle) is differentiated with the atmospheric analysis (blue diamond) which is read from a file to produce an analysis increment. **(3)** The AGCM is then rewound to 03Z and **(4)** the ensemble of coupled models is advanced until 09Z while the atmospheric analysis increments are incrementally applied over the series of time steps from 03Z to 09Z, thereby controlling the drift of the atmospheric states from the atmospheric analysis. The same six-hourly procedure **(1-4)** is then repeated until the time of the next ocean analysis (green star).

The initial testing of the augmented EnKF involves the MOM4 ocean model coupled to the GEOS-5 AGCM. However, a distinct advantage of the new system over its predecessor is that its implementation's reliance on the Earth System Modeling Framework (ESMF) and Modeling

Analysis and Prediction Library (MAPL) libraries result in a highly configure-able model-independent data assimilation system (because ESMF and MAPL provide a model-independent framework to connect diverse modeling components).

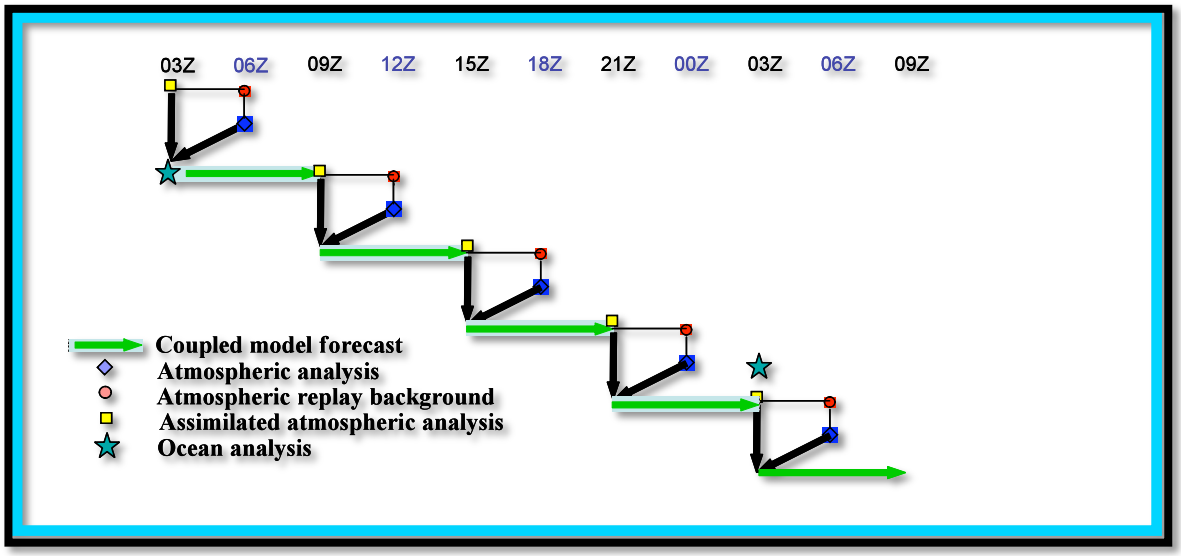

Figure 1: Schematic illustration of the coupled data assimilation procedure with "replay" of the GMAO atmospheric analysis as explained in the text.

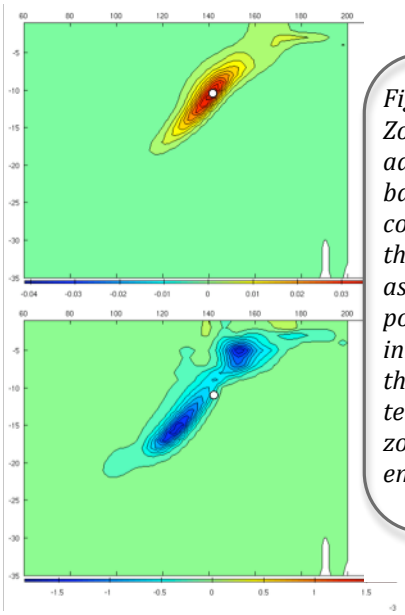

Figure 2: Zonal sections through an adaptively localized background error covariance function showing the influence (marginal assimilation increment) of a positive unit temperature innovation at the location of the white circles on (top) the temperature and (bottom) zonal current fields of one ensemble member (see text).

The EnKF implementation includes a flow-adaptive background error covariance localization and filtering procedure to mitigate the deficiencies of a limited-size ensemble. The localization for the compact support is based on neutral density. As an illustration, a zonal vertical section through an adaptively localized error covariance is shown in Figure 2. This covariance shows the marginal impact of a unit temperature innovation at a location indicated by the white circle on the temperature field of one ensemble member (upper panel). Note the tilt of the covariance pattern, which approximately follows the thermocline. The influence of the same temperature innovation on the other model prognostic fields obeys similar stratification-aware patterns. The lower panel shows the corresponding marginal zonal current increment.

Publication:

Keppenne, C.L., M.M. Rienecker, J.P. Jacob and R.M. Kovach, 2008: Error covariance modeling in the GMAO ocean ensemble Kalman filter, *Mon. Wea. Rev.*, **136**, 2964-2982.

Error Analysis of Ocean Color Data

Watson Gregg and Nancy Casey

Project Goals and Objectives: Chlorophyll is the most systematically and widely observed carbon-related variable in the oceans. In situ archives date from 1955. Satellite estimates are available on a global basis continuously since 1996. This data treasure provides a unique and irreplaceable indicator of how climate change may affect ocean carbon and vice versa. However, both in situ and satellite and data sets are flawed: in situ because of poor spatial coverage, and satellite because of accuracy and occasional sampling issues.
We intend to investigate issues related to ocean chlorophyll errors, quantify them to the extent possible, and propose solutions when possible. We will bring to bear in situ comparisons (regionally, globally, seasonally, and interannually), analysis methodologies, and data assimilation techniques. First we will assess the satellite and in situ chlorophyll error and its variability. Spatial distributions of the error will be provided using the conditional relaxation analysis method, involving in situ and satellite data. This will reveal areas and times when corrections are needed for the satellite data. We will then proceed to estimate sampling errors from satellite. Finally, a full global ocean chlorophyll assimilation system will be applied using various fields, including in situ, analysis of satellite and in situ data, and satellite data to observe overall improvement and continued regions/times where problems exist. An in situ sampling program will be proposed that will minimize the residual errors, after utilizing all available tools, i.e., satellite data, available in situ data, analysis of satellite and in situ, and data assimilation. The result of these analyses can yield information on optimization of future satellite missions, balancing sampling, reducing persistent errors locations and times, with costs.

Project Description: Quantifying ocean carbon variability is a major objective of NASA's Carbon Cycle Program. Chlorophyll is an indicator of the abundance and distribution of the living component of ocean carbon. A major focus of in situ observations, it has a very long time series, dating back to 1955 in the NOAA/National Oceanographic Data Center (NODC) archives. It is also the primary geophysical derived variable for spaceborne ocean color sensors, which have been providing routine global observations since 1996.

This vast repository of carbon-related information has led to many reports of spatial and temporal variability, and forms the basis for most large-scale estimates of photosynthetic uptake of carbon. Yet the errors, their sources and distributions, are not completely characterized. Knowledge of the errors is essential for us to have confidence in estimates of chlorophyll variability in the oceans.

While there are error estimates of satellite chlorophyll performed by NASA, these estimates utilize a pristine data set, free of most atmospheric correction problems and ancillary absorbing substances in the ocean besides chlorophyll. These estimates are critical, but emphasize the capability of the sensors. A complete analysis of the data sets, containing all of the flaws in the data processing algorithms, in all parts of the global oceans as can be used, is needed to evaluate estimates of spatial and temporal variability derived from these data sets. Gregg and Casey (2004) performed some parts of such an analysis, but this work is now outdated as the current data sets in the NASA archives use a new set of processing algorithms.

There also remain issues associated with satellite sampling errors that have not been addressed quantitatively and comprehensively. These sampling errors derive from clouds, excessive aerosols, and to a lesser extent sun glint, sensor tilt, and inter-orbit gaps that severely limit daily ocean

observational coverage. These sampling errors may creep into the monthly and annual products even though they appear to be nearly gap-free.

New methodologies have recently been developed and applied to ocean biological problems that have much potential to reduce the total error in chlorophyll estimates. We refer to data assimilation, which combines the accuracy and reliability of data with integrated representations of ocean processes. These efforts are quickly maturing. It is unclear exactly how much these new methods can contribute to reducing error in estimates of chlorophyll, or what their limitations are. A comprehensive, quantitative evaluation is lacking.

Once the chlorophyll errors are quantitatively described on a global and regional basis, and all tools to combine satellite, in situ, and modeling approaches have been implemented and characterized, the question becomes, what can be done to reduce the residual errors? At this point we intend to investigate strategies for in situ sampling, targeted in persistent problem areas that can minimize residual errors remaining from the application of state-of-the-art methodologies. Maps of areas subject to limitations by satellite observations and outside the capabilities of modern data assimilation systems can assist program managers and guide deployment of in situ sensors to maximize effectiveness.

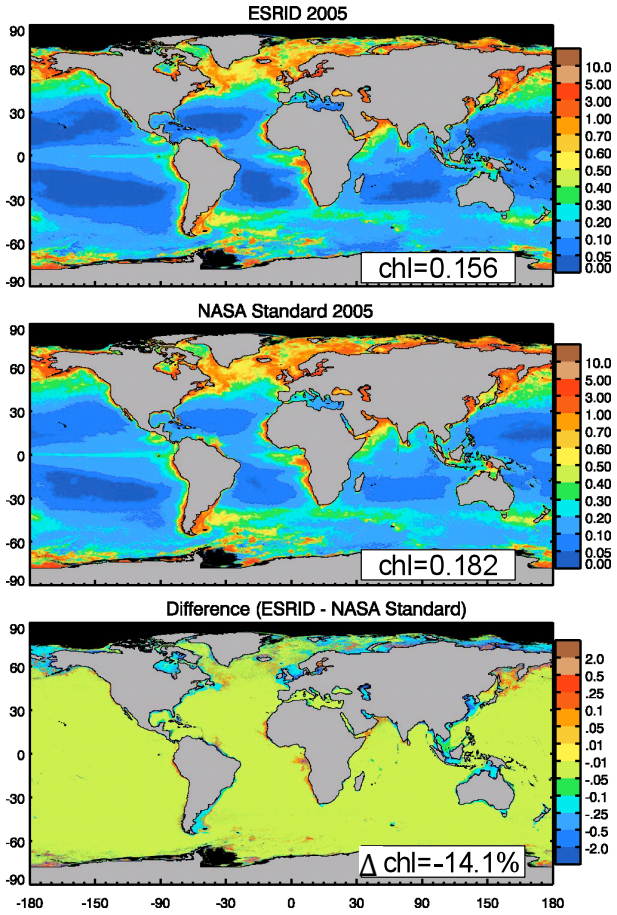

Figure 1: Global annual mean chlorophyll from SeaWiFS using ESRID, the NSA standard processing, and the difference for 2005. The global mean chlorophyll values are shown n each plot in units of mg m^3, with the difference in percent in the difference plot.

Results: A new empirical approach is developed for ocean color remote sensing. Called the Empirical Satellite Radiance-In situ Data (ESRID) algorithm, the approach uses relationships between satellite water-leaving radiances and in situ data after full processing, i.e., at Level-3, to improve estimates of surface variables while relaxing requirements on post-launch radiometric re-

calibration. The approach is evaluated using SeaWiFS chlorophyll, which is the longest time series of the most widely used ocean color geophysical product.

The results suggest that ESRID 1) drastically reduces the bias of ocean chlorophyll, most impressively in coastal regions, 2) modestly improves the uncertainty globally, and 3) reduces the sensitivity of global annual median chlorophyll to changes in radiometric re-calibration. Simulated calibration errors of 1% or less produce small changes in global median chlorophyll (<2.7%).

In contrast, the standard NASA algorithm set is highly sensitive to radiometric calibration: similar 1% calibration errors produce changes in global median chlorophyll up to nearly 25%. We show that 0.1% radiometric calibration error (about 1% in water-leaving radiance) is needed to prevent radiometric calibration errors from changing global annual median chlorophyll more than the maximum interannual variability observed in the SeaWiFS 9-year record (±3%), using the standard method. This is much smaller than the SeaWiFS goal of 5% uncertainty for water leaving radiance.

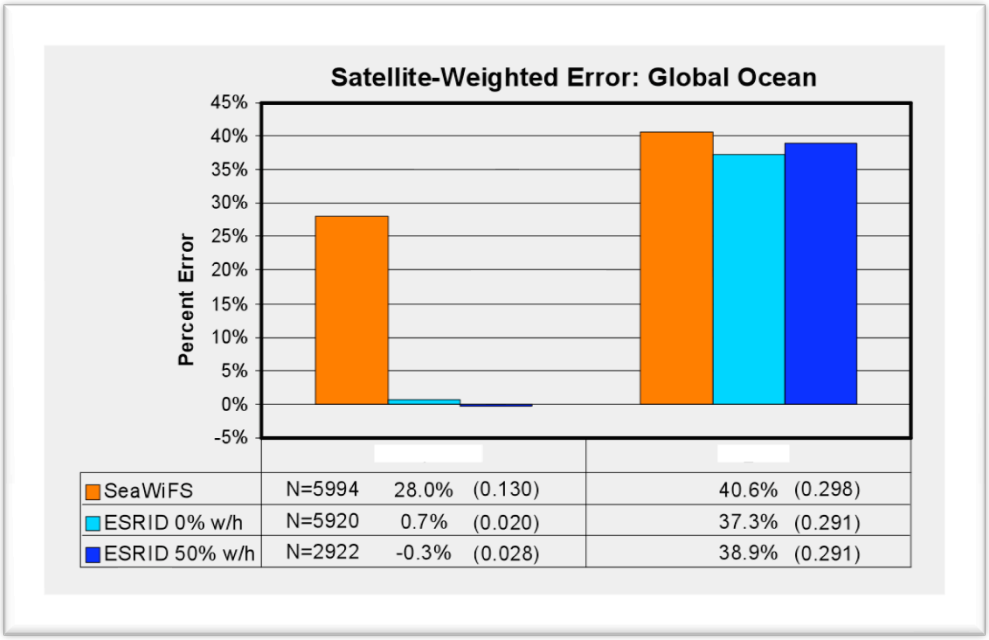

Figure 2: Satellite-weighted error statistics (bias and uncertainty) for the global ocean. Statistics from SeaWiFS are compared with two estimates from ESRID, one with no withholding of data (0% w/h), representing a lower bound of the error estimate, and one with 50% withholding (50% w/h), representing an upper bound. The statistics are show in the data table below the figures, with log error provided in parentheses.

The results suggest that ESRID, combined with a field sampling program, can improve the quality and reliability of ocean color data, while promoting a unified description of ocean biology from satellite and in situ platforms. Although the results here focused on chlorophyll, the ESRID approach can be applied to any surface variable potentially observable by visible remote sensing.

Publication/Reference:

Gregg, W.W., N.W. Casey, J.E. O'Reilly, and W.E. Esaias, 2009: An Empirical Approach to Ocean Color Data: Reducing Bias and the Need for Post-Launch Radiometric Re-Calibration. *Remote Sensing of Environment*, revision in review.

Gregg, W.W., and N.W. Casey, 2004: Global and Regional Evaluation of the SeaWiFS Chlorophyll Data Set. *Remote Sensing of Environment*, **93**, 463-479. DOI: 10.1016/j.rse.2003.12.012.

GEOS-5 – CloudSat Intercomparisons

Julio Bacmeister

Project Objectives: The purpose of this study is twofold. First we would like to place the huge CloudSat database in the correct meteorological setting in the hope of shedding light on the large scale dynamical controls exerted on convective systems by the atmosphere, using a state-of-the-art high resolution GEOS-5 Data assimilation System (DAS). Second we would like to directly compare the output of the current convective and cloud parameterizations operating in the AGCM component of the GEOS-5 DAS with CloudSat observations.

Project Description: Parameterization of clouds and convection remains a vexing problem for global models. Convective updrafts and downdrafts in the atmosphere have horizontal scales from 100s of meters to several kilometers. These motions are well below the horizontal resolution of current global atmospheric models and will probably not be resolvable in global models for a decade or more. Nevertheless, convection exerts a first order effect on our climate and atmospheric circulation. This effect is currently included in global models using simplified representations (or parameterizations) that are driven by the resolved flow features of the global model.

CloudSat, a satellite-borne cloud profiling radar (CPR) designed to detect small cloud particles, provides profiles of cloud-induced radar-reflectivity with a vertical resolution of 500 m. Profiles are measured approximately every 1-2 km along the satellite ground track and provide an unprecedented view of the vertical structure of clouds. This study examines the relationships between CloudSat derived cloud parameters and other atmospheric variables, using global atmospheric fields from MERRA. Our focus is on convective systems which are poorly represented in models and which have so far eluded efforts to correlate simulations with CloudSat observations.

Cloud or convective depth scale, a critical parameter for a number of atmospheric processes including tracer transport, radiative forcing, and diabatic heating, is typically underestimated in climate models. Here we determine climatologies of cloud depth from CloudSat and relate them to predictors of cloud depth based on local atmospheric profiles of u, v, T and q. We use the following algorithm to automate estimates of cloud depth from CloudSat data. Raw GEOPROF-2B radar reflectivities are the starting point. Each granule of radar reflectivity consists of around 37,000 profiles with 125 range bins (levels) containing returns from different altitudes. Centers of the altitude range bins are spaced about 240 m apart although vertical feature resolution is around 500 m. For the analysis, each granule is subdivided into overlapping segments of 100 profiles, with centers spaced 50 profiles apart (Figure 1). The correlation between each pair of vertical levels in the segment is then calculated. Only those between level 105, the typical surface return level, and level 45 at ~ 15 km are used. The result is a 60x60 correlation matrix for each segment (Figure 1c). A two-sided, one-parameter Gaussian fit is then made to the correlations from each level. This gives two correlation length scales (up and down) for each level in the CloudSat data (Figures 1d, e).

We use the 1/2°×2/3° MERRA fields interpolated onto CloudSat tracks in both space and time to derive a number of predictors for convective cloud depth. One of the simplest of these is the height to which an undiluted surface parcel would rise before losing buoyancy. This depends primarily on the moist static energy near the surface and the temperature profile aloft, as illustrated schematically in Figure 2. The undiluted surface parcel height is a simple estimate of the maximum possible convective cloud height for given atmospheric profiles of T and q.

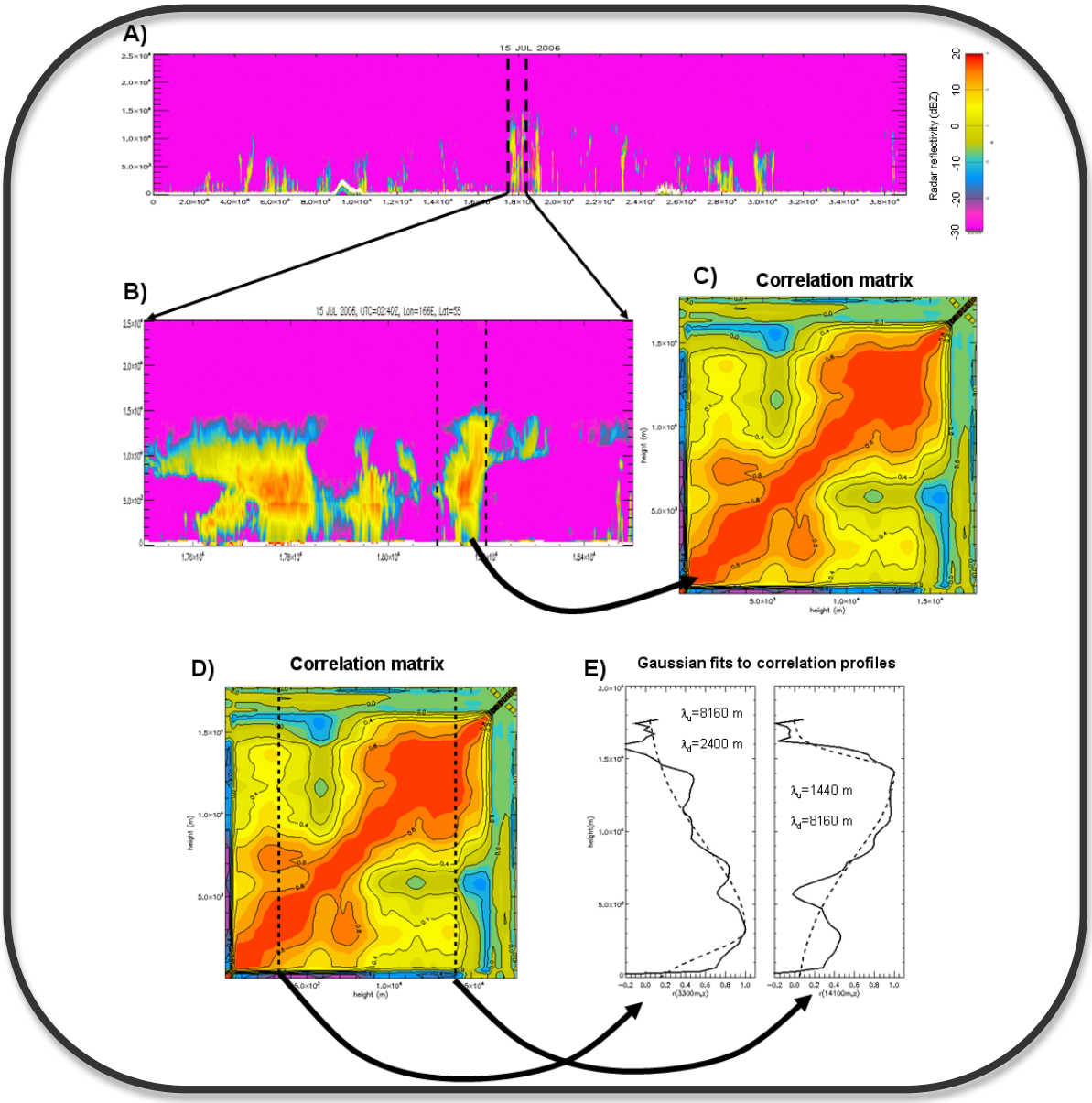

Figure 1: Illustration of analysis procedure for GEOPROF-2B radar reflectivity granule (#01132, July 15, 2006, 01:52:00Z to 03:31:00Z). Panel A shows raw reflectivity from CloudSat for the entire granule of around 37,000 profiles. Panel B zooms in on convective clouds observed in W Pacific (5N-5S, ~165W). The section bounded by the dashed lines contains 100 profiles. Panel C shows the level-to-level correlation matrix calculated for this section, from near mean sea level to ~ 15 km altitude. Panels D and E illustrate the estimation of upward and downward correlation scales from each vertical level. The dashed vertical lines in D are at 3.3 km and 14.1 km. In E, solid lines show the corresponding correlation profiles, dashed lines show best-fit one parameter Gaussians.

Results: Figure 3 shows a joint PDF of CloudSat vertical correlation scale from the surface upwards and the undiluted surface parcel height from MERRA for July 2006. There is a clear statistical relationship between this simple predictor of convective cloud depth and observed cloud vertical correlation scales. Observed cloud vertical scales rarely exceed the undiluted parcel height estimated by MERRA. The shape of the PDF for a given value of the undiluted parcel height is approximately exponential, with many more observed correlation scales close to zero than to the maximum possible height predicted by the analysis. The close match between the upper limit of the PDF in the horizontal and the y=x line may be fortuitous consequence of our analysis, but the

general character of the joint PDF is not.

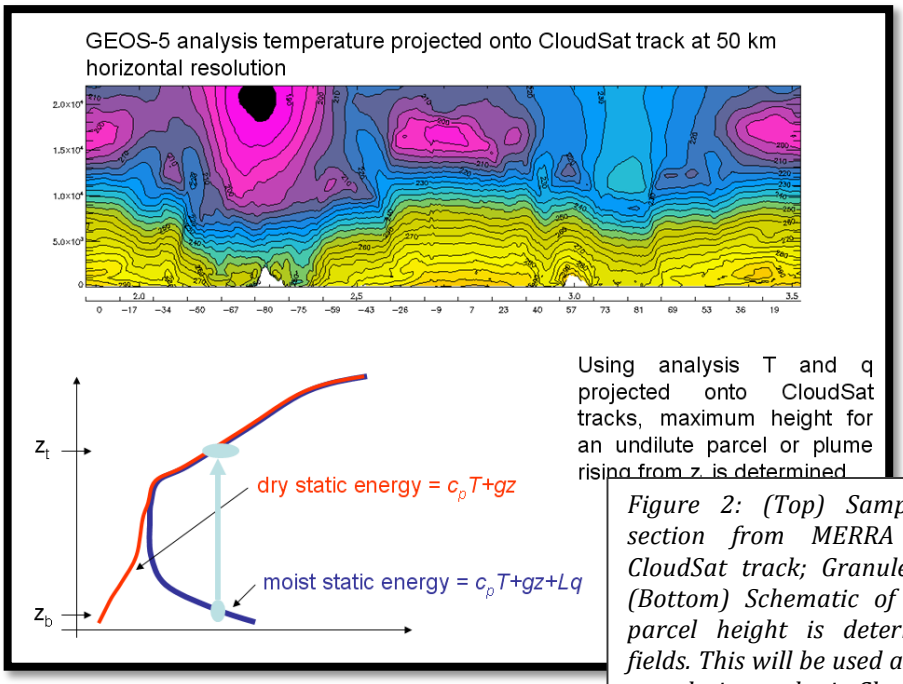

Figure 2: (Top) Sample temperature cross-section from MERRA interpolated onto a CloudSat track; Granule 01132, July 15 2006. (Bottom) Schematic of how undiluted surface parcel height is determined from reanalysis fields. This will be used as a predictor for vertical correlation scales in CloudSat data.

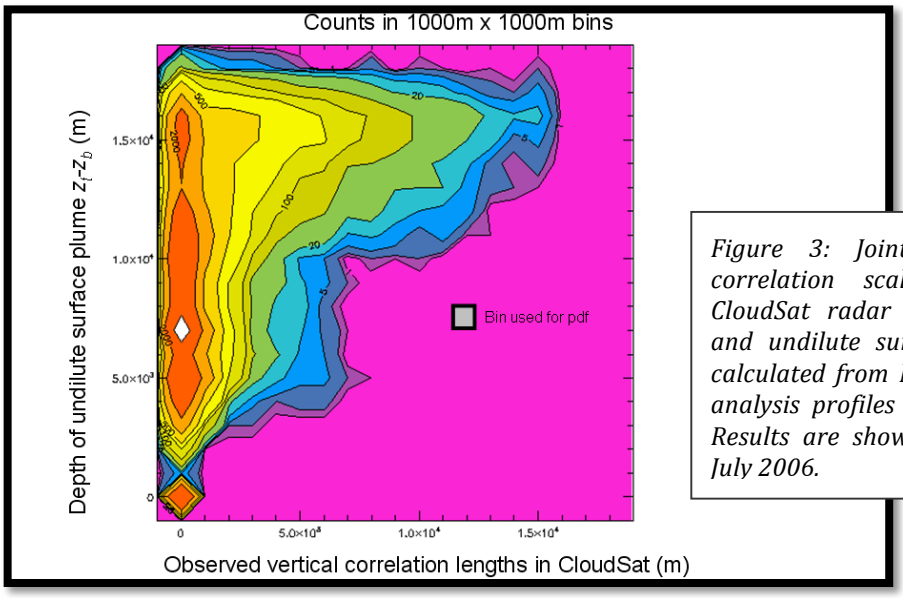

Figure 3: Joint PDF of vertical correlation scales obtained from CloudSat radar reflectivites (x-axis) and undilute surface parcel heights calculated from MERRA retrospective analysis profiles of T and q (y-axis). Results are shown for the month of July 2006.

The result in Figure 3 is encouraging. A simple analysis derived predictor for cloud height yields a good and physically reasonable description of the statistics of vertical correlation scales in the CloudSat data. The lack of a good deterministic relationship between our simple analysis predictor and observed cloud vertical scales is almost certainly due in part to sampling issues related to CloudSat, but may also reflect a real underlying stochastic character in atmospheric convection. Refinements in the analysis predictor could produce a tighter relationship with the observations. However, we believe that issues of sampling and inherent stochasticity are likely to dominate in comparisons of CloudSat convective cloud observations with large-scale models. Cloud resolving models should prove useful in interpreting results such as those in Figure 3.

Cloud Parameterization using CRM simulations and Satellite Data

Peter Norris and Arthur Hou, with Lazaros Oreopoulos (613.2), Wei-Kuo Tao and Xiping Zeng (613.1)

Project Objectives: Clouds play an essential role in moderating the climate. This has prompted continuing efforts to improve the representation of clouds in global climate models. What is currently needed is the ability to test these cloud representations against different sources of observed cloud data with global or large-scale coverage. In particular, NASA has made a large investment in high-resolution satellite cloud observing systems (e.g., MODIS, AMSR-E and CloudSat) that can be used for this purpose. The goal of our work is to use retrieved cloud data to validate cloud properties within the Goddard Earth Observing System (GEOS) model, to measure the capability of trial cloud representations, and to assimilate cloud measurements directly into the GEOS data assimilation system. This task is particularly concerned with developing climate model cloud representations that benefit from realistic statistical descriptions of the cloud scale variability provided by high-resolution NASA cloud data.

Project Description: Currently, climate models have grid sizes too large (due to computational restrictions) to model many important cloud processes, so several solutions are currently being explored by the GCM community. One approach is to model not just the mean properties of a model gridbox, but other statistical properties as well. The so-called statistical or assumed probability distribution function (PDF) cloud schemes fall into this category. These schemes assume a certain parametric form for the PDF of subgrid-scale moisture variability, from which the cloud fraction and condensed water content are diagnosed. To close the system, the PDF parameters must be diagnosed or prognosticated by the GCM.

In addition to the layer-by-layer statistical properties of the cloud fields, a proper treatment of vertical cloud overlap statistics is crucial for realistically modeling the transmitted solar radiation and other radiative properties of the grid column, and also the surface precipitation flux and other hydrological quantities.

Our research has focused on these statistical cloud parameterization tasks, both because they provide a more sound theoretical basis for cloud parameterization than many of the ad-hoc methods currently used, and also because the current availability of high resolution cloud data (from MODIS, CloudSat, and other sources) now make it practical to constrain these statistical properties

Results: Our focus for the current year has been on formulating a sufficiently general theoretical model for horizontal subgrid-scale moisture variability, and its vertical correlation among layers. We have published a new contribution to the GCM cloud parameterization community that uses so-called copula functions to achieve the above task with far more flexibility than previous methods.

We have made significant advances in two theoretical/modeling studies aimed at improving statistical cloud parameterizations for use in climate models. The first development allows the correlation of the PDFs of moisture and temperature among different layers of a model grid column using statistical functions called copulas. The work provides a significant advance in the treatment of the thorny cloud overlap problem and in the calculation of cloudy radiative fluxes within complex cloud systems. Previous work had excluded temperature variability and also restricted direct inter-layer correlations to neighboring layers. The new approach was tested using high-

resolution cloud data from the Goddard Cumulus Ensemble (GCE) cloud resolving model and found to give very promising results compared with existing methods. The new approach is very suitable for use by Monte-Carlo grid column radiative transfer schemes, which have been developed by others recently. Figure 1 shows the good performance of our Gaussian Copula method against two other modern cloud overlap schemes. Figure 2 shows that the new method can model complex inter-layer moisture correlations very well.

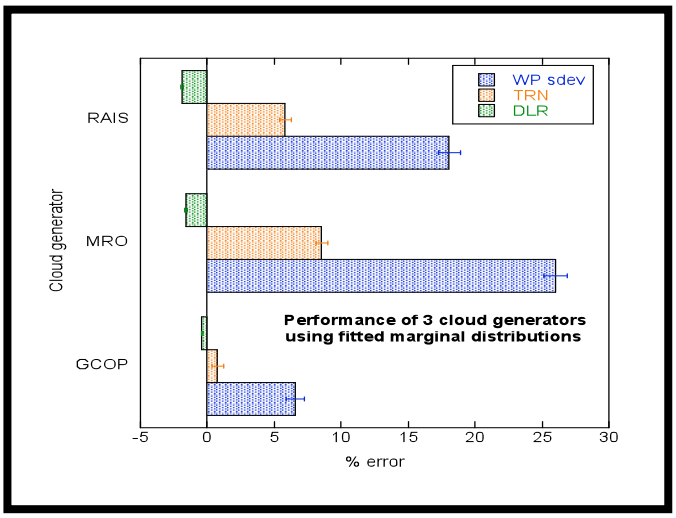

Figure 1: Percent biases in GCM-domain-sized estimates of the standard deviation of liquid water path (WP sdev), transmitted solar flux to the surface (TRN) and downwelling longwave radiation to the surface (DLR) of three cloud generators (GCOP=Gaussian Copula, MRO=Maximum Random Overlap, RAIS=Räisänen et al. (2004) total water generator) relative to exact GCE independent-column values. The results come from 100 generator realizations with the bias spread shown as superimposed error bars. The performance of the Gaussian copula method is clearly superior.

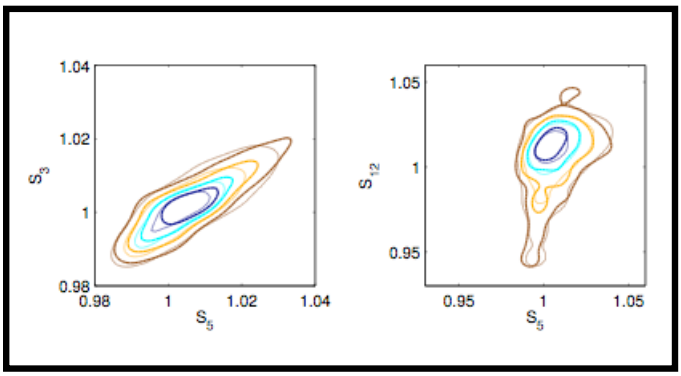

Figure 2: Contours containing 80% (brown), 60% (orange), 40% (cyan) and 20% (blue) of the joint inter-layer moisture probability, such that the probability densities within each contour are larger than those outside. Thick contours are for the raw GCE subcolumns and the thin contours are for subcolumns generated from the Gaussian copula. The good copula fits are evident. The layer separations are 256 m (left panel) and 1652 m (right panel. The closer layers are more correlated, as expected.

The second development started as an expansion of the above study to four case studies with very different synoptic conditions. In the process of that analysis it was discovered that a more flexible parametric form would be required for the PDFs of moisture and temperature variation within each layer, which are often highly skewed and can be multimodal. Norris et al. (2008) focuses on inter-layer variability. Now we are focusing on the variability within a single layer and are developing a flexible new skewed distribution, with separate control of central and tail skewness.

Publication:

Norris, P.M., L. Oreopoulos, A.Y. Hou, W.-K. Tao, X. Zeng, 2008: Representation of 3D heterogeneous cloud fields using copulas: Theory for water clouds. *Q. J. R. Meteorol. Soc.*, **134**: 1843-1864. doi:10.1002/qj.321.

Modeling Diurnal Cycle of Warm-Season Precipitation in GCMs

Myong-In Lee, Siegfried Schubert and Max Suarez, with Jae Schemm, Hua-Lu Pan, Jongil Han and Soo-Hyun Yoo (NOAA/NCEP)

Project Goals: The goal of this project is to improve our understanding of the mechanisms that drive the diurnal cycle of warm-season precipitation, with a broader goal of improving the parameterization of the mechanisms that drive the diurnal cycle in current GCMs.

Project Description: The diurnal cycle is a fundamental component of the warm season climate of the continental United States and northern Mexico. However, it still remains a difficult test for GCMs. In general, deep convection tends to develop too early over land, where they produce too much rainfall in the daytime. The model deficiencies are particularly pronounced over the Great Plains where the models generally fail to capture the nocturnal rainfall maximum found in the observations. This problem extends beyond GCMs to impact the quality of many data assimilation products, suggesting there is a common, intrinsic problem, apparently associated with deficiencies in the parameterized model physics.

This project aims to evaluate, understand, and improve the warm-season diurnal cycle of precipitation in current GCMs. From our previous assessment, the NCEP GFS model produced a realistic nocturnal rainfall signal over the Great Plains. Here we examine the nature and realism of the mechanisms responsible for the diurnal cycle of precipitation in this model. We particularly focused on the role of various convection triggers implemented in the model.

Results: We have run a set of experiments designed to assess the impact of several convection triggers implemented in the Simplified Arakawa-Schubert (SAS) scheme in the NCEP GFS. Figure 1 compares the amplitude and the phase of the maximum of the diurnal cycle of precipitation from the control (CTRL) and four sensitivity runs (EXP1–4), and those from the surface rain-gauge observations (HPD). The control simulation (CTRL) is quite reasonable in reproducing large-scale coherent patterns of the phase of the maximum. The model shows good correspondence with the observations in the nighttime maxima over the Great Plains. Over the rest of the continent, the model exhibits a precipitation maximum in the afternoon or evening, which is consistent with the observations, although the peak times are in general a few hours earlier than in the observations.

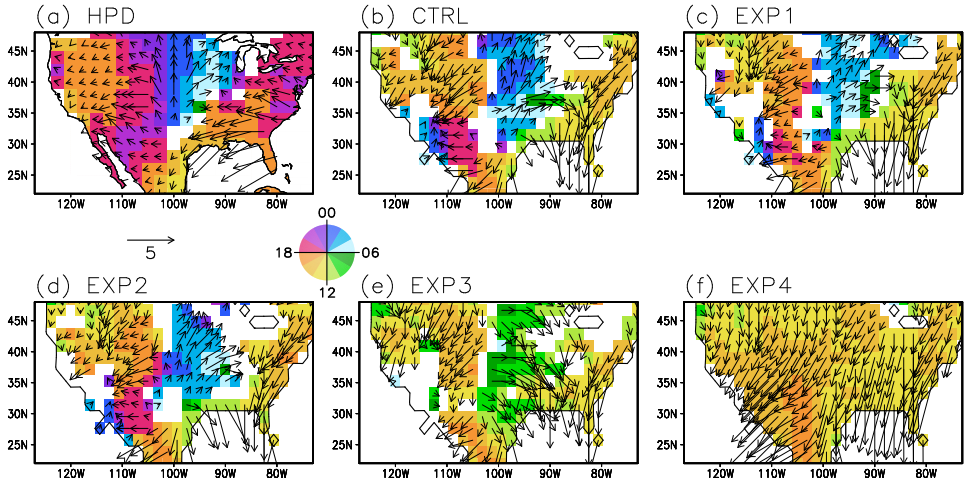

Figure 1: Amplitude and maximum phase of the diurnal cycle of precipitation in (a) the observations (HPD, 1983–2002) and (b–f) the model simulations (ensemble means). Length of the arrow indicates the amplitude (mm d^{-1}); the arrow direction indicates the maximum phase in LST (local solar time). The maximum phases are also indicated in color shading. Only grid points over land and significant at the 90% level are shown. The land-sea boundary that was used in the model is indicated in panels b–f.

From the sensitivity experiments, it was found that the simulated amplitude and phase of the diurnal cycle is insensitive to modifications in the convection scheme that disabled the dependency of the cloud work function (CWF) and the relaxation timescale on the grid-scale vertical motion (EXP1 and EXP2, respectively). On the other hand, the simulation was found to be sensitive to the choice of the convection starting level (EXP3) and the model-specific LFC (level of free convection) condition (EXP4). When the convection starting level is set to be the model level closest to the ground (in EXP3), rather than the level of maximum moist static energy (as defined in the standard SAS scheme in CTRL), the simulated nocturnal precipitation disappears over the Great Plains and the peak in the precipitation is shifted to the daytime. A similar sensitivity was obtained when the LFC condition is relaxed substantially (set to a condition less than 500 hPa from the convection starting level in EXP4 from the standard setting of 150 hPa in CTRL).

Further analysis indicates that the convection trigger associated with the LFC condition, which crudely represents an upper limit of convective inhibition, produced a significant impact on the phase of the diurnal convection (see the schematic in Figure 2). In particular, the nighttime elevation of the convection starting level above the nocturnal inversion layer provides a favorable condition for the nocturnal development of precipitation over the Great Plains. On the other hand, daytime convection appears to be largely suppressed as the convection starting level is closer to the ground and consequently the convective inhibition (i.e., the depth of the LFC from the convection starting level) becomes larger, although the potential convective instability of the column (as represented by CWF) is much larger during the day than at night. This mechanism appears to be effective in the inland regions such as the Great Plains where the relatively dry PBL air causes an elevation of the LFC and large convective inhibition. This feature is qualitatively consistent with the Atmospheric Radiation Measurement (ARM) sounding observations over the Great Plains.

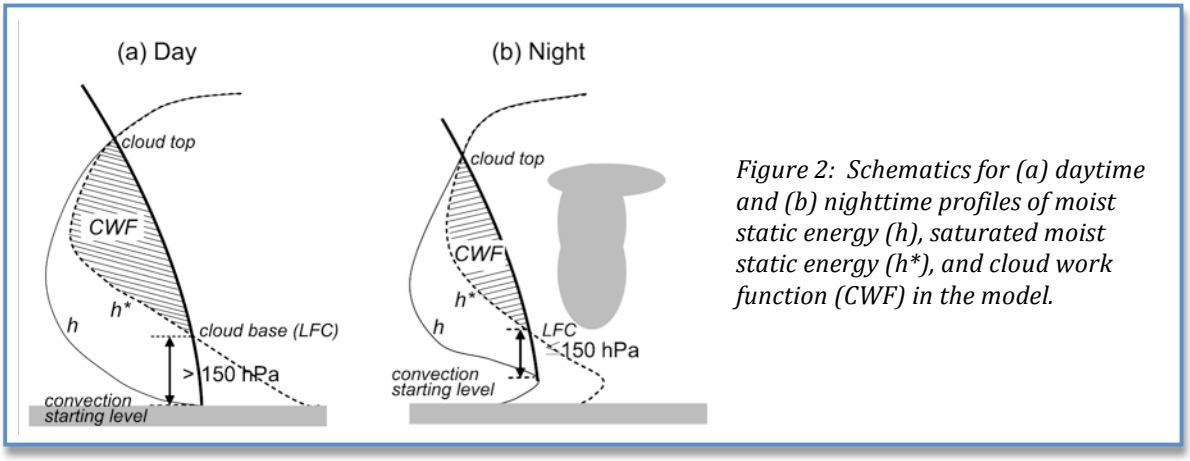

Figure 2: Schematics for (a) daytime and (b) nighttime profiles of moist static energy (h), saturated moist static energy (h), and cloud work function (CWF) in the model.*

We plan to test the same convection triggers with the GEOS-5 GCM to improve its representation of the diurnal cycle of precipitation. The implementation in GEOS-5 seems to be straightforward as the convective scheme of GEOS-5 is the relaxed Arakawa-Schubert, which is very close to that of GFS.

Publications:

Lee, M.-I., and S. D. Schubert, 2008: Validation of the Diurnal Cycle in the NASA's Modern Era Retrospective-Analysis for Research and Applications (MERRA). Proc. the 88th AMS Annual Meeting, 20-24 January, New Orleans.

Lee, M.-I., S. D. Schubert, M. J. Suarez, J.-K. E. Schemm, H.-L. Pan, J. Han, and S.-H. Yoo, 2008: Role of convection triggers in the simulation of the diurnal cycle of precipitation over the United States Great Plans in a general circulation model. J. Geophys. Res.,113, D02111, doi:10.1029/2007JD008984.

Moist Benchmark Calculations for Atmospheric GCMs

Myong-In Lee and Max Suarez, with In-Sik Kang and Daehyun Kim (SNU), and Isaac Held (NOAA/GFDL)

Project Goals and Objectives: The goal of the project is to develop and implement a simplified benchmark test for general circulation models (GCMs). The benchmark test is a set of idealized GCM experiments in which the full moist physics parameterizations are retained but the lower boundary of the model is coupled with a slab ocean – a homogenous, wet, low-heat-capacity surface. The project focuses specifically on evaluating the usefulness and limitations of the test in comparing the moist physics parameterizations of GCMs in the ocean-atmosphere coupled framework.

Project Description: Although GCMs are indispensable to weather/climate prediction and climate change studies, many uncertainties in parameterized physics remain. The uncertainties, particularly in moist convection and its interaction with cloud and large-scale circulation, produce large differences among the models as well as systematic deviations from observed climate. To pin down the problem in a complicated GCM simulation is neither simple nor straightforward since model behaviors are often masked by the complexity of the forcing and boundary conditions, including zonal asymmetries due to the prescribed sea-surface temperatures (SSTs), topography, and land-ocean distributions that complicate the interpretation of the model responses.

This project is to develop a simplified yet useful benchmark test to the current GCMs, in order to help identify common problems and differences between the models associated with moist physics parameterization. The test is highly idealized, in the spirit of the dynamical core benchmarks proposed by Held and Suarez (*BAMS,* 1994), but extended to moist atmospheres. All physical parameterizations and dynamical assumptions of the models are retained, but the models are run over a flat, homogenous, saturated ocean surface with a small, but non-zero heat capacity. A simple mixed layer ocean is included to enable air-sea coupling processes and allow for a crude, but more straightforward analysis of the climate sensitivity than with realistic coupled GCMs.

Results: In calculations with several GCMs (NSIPP, GFDL AM2, SNU, and GEOS-5), the idealized test produces very strong zonal-mean flow and exaggerated ITCZ strength. Nevertheless, the model simulations remain sufficiently realistic to justify the use of this framework in isolating key differences between models. Because surface temperatures are free to respond to model differences, the simulation of the cloud distribution, especially in the subtropics, affects many other aspects of the simulations. The simulated subtropical cloud distributions are especially important in characterizing different models, determining planetary albedos, global-mean temperatures, and ITCZ precipitation. The degree to which low-level clouds control the climate in this benchmark was further explored in the NSIPP model, which in the control runs was an outlier, producing by far the warmest climate. By changing the cloud parameterization in this model to produce more low-level subtropical cloudiness, its climate is more in agreement with those in the other models.

The analysis of simulated tropical transients highlights the importance of convection inhibition and air–sea coupling as affected by the mixed layer depth. The subseasonal variances and the eastward propagation speeds are quite different among the models. We suggest that these differences are largely due to differences in the convection inhibition. The shallower heating structure from the grid-scale condensation scheme that results when convection is inhibited seems to explain the slower propagation of the convectively coupled equatorial waves, a result that is consistent with expectations from previous studies, and also consistent with observations. The oceanic heat

capacity also turns out to be an important parameter in affecting the mean climate and transients, with a tendency for stronger simulated zonal-mean circulation and ITCZs with deeper mixed layers.

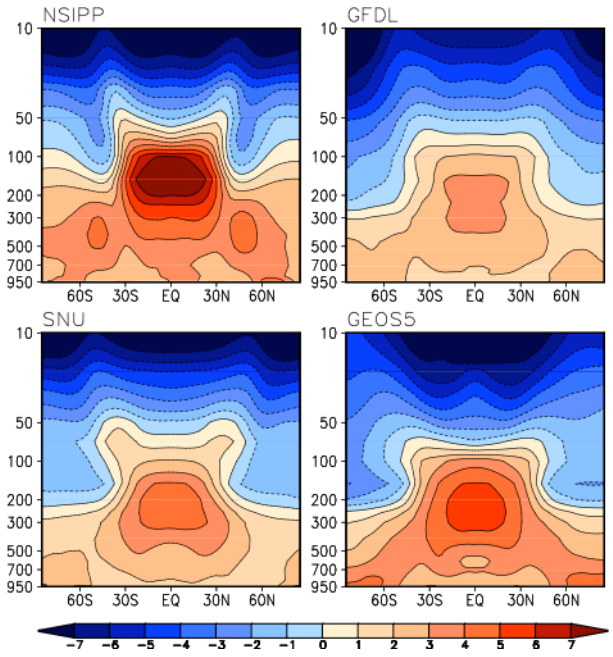

Figure 1: Zonal-mean distributions of temperature change (2xCO_2-Control) in the four idealized aqua-planet GCM simulations (NSIPP, GFDL, SNU, and GEOS-5). Units are K.

The moist physics sensitivity to increased greenhouse forcing was also evaluated by doubling CO_2 concentration. The models tend to produce different amplitudes of global mean responses in surface temperature and precipitation. Although the GCMs also exhibit different sensitivity in the latitude-height distributions of the zonal-mean temperature change, all models show a consistent signal of overall warming in the troposphere and cooling in the stratosphere (Figure 1). The percentage changes in global-mean precipitation are closely proportional to changes in global-mean surface temperature, increasing at a rate of 2.5% K^{-1} (Figure 2), quite close to the value (2.2% K^{-1}) from the IPCC AR4 runs (Soden and Held, *J. Climate,* 2006). In the warmer climate, the models consistently simulate an enhanced water vapor transport toward the equator, a reduction of dry stability, a weakening of the Hadley circulation, and a reduction in cloudiness and tropospheric relative humidity. The net changes in cloud radiative forcing in the four models, on the other hand, differ in sign and magnitude.

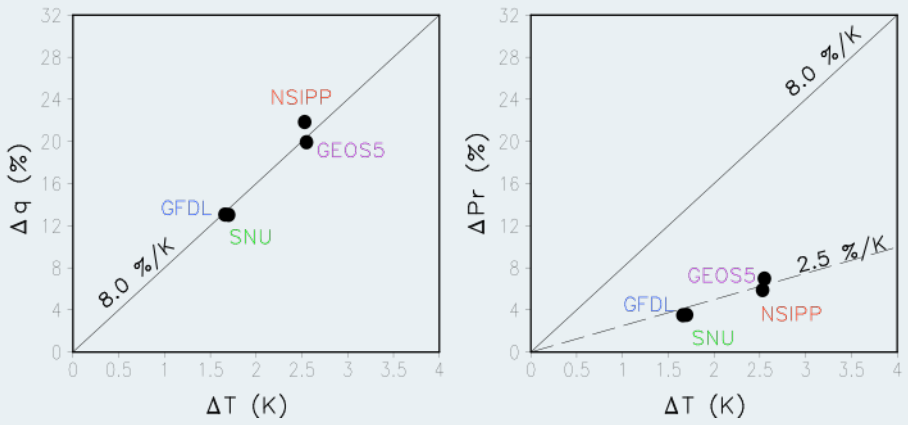

Figure 2: The change (in %) in the global-mean column-integrated moisture (left) and precipitation (right) vs the global-mean change in surface temperature at 2X CO_2 in the four AGCMs. Solid lines indicate the linear fit of the increase rate in column-integrated water vapor (8.0 % K^{-1}), and the dashed line indicates the linear fit of the precipitation increase at a rate of 2.5 % K^{-1}.

In summary, preliminary comparisons from the moist benchmark test demonstrate that it provides a discriminating framework for understanding the impacts of model physics parameterizations.

Publications:

Lee, M.-I., M.J. Suarez, I-S. Kang, I.M. Held, and D. Kim, 2008: A moist benchmark calculation for atmospheric general circulation models. *J. Climate,* **21**, 4934-4954.

Mechanisms and Prediction of Long-Term Drought

Siegfried Schubert and the extended USCLIVAR Drought Working Group*

Project Goals and Objectives: The goals of this project are to address fundamental issues about the causes and predictability of drought throughout the world. The study addresses the role of the leading patterns of interannual SST variability, with a focus on understanding and quantifying the physical mechanisms linking global-scale SST variations to regional drought, the potential predictability those linkages entail, and the limitations on realizing that predictability resulting from deficiencies in current global climate models. The study takes advantage of simulations made with global climate models developed at NASA, NOAA and NCAR.

Project Description: The El Niño/Southern Oscillation (ENSO) and other long-term changes in sea surface temperature (SST) can have a profound impact on regional hydroclimate variability including high impact events such as droughts. In certain regions of the world land-atmosphere feedbacks can act to amplify drought or pluvial conditions. This project addresses a number of questions concerning the mechanisms that maintain drought across the seasonal cycle and from one year to the next including: What is the role of the leading patterns of SST variability, and what are the physical mechanisms linking the remote SST forcing to regional drought? What is the role of land-atmosphere coupling? What are the implications for the predictability of drought on seasonal and longer time scales? In order to address these questions the USCLIVAR Drought Working Group initiated a series of global climate model experiments in which the models were forced with the leading patterns of SST variability including a Pacific ENSO-like pattern, a pattern that resembles the Atlantic Multi-decadal Oscillation (AMO), and a global trend pattern.

A number of groups participated in this project. The GMAO contributed runs made with version one of the NASA Seasonal-to-Interannual Prediction Project (NSIPP-1) AGCM – a precursor to the GEOS-5 model. NOAA's Climate Prediction Center, with support from the Climate Test Bed, contributed runs made with the Global Forecast System (GFS) AGCM, and NOAA's GFDL contributed runs made with the AM2.1 AGCM. The Lamont-Doherty Earth Observatory of Columbia University contributed runs made with the NCAR CCM3.0 AGCM, and NCAR contributed runs made with the CAM3.5 AGCM. An additional set of runs was made by COLA/University of Miami with the (coupled) CCSM3.0 model employing a novel adjustment technique to nudge the coupled model towards the imposed SST forcing patterns.

Results: While a large number of different experiments were run, we report here on results from the baseline experiments in which the models were forced with all eight combinations of the *Pacific* and *Atlantic* patterns. The runs are labeled according to whether the SST patterns contributing to the forcing are in their cold, warm or neutral phase. For example, PwAc indicates that a model is forced with the warm phase of the *Pacific* and the cold phase of the *Atlantic* patterns. PwAn indicates that a model is forced with the warm phase of the *Pacific* and the neutral phase

* Siegfried Schubert, David Gutzler, Hailan Wang, Aiguo Dai, Tom Delworth, Clara Deser, Kirsten Findell, Rong Fu, Wayne Higgins, Martin Hoerling, Ben Kirtman, Randal Koster, Arun Kumar, David Legler, Dennis Lettenmaier, Bradfield Lyon, Victor Magana, Kingtse Mo, Sumant Nigam, Philip Pegion, Adam Phillips, Roger Pulwarty, David Rind, Alfredo Ruiz-Barradas, Jae Schemm, Richard Seager, Ronald Stewart, Max Suarez, Jozef Syktus, Mingfang Ting, Chunzai Wang, Scott Weaver, Ning Zeng

(climatological SST) of the *Atlantic* patterns. In each case the amplitude of the pattern was set at 2 standard deviations of the annual mean variability. In the following we focus on the response over the United States.

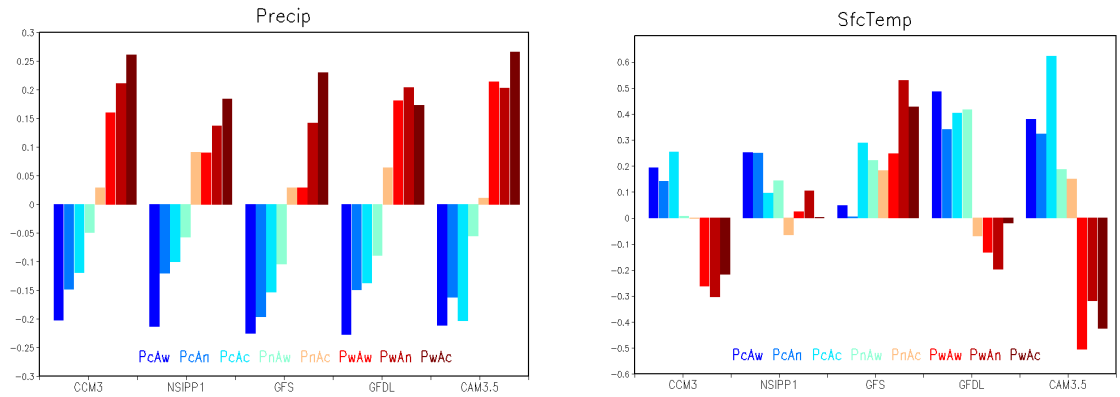

The annual and continental United States mean responses for a) precipitation and b) surface temperature for all 8 combinations of the Pacific and Atlantic patterns for the 5 AGCMs.

A key result is that all the models agree that the combination of a cold *Pacific* and warm *Atlantic* (PcAw) tends to produces the largest precipitation deficits, while the combination of a warm *Pacific* and cold *Atlantic* (PwAc) tends to produce the largest precipitation surpluses. An unexpected result is that the surface temperature response shows less agreement among the models than that found for the precipitation response.

As a measure of potential predictability, the signal-to-noise ratio is defined as $R = (\bar{x} + \bar{y}) / s_{xy}$, where x and y represent seasonal values from the experiment and control runs respectively, the overbar denotes a time mean, and $s_{xy}^2 = \left(s_x^2 + s_y^2\right)/2$, where s_x^2 and s_y^2 are the variance estimates of x and y, respectively.

For all the models, the largest values occur in spring with surprisingly small (not significant) values during winter. The results for the U.S. as a whole reflect those in the Great Plains and the southwest, particularly the southern Great Plains. In contrast to the results for precipitation, the values of the surface temperature response to the *Pacific* forcing (not shown) are generally lower and show considerably less agreement among the models. The results presented here are part of a more complete study submitted for publication (Schubert et al., 2009) in a special Journal of Climate issue on drought that focuses on the analysis of these runs as well as those from DRICOMP[1].

We plan to repeat many of the above runs with the latest version of the GEOS-5 AGCM. A follow-on study will begin tackling the full predictability problem on decadal time scales in support of IPCC. A key focus will be on assessing the nature and predictability of PDO-like and AMO-like SST variations on interannual to decadal time scales.

URL: http://gmao.gsfc.nasa.gov/research/clivar _drought_wg/index.html

[1] The Drought in Coupled Models Project is coordinated by USCLIVAR and is funded by NSF, NOAA, NASA, and DOE.

Publications:

Siegfried Schubert, David Gutzler, Hailan Wang, Aiguo Dai, Tom Delworth, Clara Deser, Kirsten Findell, Rong Fu, Wayne Higgins, Martin Hoerling, Ben Kirtman, Randal Koster, Arun Kumar, David Legler, Dennis Lettenmaier, Bradfield Lyon, Victor Magana, Kingtse Mo, Sumant Nigam, Philip Pegion, Adam Phillips, Roger Pulwarty, David Rind, Alfredo Ruiz-Barradas, Jae Schemm, Richard Seager, Ronald Stewart, Max Suarez, Jozef Syktus, Mingfang Ting, Chunzai Wang, Scott Weaver, Ning Zeng, 2009: A USCLIVAR Project to Assess and Compare the Responses of Global Climate Models to Drought-Related SST Forcing Patterns: Overview and Results. *J. Clim*. (submitted).

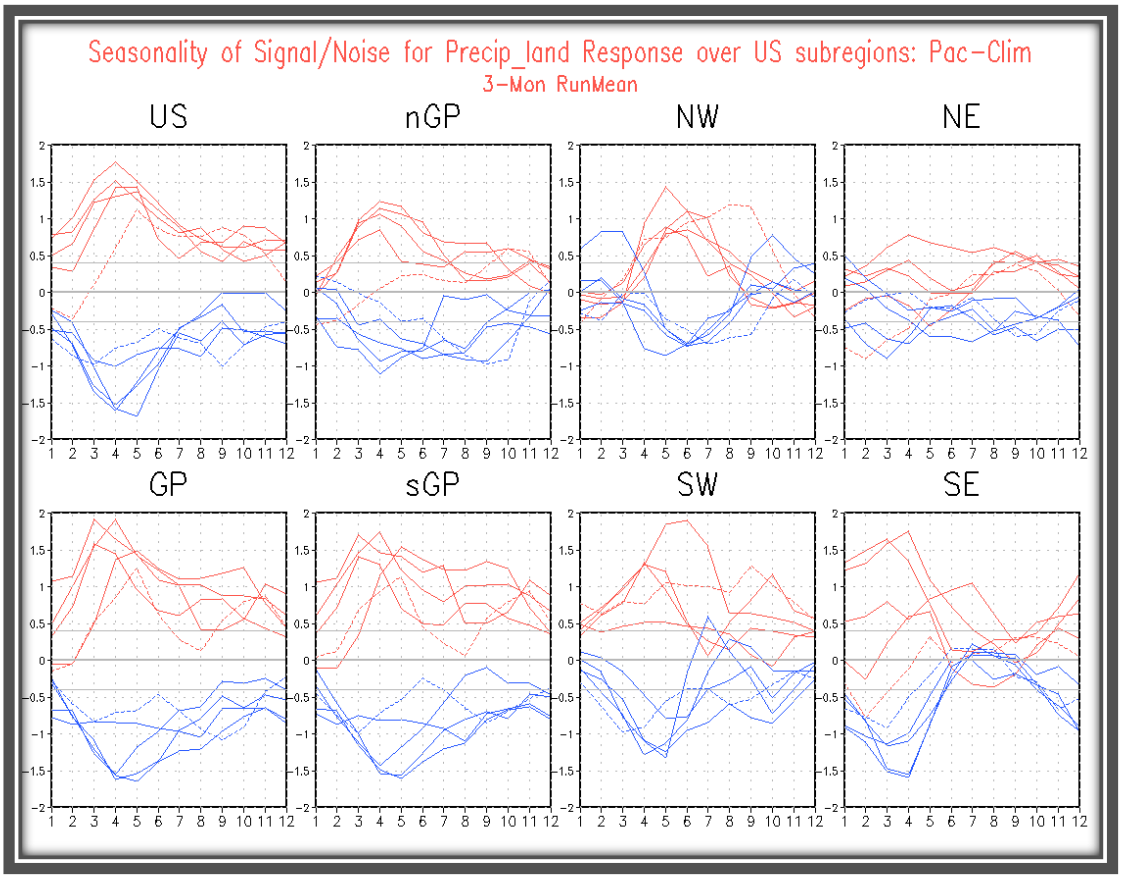

Seasonality of the signal to noise ratios (R –see text) of the 3-month mean precipitation responses for each model over various regions of the United States to the Pacific warm (red curves) and cold (blue curves) SST anomaly pattern. The numbers along the abscissa refer to the center month of the 3-month means. Results are based on 50-year simulations except for the GFS model (dashed lines), which was run for 35 years. See text for the definition of the signal-to-noise ratio. The thin horizontal lines denote the 5% significance levels based on a t-test (for the GFS model the critical t-value is 0.49). Areas consist of the continental United States (US) and various sub-regions consisting of the northern Great Plains (nGP), Northwest US (NW), Northeast US (NE), US Great Plains (GP), southern Great Plains (sGP), Southwest US (SW), and Southeast US (SE). Units: dimensionless.

Impact of SST Modes on Warm Season Central U.S. Hydroclimate in Observations and GCM Simulations

Scott Weaver, Siegfried Schubert, and Hailan Wang

Project Goals and Objectives: To assess the influence of recurring modes of SST variability on the regional mechanisms for warm season central U.S. hydroclimate variations in observations and a multi-model AGCM framework as part of the US CLIVAR Drought Working Group. The focus is on the role of the Great Plains Low-Level Jet.

Project Description: The central U.S. is a hydroclimatically and economically sensitive region given its agricultural prominence and significant warm season precipitation variability. The proximity of this region to the Rocky Mountains, Gulf of Mexico, and Atlantic and Pacific Oceans provide a unique combination of potential climate influences. As such, the central U.S. is prone to drought and pluvial conditions, highlighted most recently by the flooding during the spring of 2008. Given the recent evidence for SST variability in producing precipitation anomalies over the Great Plains on seasonal to interannual timescales, it is necessary to understand the mechanisms through which slowly varying SST modes generate regional hydroclimate variability. In this initial study we focus on an important mechanism for central U.S. warm season precipitation, the Great Plains low-level jet (GPLLJ).

Results: Interannual variability of the GPLLJ is shown linked to global scale SST variability during the warm season over the period 1949-2002 in the NCEP/NCAR reanalysis and NSIPP1 and CCM3 AMIP climate model simulations. An interesting finding is the seasonal dependence of the link between SST and GPLLJ variability. The strongest correlations of the GPLLJ to SST and central U.S. precipitation are found during the JAS season.

Applying regressions of the GPLLJ index anomalies it is found that NSIPP1 and CCM3 ensemble mean AMIP simulations produce some characteristics of the observed GPLLJ related precipitation variability over the U.S., Mexico, and Gulf of Mexico, however, the magnitude of the AMIP response gives weaker precipitation anomalies over the Great Plains and stronger ones over the West Coast of Mexico, Gulf of Mexico, and Caribbean Sea as compared to those in observationally constrained data. Correlations of the GPLLJ with SLP and 200 hPa heights in the NCEP/NCAR reanalysis reveals that the GPLLJ is related to a large scale Pan Pacific wave train pattern and an Atlantic based subtropical SLP

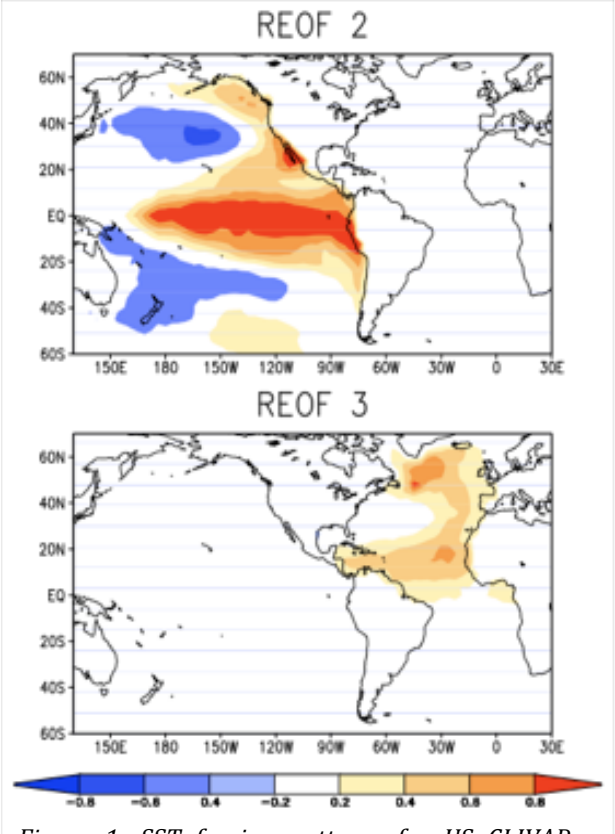

Figure 1: SST forcing patterns for US CLIVAR Drought Working Group AGCM Experiments. The shading interval is 0.2. Only the positive polarity is shown.

anomaly. The CCM3 and NSIPP1 AMIP ensemble mean correlations show varying 200 hPa height anomaly structures, however they agree in the location of the SLP anomaly, especially the maximum over the Gulf of Mexico.

As part of the U.S. CLIVAR Drought Working Group, we conducted idealized SST simulations with the NSIPP-1 AGCM using forcing patterns gleaned from a rotated EOF analysis of annual SST anomalies during 1901-2004 from the Hadley Centre (Figure 1). The seasonal cycle of the GPLLJ and northern Great Plains precipitation in idealized SST climate model simulations indicates that a warm Pacific combined with a cold Atlantic enhances the strength of the GPLLJ and northern Great Plains precipitation. Additionally, the timing and sensitivity of the seasonal cycle of the GPLLJ and precipitation is impacted under this idealized forcing. In particular the GPLLJ response is not sensitive to the sign of the spring SST anomaly as compared to summer, where the spread is large, and the peak timing of the GPLLJ is a month earlier in the cold Pacific – warm Atlantic (PcAw) case than in the warm Pacific – cold Atlantic (PwAc) (Figure 2).

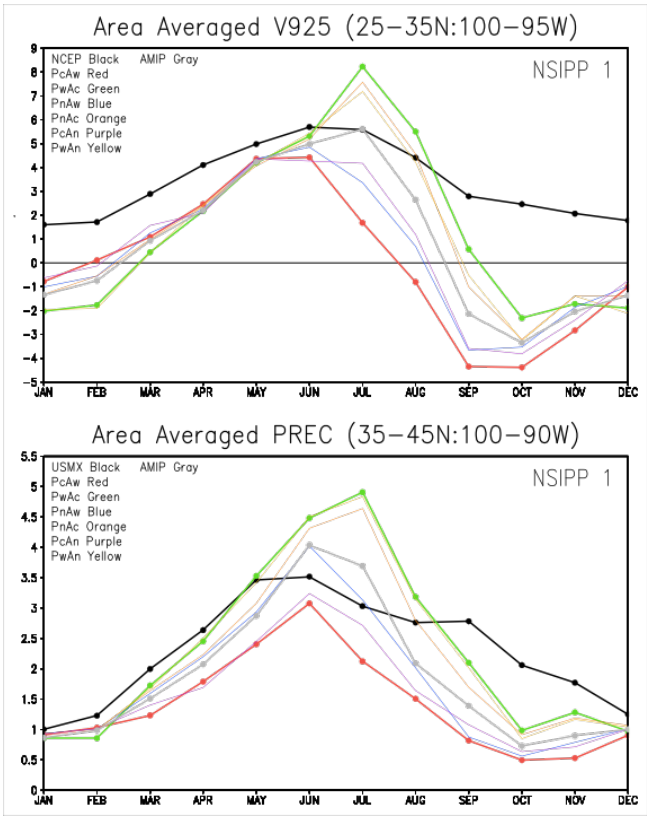

Figure 2 Mean seasonal cycle of the Great Plains LLJ (top, m s^{-1}) and precipitation (bottom, mm day^{-1}) in the NSIPP1 idealized SST experiments

The idealized simulations offer an opportunity to examine the spatial structure of regional GPLLJ, precipitation, and SLP anomalies and the relative roles of the Pacific and Atlantic SSTs by examining the model responses to forcing from either basin while keeping the other neutral. Interestingly, the low-level circulation (i.e., the GPLLJ and SLP) and precipitation were similar in the model simulations regardless of the prescribed forcing (i.e., warm Pacific/neutral Atlantic or cold Atlantic/neutral Pacific) and place a maximum in SLP over the Gulf of Mexico.

An examination of moisture fluxes, their convergences, and precipitation over the western hemisphere warm pool region in the NSIPP1 model shows that the precipitation response (and thus latent heating) to an SST anomaly is preferentially located over the area of maximum climatological SST. Interestingly, this response is not sensitive to the basin receiving the anomalous SST forcing, perhaps implicating the importance of the anomalous zonal and meridional SST gradients in generating this circulation feature (i.e., the structure of the regional SST forcing).

URL: http://gmao.gsfc.nasa.gov/research/clivar _drought_wg/index.html

Publications:

Weaver, S.J., S. Schubert, and H. Wang, 2009: Warm season variations in the low-level circulation and precipitation over the central U.S. in observations, AMIP simulations, and idealized SST experiments. *J. Clim. (submitted).*

On the Impact of Global SST Changes on Climate Variability and Trends over the U.S. during 1950-2000

Hailan Wang, Siegfried Schubert, Max Suarez, and Junye Chen, in collaboration with Martin Hoerling (NOAA/ESRL/PSDR), Arun Kumar and Philip Pegion (NOAA/NCEP/CPC)

Project Goals and Objectives: The goal of this project is to improve our understanding of the causes of the regional and seasonal variations in the surface temperature and precipitation trends over the U.S. The focus is on determining the roles of the leading patterns of low frequency variability of sea surface temperature (SST) in the Indo-Pacific and Atlantic basins, as well as a global warming pattern.

Project Description: Recurring patterns of SST variability exert profound impacts on a number of regional climates throughout the world at interannual to decadal and longer time scales. For North America, the most important SST variations are those associated with El Niño-Southern Oscillation (ENSO), and at longer time scales, a decadal pan-Pacific pattern related to the PDO, and the AMO in the north Atlantic. In addition, SST variations in the Indian Ocean and a global linear trend pattern appear to be important. This project examines the extent to which these low frequency SST changes contribute to the regional and seasonal variations in the surface temperature and precipitation trends over the U.S. during 1950-2000.

Results: Using the NSIPP-1 AGCM, we have investigated the causes of seasonality and regionality of climate trends over the U.S. during 1950-2000 by linking these climate trends to the leading patterns of SST variability including a global warming (GW) pattern and a PDO-like pattern.

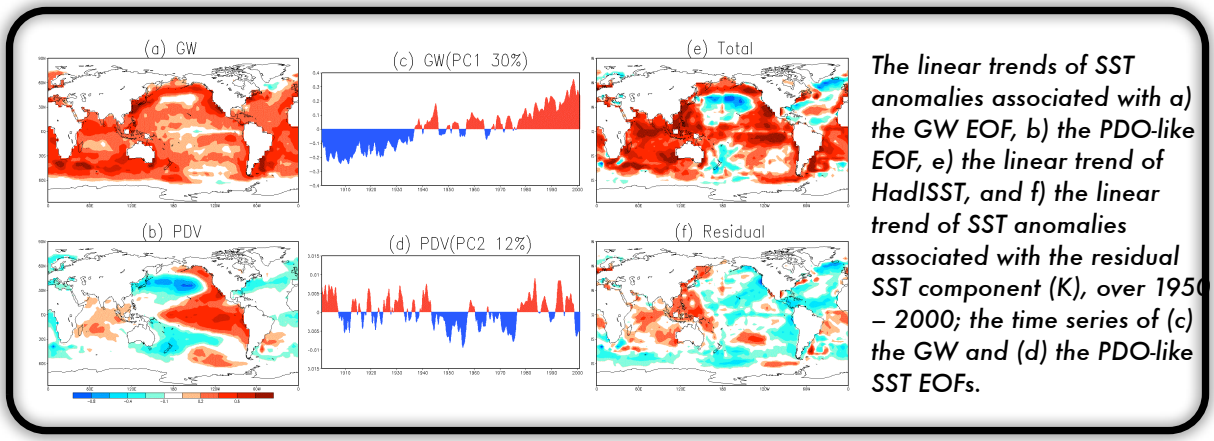

The linear trends of SST anomalies associated with a) the GW EOF, b) the PDO-like EOF, e) the linear trend of HadISST, and f) the linear trend of SST anomalies associated with the residual SST component (K), over 1950 – 2000; the time series of (c) the GW and (d) the PDO-like SST EOFs.

The observed climate trends over the U.S. during 1950–2000 exhibit distinct seasonality and regionality. The surface temperature over the U.S. exhibits a warming trend during winter, spring and early summer and a modest countrywide cooling trend in late summer and fall, with the strongest warming occurring over the northern U.S. in spring. Precipitation trends (not shown) are positive in all seasons, with the largest trend occurring over the central and southern U.S. in fall. This study investigates the causes of the seasonality and regionality of those trends, with a focus on

the intriguing cooling and wetting trends in the central U.S. in late summer and fall.

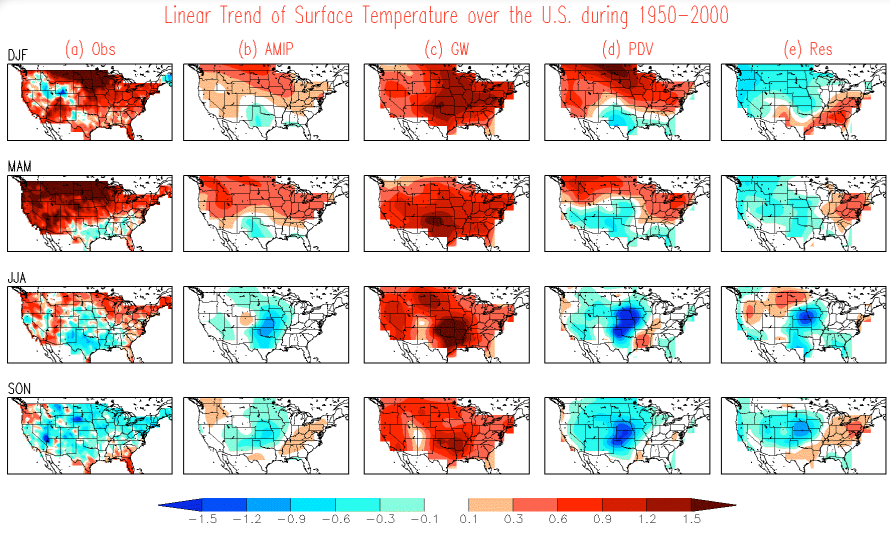

The linear trends of surface temperature (K) computed from a) station observations, b) the NSIPP-1 AMIP ensemble mean simulations. The response in the AGCM surface temperature to the linear trends of SST anomalies associated with c) the global warming (GW) mode, d) the Pacific decadal oscillation (PDO)-like mode, and (e) the residual SST component, for DJF (top row), MAM (2nd row), JJA (3rd row) and SON (bottom row).

The strong similarity between the observations and the AMIP ensemble mean simulations above suggests that the observed surface temperature trends over the U.S. during 1950-2000 are to a large extent explained by changes in SST. A series of idealized AGCM experiments were performed, forced by SST trends associated with the GW and the PDO-like SST patterns, as well as a residual trend pattern. The GW and PDO-like SST patterns were obtained as the first and second leading EOFs of the observed Hadley SST that has ENSO signal linearly removed, and the residual trend pattern was obtained by removing the GW and the PDO contributions from the linear trend of Hadley SST.

The results above show that, among the leading patterns of SST variability, the PDO-like pattern plays a prominent role in producing both the seasonality and regionality of the climate trends over the U.S. In particular, it is the main contributor to the apparent cooling and wetting (precipitation responses not shown) trends over the central U.S. in late summer and fall. The residual SST trend, a manifestation of phase changes of the AMO SST variation during 1950–2000, also exerts influences that show strong seasonality with important contributions to the central U.S. temperature and precipitation during the summer and fall seasons. In contrast, the response over the U.S. to the GW SST pattern is an overall warming with little seasonality or regional variation.

This study suggests that, while the global warming SST pattern plays a key role in annual continental and larger-scale warming trends, the decadal and multi-decadal variability in the Pacific and Atlantic are key factors in explaining the seasonal and regional variations of the observed climate trends over the U.S. during the period 1950-2000.

Publications:

Wang, H., S. Schubert, M. Suarez, J. Chen, M. Hoerling, A. Kumar and P. Pegion, 2009: Attribution of Seasonality and Regionality of the Climate Trends over the United States during 1950-2000, *J. Climate (in press*).

Drought Studies, with an Eye toward Applications

Randal Koster, Greg Walker (Code 613.2), Sarith Mahanama, and Yogesh Sud (Code 613.2)

Project Goals and Objectives: The project aims to use GMAO modeling systems to generate information of value to users interested in drought monitoring and prediction. Three relevant topics have been examined: (i) the interpretation of GMAO seasonal forecasts in terms of predicted soil moisture deficits; (ii) the examination of drought-induced warming and how it relates to local hydroclimatic regime; and (iii) the examination of the potential for improved streamflow prediction during the spring snowmelt season given information on winter snow and soil moisture, as perhaps measured by satellite.

Project Description: This project grew out of the realization that GMAO's quasi-operational seasonal forecasts could provide valuable information on drought to a wide variety of potential users. We focused in 2008 on processing (for the first time) seasonal forecasts of soil moisture produced by the GMAO into a form suitable for transfer to the NCEP personnel generating the U.S. Drought Monitor and U.S. Drought Outlook, two tools in wide use across the applications community. Two valuable side analyses evolved along the way. First, multi-decadal AGCM simulations were examined in the context of a well-known hydroclimatological framework to explain why some regions tend to get warmer during dry periods (thereby exacerbating drought) and others do not. These findings were applied to historical temperature and precipitation observations to delineate regions particularly susceptible to drought-induced warming. Second, offline (land-only) simulations with the GMAO land surface model were used to investigate how knowledge of snow and soil moisture conditions during winter contributes to forecasts of streamflow (and thus water resources) during the snowmelt season. Supplemental simulations isolated the specific contribution of soil moisture knowledge to forecast skill, identifying a potentially valuable application of upcoming SMAP data streams.

Results: i) Soil Moisture Forecasts. We first analyzed existing seasonal forecasts over multiple years to provide two crucial pieces of information: (i) the distribution of potential predictability, or the degree to which soil moisture can be predicted months in advance given an inherently chaotic atmospheric system, and (ii) "skill levels" associated with drought prediction. We put the term "skill levels" in quotes because by necessity (given an overwhelming paucity of relevant measurements), we evaluate our predictions against a model-based proxy for observed soil moisture, generated by driving our land model globally offline with observed meteorological forcing. Still, the land model used has reasonable memory characteristics, and we learn at the very least the degree to which poor forecasts of forcing reduce the skill of agricultural drought prediction.

This information provides needed background for evaluating our more direct contribution to the community: the real-time provision, every month, of seasonal soil moisture forecasts to NCEP's Drought Outlook and Drought Monitor. Figure 1 shows an example of such a contribution. The top left plot shows the initial set of soil moisture anomalies imposed on the forecast, derived by forcing the land model globally with observations-based meteorological data. The data, expressed in terms of standard normal deviates, show the far west and the eastern part of the country to start out drier then average. The other three plots show the corresponding GMAO forecasts of soil moisture for the

first day of the 2nd (top right), 3rd (bottom left), and 4th (bottom right) months of the forecast. The dry areas generally (but not always) weaken with time; their strength and location depend on both the inherent soil moisture memory in the model and the ability of the model to forecast meteorological drivers.

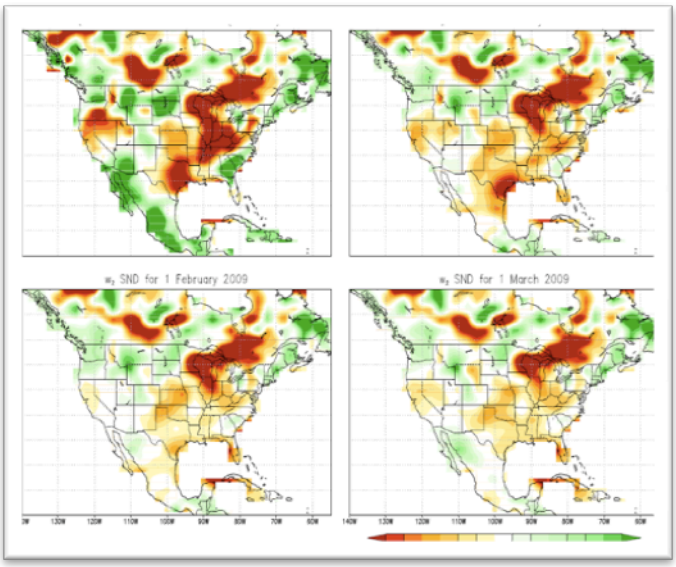

Figure 1: Real-time forecasts of soil moisture deficit (expressed in standard normal deviates), an indicator of agricultural drought.

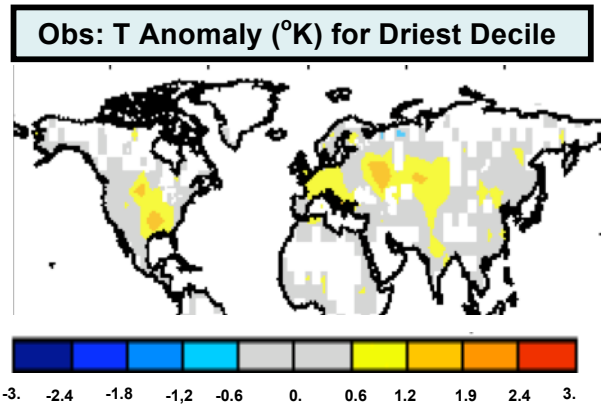

Figure 2: Average JJA temperature anomaly during driest tenth of years, from historical data.

ii) Drought-Induced Warming. Our analysis of AGCM precipitation and temperature fields produced a wealth of understanding regarding the degree to which the land surface can exacerbate drought through evaporation feedback on air temperature. This understanding was then applied to historical precipitation and air temperature data, with results like those shown in Figure 2. The figure shows the average seasonal temperature anomaly (in K) for dry boreal summers (years with JJA precipitation in the lowest decile); note that because this represents a full seasonal average, anomalies of 1 or 2 degrees are quite large. This field, which is consistent with AGCM data and can be explained via simple hydroclimatological arguments, shows that the southern U.S. is particularly prone to seasonal heat waves associated with drought. Another valuable result (not shown here) is the delineation, from observations alone, of the areas for which JJA evaporation is controlled by interannual variations in soil moisture – something never before derived without the use of models.

iii) Snow and Soil Moisture Impacts on Spring Streamflow Prediction. Offline (land-only) simulations of 80+ years of hydrology over the continental United States provide a unique opportunity to determine how knowledge of wintertime soil moisture and snow contributes to accurate predictions of spring (March-May) runoff. Two simulations were performed: (a) one in which initial soil moisture and snow water equivalent (SWE) are known on January1 but meteorological forcing for January – May is unknown (climatological forcing is used), and (b) a repeat of this simulation, except that only snow water equivalent on Jan. 1 is assumed known. Comparison of the simulated springtime runoffs against "truth" (the values from a full simulation, including all known meteorological forcing) isolates the degrees to which knowledge of winter SWE and/or soil moisture contribute to streamflow forecast skill. Preliminary results show that these contributions are indeed significant. Such information is critical for quantifying potential SMAP applications to the streamflow prediction problem.

GLACE-2: Determining How Soil Moisture Initialization Affects Subseasonal Forecast Skill

Randal Koster and Tomohito Yamada

Project Goals and Objectives: GLACE-2, an international project led by GMAO scientists, is using a wide variety of modeling systems to examine the degree to which the proper initialization of soil moisture improves forecasts of monthly precipitation and air temperature. For the first time ever, a global consensus should emerge regarding the value of land initialization for forecasts, perhaps motivating national forecast centers to make full use of land initialization in their own operations.

Project Description: A major motivation for the study of the coupled land-atmosphere system is the idea that soil moisture anomalies may affect future precipitation through their effects on future surface energy and water budgets. If true, the accurate initialization of soil moisture in a subseasonal or seasonal precipitation forecast may improve forecast skill.

To address this issue, participants in GLACE-2 are performing two series of forecasts: (i) a series of 100 2-month warm-season ensemble forecasts (each ensemble consisting of 10 simulations) in which land surface conditions (mainly, soil moisture), sea surface temperatures, and atmospheric states are initialized to realistic values, and (ii) an equivalent series, except that initial land conditions are assumed unknown and are instead taken from a probability distribution function of possible values. The evaluation of forecasted precipitation and air temperature data from the two series against observations allows us to isolate the contribution of soil moisture information to forecast skill. Additional processing of the data reveals the potential predictability associated with land initialization – the upper bound of potential skill for the model.

Results: Accomplishments for FY2008 include the following:
a) *Identification/coordination of participants.* The first task was to identify the institutions that are interested and willing to perform the computationally intensive GLACE-2 experiments. At this time, 10 institutions, representing 12 modeling systems, are actively involved:

(i) NASA/GSFC (new and old seasonal forecast systems)
(ii) COLA (COLA and NCAR/CAM AGCMs)
(iii) Princeton (NCEP AGCM)
(iv) IACS (Switzerland): (ECHAM AGCM)
(v) KNMI (Netherlands): ECMWF system (atmosphere only)
(vi) ECMWF (UK): coupled atmosphere-ocean system
(vii) GFDL: (GFDL AGCM)
(viii) U. Gothenberg (Sweden): (NCAR AGCM, older version)
(ix) CCSR/NIES/FRCGC (Japan): CCSR AGCM
(x) FSU/COAPS: FSU AGCM

b) *Generation of SST boundary conditions.* In the experiment, prescribed SSTs over the forecast period must be based on the known SST anomalies at the start of the period and a persistence time scale derived from SST observations outside the year of forecast. We have computed and transformed those persistence time scales into SST boundary conditions for the forecasts – both as absolute SST values and as anomalies.

c) *Activity involving GMAO and Japanese forecast systems*. GMAO scientists have been setting up the GLACE-2 experiments on two of the AGCMs used for this study: the GMAO GEOS-5 AGCM and the CCSR/NIES/ FRCGC AGCM (MIROC) based at the University of Tokyo.

d) *Analysis of participant contributions.* A handful of results from other institutions have already been submitted to GMAO data archives and are in the process of being analyzed. For example, the COLA group has already provided data, from which we have since computed global fields of precipitation and air temperature predictability as a function of lead time into the forecast. We have quantified forecast skill for this system (Figure 1). The top left panel shows the skill of precipitation prediction (measured as the square of the correlation coefficient, r^2, between predicted and observed rainfall during the first 15-day period given start dates in April-June) for the case without realistic land initialization. The top middle panel shows the corresponding skill levels obtained when the land initialization is realistic, and the top right panel shows the differences, i.e., the isolated contribution of land initialization to the forecast skill. The land contribution is not huge, but it is generally statistically significant where it does appear, and it is indeed large in the context of subseasonal forecasting.

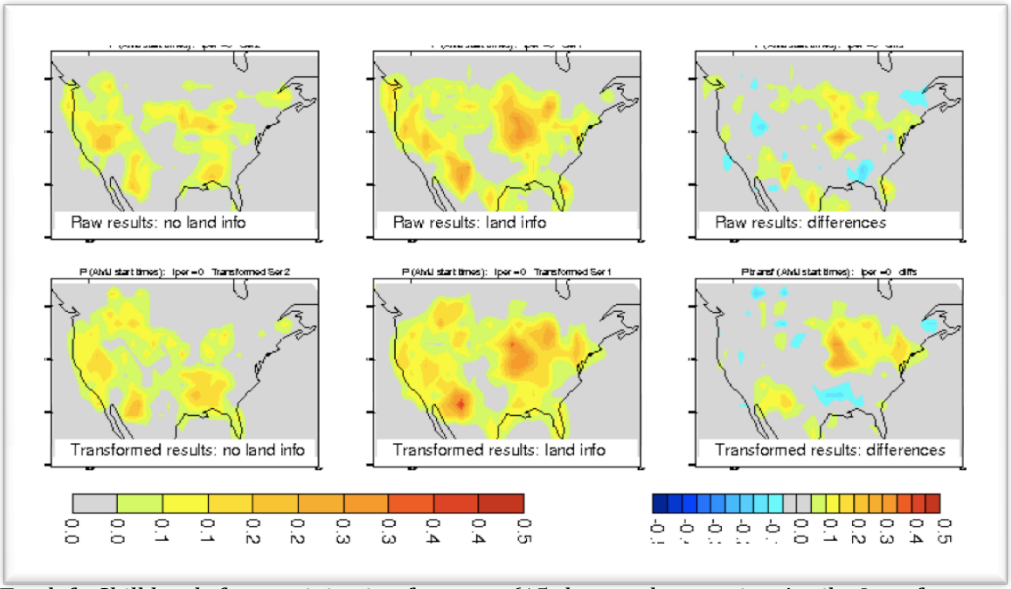

Figure 1.: Top left: Skill levels for precipitation forecasts (15-day totals, covering April – June forecast start dates), measured as the r^2 between the forecasted and observed rates. Top middle: Same, but for the case when the land is realistically initialized. Top right: Differences, i.e., isolated impact of land initialization on forecast skill. Bottom panels: corresponding plots obtained after applying an objective statistical transformation to the forecasted quantities. In all cases, given the experimental design behind this particular contribution, the atmospheric initialization has a relatively small impact on the forecast skill.

The bottom panels in the figure show the corresponding skill levels obtained when the objective forecast transformation technique of Koster et al. (2008) is applied. (This will be a standard part of the GLACE-2 analysis.) The land contribution to skill is markedly increased.

Publications/References:

Koster, R. D., 2007: The Global Land-Atmosphere Coupling Experiment – Phase 2. *GEWEX News*, **17**, 7-8.

Koster, R. D., T. L. Bell, R. Reichle, M. J. Suarez, and S. D. Schubert, 2008: Using observed spatial correlation structures to increase the skill of subseasonal forecasts. *Mon. Wea. Rev.*, **136**, 1923-1939.

The African Easterly Jet: Structure and Maintenance

Man Li Wu, Siegfried Schubert, Max Suarez, Randy Koster, Phil Pegion, with Oreste Reale (Code 613)

Project Goals: The goal of this project is to improve our understanding of the controls on the interannual variability of the African Easterly Jet (AEJ) and its downstream effects including impacts on African Easterly Waves (AEWs) and tropical storms. The long-term goal is to improve forecast skill of tropical storm activity on sub-seasonal and longer time scales. As a first step, we concentrate on understanding the AEJ structure and the forcings that contribute to its maintenance.

Project Description: Major gaps exist in our understanding of the controls of interannual variability of Atlantic storms and hurricanes due to the complexity of the multi-scale phenomena involved. Some hurricanes make landfall over the United States causing extensive damage to many aspects of the economy, while some curve northward early and do not make landfall at all. The African Easterly Jet (AEJ) and African Easterly Waves (AEWs) are known to affect storms, and also influence rainfall over West Africa, which impacts water resources, agriculture, and health across Africa. Although the AEJ and AEWs have been studied for more than 40 years, little is known about what controls the interannual variability of the AEJ and AEWs, and what the steering mechanism of the storm tracks are. In order to begin addressing this issue we focus on improving our understanding of the basic structure of the AEJ (e.g., what controls the position, width, strength, and height of the jet); the impact of the structure of the AEJ on the AEW activity over Africa (AEWs need energy for growth); and the role of AEWs and the Atlantic Ocean environment on cyclogenesis and storm/hurricane tracks. We will focus on both local and remote control on the interannual variability. Regarding local control, we will focus on the impact of land-use change over Africa; and in the case of remote control, we will focus on the impact of the North Atlantic Oscillation, El Nino Southern Oscillation, and the Madden Julio Oscillation.

Results: We use the NSIPP-1 atmospheric general circulation model to produce a 3-member 73-year ensemble run forced by observed SST to serve as the Control run. The AEJ, as produced by the Control, is compared with the representation of the AEJ in the European Center for Medium Range Forecast Reanalyses (ERA-40) and other observational data sets and is found to be very realistic. Five Experiments are then performed, each represented by sets of 3-member 22-year long (1980-2001) ensemble runs. The goal of the experiments is to investigate the role of meridional soil moisture gradients, different land surface properties and orography. Unlike previous studies, which have suppressed soil moisture gradients within a highly idealized framework (i.e., the so-called bucket model), terrestrial evaporation control is here achieved with a highly sophisticated land-surface treatment and with an extensively tested and complex methodology. The results show that the AEJ is suppressed by a combination of absence of meridional evaporation gradients over Africa and constant vegetation, even if the individual forcings taken separately do not lead to the AEJ disappearance, but only its modification. Moreover, the suppression of orography also leads to a different circulation in which there is no AEJ. This work suggests that it is not only soil moisture gradients, but also a unique combination of geographical features present only in northern tropical Africa, which cause and maintain the jet.

In the following, three figures illustrate: (1) that the AEJ is strongly constrained by boundary forcings, and the variations in these constraints may lead to completely different atmospheric regimes (Figure 1), and (2) three reanalyses (ERA-40, NCEP R2, and the JRA-25) display slightly different AEJ properties, and structure of the AEJ with respect to the meridional horizontal shear of

the zonal wind (Figures 2 and 3). The meridional horizontal shear of the zonal wind is indicative of barotropic instability. All three reanalyses show a strip of positive values on the southern flank of the AEJ. The corresponding meridional cross-sections localize the heights and latitudes that appear, according to these data sets, more likely to be barotropically unstable. All the reanalyses agree that the strongest cyclonic shear induced by the AEJ is at about 600 hPa and at about 10°N but ERA-40 displays a more confined maximum. The cross-sections also emphasize that in ERA-40 the cyclonic shear appears to slope equatorward with height, which is opposite to what is obtained from JRA-25.

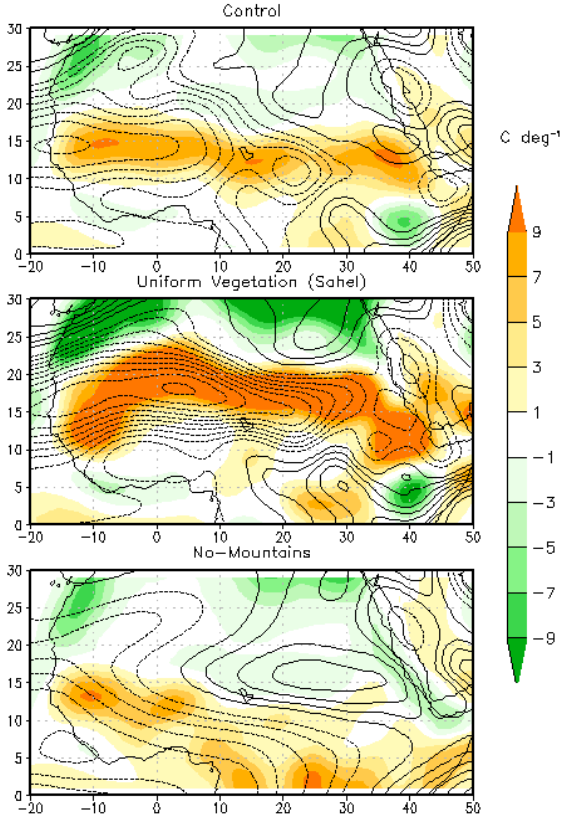

Figure 1: 600 hPa zonal wind (ms^{-1}, CI is 1 ms^{-1}, the zero contour is omitted) in the Control and experiments designed to investigate the impact of vegetation and orography on the AEJ, compared with meridional surface temperature gradient (shaded values, K^{-1}).

To further investigate the problem of barotropic instability in the AEJ, we plot the quantity,

$$\mathrm{K}(y) = \frac{\partial}{\partial y}\left[f(y) - \frac{\partial U}{\partial y} \right],$$

where f is the Coriolis parameter, and U is the zonal wind. K(y) = 0 represents the well-known necessary condition for barotropic instability to occur in response to the zonal component of the flow. In our case, K(y) = 0 on the cyclonic side of a flow indicates locations where barotropic instability is possible. This corresponds to K(y) being zero to the north of positive values of K and to the south of negative values of K (when the flow is easterly). In Figure 3, K(y) is plotted against the zonal wind. The three data sets differ substantially in this regard. In particular ERA-40 builds a contiguous line with K=0 on the southern flank of the AEJ, indicating that a strip of latitudes at about 10°N across the entire continent is potentially unstable for cyclonic disturbances to grow at the expense of the mean flow. This contiguous feature is absent from the other data sets. Most remarkable is the presence, again in ERA-40, of a contiguous vertical line of K(y) = 0 sloping slightly poleward with increasing latitude and decreasing height, almost reaching the surface at about 12°N.

Publication:

Wu, M-L. C., O. Reale, S. D. Schubert, M. J. Suarez, R. Koster, and P. Pegion 2009: African Easterly Jet:

Structure and Maintenance. *J. Climate* (accepted).

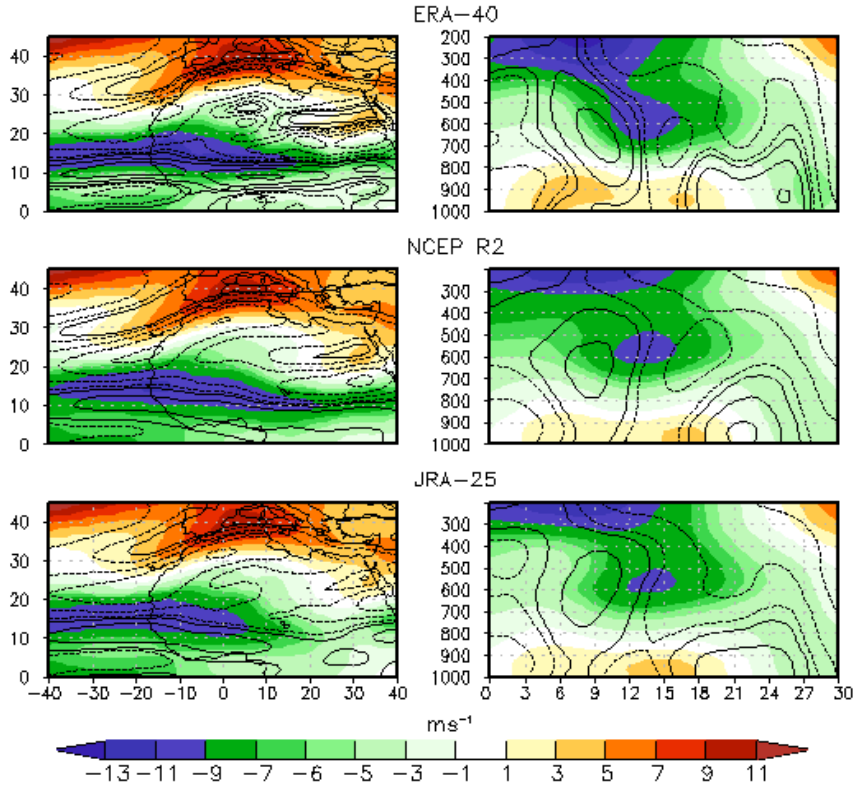

Figure 2: July zonal wind (ms^{-1}, CI is 1 ms^{-1}, the zero contour is omitted) climatology (1980-2001) based on ERA-40, NCEP R2, and JRA-25 reanalyses, and meridional horizontal shear (contours at +/- 2, 1.5, 1, 0.5 x 10^{-6}. The left-hand column shows the fields at 600 hPa. The right-hand column is a vertical cross section at 0°E.

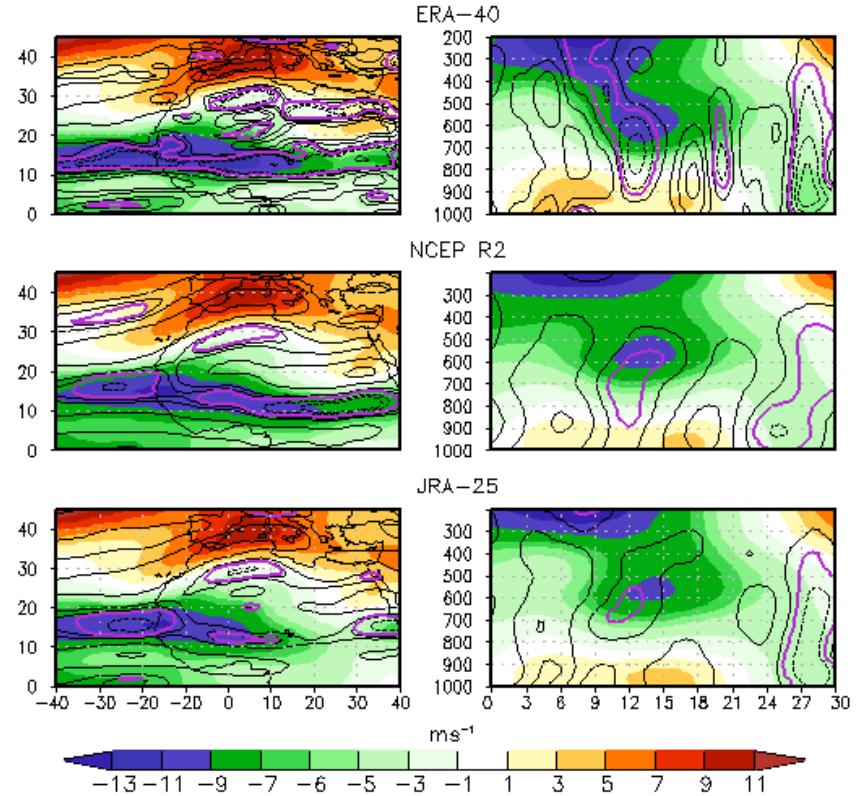

Figure 3: July zonal wind (ms^{-1}, CI is 1 ms^{-1}, the zero contour is omitted) climatology (1980-2001) based on ERA-40, NCEP R2, and JRA-25 reanalyses, and K(y) (contours at +/- 2, 1.5, 1, 0.5 x 10^{-11}. The left-hand column shows the fields at 600 hPa. The right-hand column is a vertical cross section at 0°E.

An Analysis of Moisture Fluxes into the Gulf of California

Man Li Wu, Siegfried Schubert, Max Suarez, with Norden Huang

Project Goals: The goal of this project is to improve our understanding of episodes of enhanced warm-season moisture flux into the Gulf of California. By examining the spatial structure, primary time scales, and upstream development of the fluxes, this study provides new insights into the nature and potential predictability of sub-seasonal fluctuations in the monsoonal flows impacting the summer climates of Mexico and the southwestern United.

Project Description: This project is part of a broader effort within the GMAO to improve our understanding and predictive capabilities on sub-seasonal time scales. The focus of this study is on the sub-seasonal fluctuations in the moisture fluxes over the Gulf of California. The Gulf of California moisture surges are a summertime phenomenon in the southwestern United States. They represent an important mechanism in the transport of moisture from the eastern Pacific Ocean through the Gulf of California into southwestern United States. This study focuses on understanding the spatial structure and primary time scales of low-level moisture fluxes into the Gulf. We use the ECMWF ReAnalysis-40 data for the period 1980-2001 and a compositing technique that is keyed on the low-level moisture fluxes into the Gulf.

Results: The results show that the low level moisture fluxes have a rich spectrum of temporal variability, with periods of enhanced transport over the Gulf linked to African easterly waves on sub-weekly (3–8 day) time scales, the Madden-Julian Oscillation (MJO) at intra-seasonal time scales (20-90 day), as well as intermediate (10-15day) time scale disturbances that appear to originate primarily in the Caribbean Sea/western Atlantic Ocean.

In the case of the MJO, enhanced low level westerlies and large-scale rising motion provide an environment that favors large-scale cyclonic development near the west coast of Central America. Over the course of about two weeks, this feature expands northward along the coast eventually reaching the mouth of the Gulf of California where it acts to enhance the southerly moisture flux in that region. On a larger scale, the development includes a northward shift in the eastern Pacific ITCZ, enhanced precipitation over much of Mexico and the southwestern U.S., and enhanced southerly/southeasterly fluxes from the Gulf of Mexico into Mexico and the southwestern and central United States. In the case of the easterly waves, the systems that reach Mexico appear to redevelop/reorganize on the Pacific coast, and then move rapidly to the northwest to contribute to the moisture flux into the Gulf of California. The most intense fluxes into the Gulf on these time scales appear to be synchronized with a mid-latitude short–wave trough over the west coast of the United States and enhanced low level southerly fluxes over the U.S. Great Plains. The intermediate (10-15 day) time scale systems have zonal wave lengths roughly twice that of the easterly waves, and their initiation appears to be linked to an extra-tropical U.S. east coast ridge and associated northeasterly winds that extend well into the Caribbean Seas during their development phase. The basic structure of the fluxes associated with the three time scales is shown in Figure 1.

One of the key findings is that the high frequency variability is modulated by the low-frequency variations. In particular, the short (3-8 days) and, to a lesser extent, the intermediate (10-15 day) time scale fluxes tend to be enhanced when the convectively active phase of the MJO is situated over the Americas (Figure 2).

Publication:

Wu, M-L. C., S. D. Schubert, M. J. Suarez, N. E. Huang, 2009: An analysis of moisture fluxes into the Gulf of California. *J. Climate* (accepted).

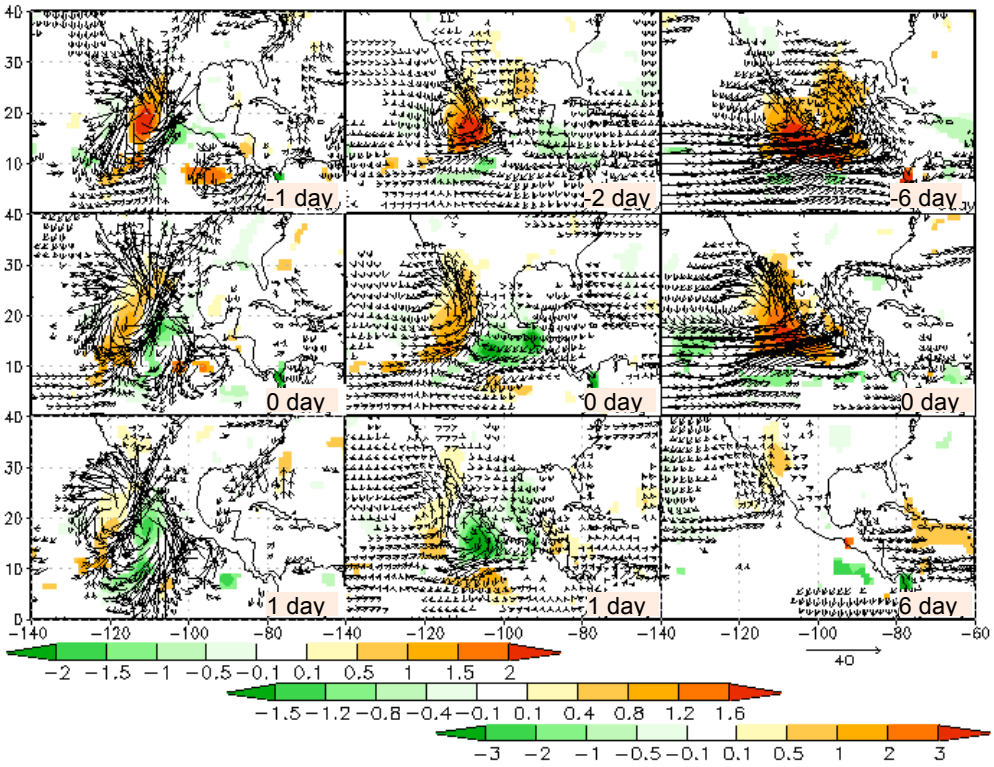

Figure 1: Composites of precipitation (mm day^{-1}) and moisture transport at 850hPa (gkg^{-1}ms^{-1}) using the northward flux (vq850) at 22°N and 110°W as the base point. The times in the lower right of each panel indicate the time lags with respect to the maximum northward flux (vq850) at the base point. The results in the left-hand panels are based on data with a 3-8 day filter applied. The results in the middle panels are based on 10-15 day filtered data and the results in the right-hand panels are based on 20-90 day filtered data. Only values that are significant at the 95% level are plotted.

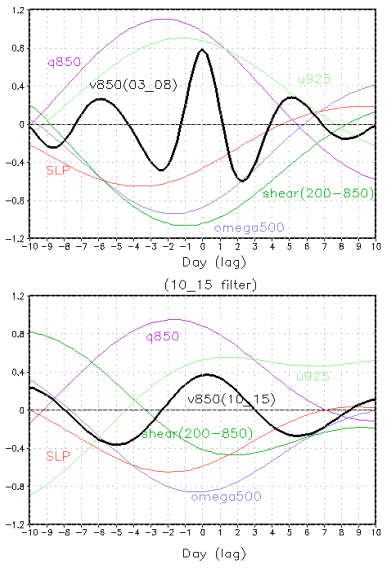

Figure 2: Composites of various quantities based on an index of (3-8 day) filtered (top panel), and (10-15 day) filtered (bottom panel) vq850 at 22°N and 110°W from ERA-40 data (1980-2001). In the top panel the heavy black line is the (3-8 day) filtered v850 (ms^{-1}) and in the bottom panel the heavy black line is the (10-15 day) filtered v850. The thin lines show various quantities (q850 hPa in gkg^{-1}, vertical motion or omega500 hPa in hPa s^{-1}, SLP in hPA, 200-850 hPa shear in ms^{-1}, u925 hPa in ms^{-1}) that have been filtered to retain time scales of 20 to 90 days and composited on either the 3-8 day index (top panel) or the 10-15 day index (bottom panel). All values are area averages over the region (115°W-105°W, 14°N-20°N). For plotting purposes, some quantities have been scaled by the following values: q850 hPa: 0.5; omega500 hPa: 0.03; 200-850 hPa shear: 2.0; v850 hPa: 2.0.

Dynamical MJO Hindcast Experiments: Sensitivity to Initial Conditions and Air-Sea Coupling

Yehui Chang, Siegfried Schubert and Max Suarez

Project Goals: The goals of this project are to measure the capability of the GEOS-5 coupled and uncoupled model to predict the MJO and intraseasonal variability in the tropics, and to identify the causes of substantial temporal changes in prediction skill.

Project Description: The Madden-Julian Oscillation (MJO) is the dominant mode of intraseasonal variability in the tropics. It can essentially be characterized by an eastward propagation of tropical deep convective precipitation anomalies over the warm pool from the equatorial Indian Ocean over the Maritime Continent into the western Pacific region. The ability to accurately forecast such a significant tropical mode as the MJO will be crucial to the success of predictions on sub-seasonal time scales. It is in fact a key source of untapped predictability in the tropics and subtropics.

The study uses the GEOS-5 atmospheric and coupled atmosphere-ocean general circulation models (AGCM and AOGCM, respectively). Our approach is to utilize the idealized data assimilation technology developed at the GMAO. The technique, called "replay", allows us to assess, for example, the impact of the surface wind stresses and/or precipitation on the ocean in a controlled environment. By running the AOGCM in replay mode we can in fact constrain the model using any existing reanalysis data set. For this study we replay the model constraining (nudging) it to the MERRA Scout (2°) run for the period 1979-2005. The fields u,v,T,q,p_s are adjusted towards the 6-hourly analyzed fields in atmosphere. In the case of the coupled model, the focus is on the tropical oceans. In particular, we examine the model's ability (when forced in replay mode) to reproduce the ocean variability associated with the major anomalous events of 1983, 1988, and 1997. The events in 1983 and 1997 are closely associated with a major warm anomaly while the 1988 event is a cold event in the tropical Pacific. The main finding from this coupled replay experiment is that the variations of the tropical oceans are very well simulated. In particular, the thermocline depth displays a very realistic seasonal cycle and inter-annual variability.

In the case of coupled model predictions, initial states are typically created using uncoupled assimilations. For example, starting from independently generated ocean and atmosphere initial states, the forecast systems undergo initialization shocks that can be detrimental to forecast skill, especially for sub-seasonal forecasts. In this study, the use of coupled replay provides a natural set of physically consistent initial conditions. The system can better preserve the coherent air-sea fluxes leading to improved forecast skill.

Results: We have made a series of MJO hindcast experiments with the GEOS 5 AGCM and AOGCM during 1979, 1996-97 and 2002. These hindcasts are initialized daily from states generated by the GEOS-5 replay system. Figure 1 shows the differences in the MJO forecasting skills between 1979 and 2002. Additional hindcasts with degraded moisture observations in the initial conditions for 2002 revealed that the higher forecast skill during 2002 is likely the result of satellite moisture observations that were not available during 1979. There are also clear shorter-term temporal variations in prediction skill (not shown). Both the AGCM and AOGCM predicted realistic MJO signals.

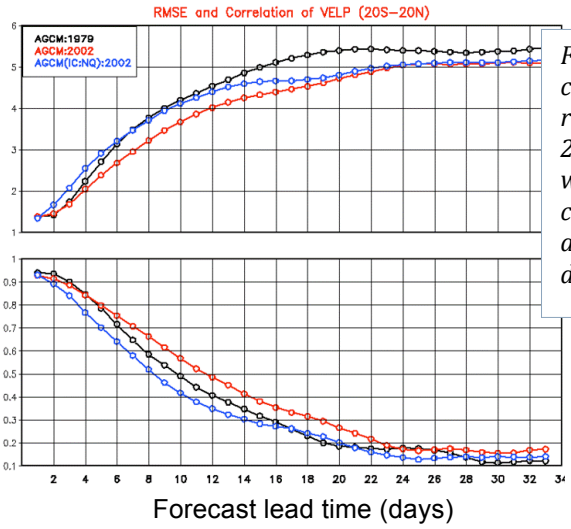

Figure 3: RMSE (top) and Correlation coefficients (bottom) between predicted and reanalysis velocity potential at 200mb (20S-20N) for 1979 (black), 2002 (red) and 2002 with degraded moisture fields in initial conditions (blue). The RMSE and correlations are shown as function of forecast lead-time in days.

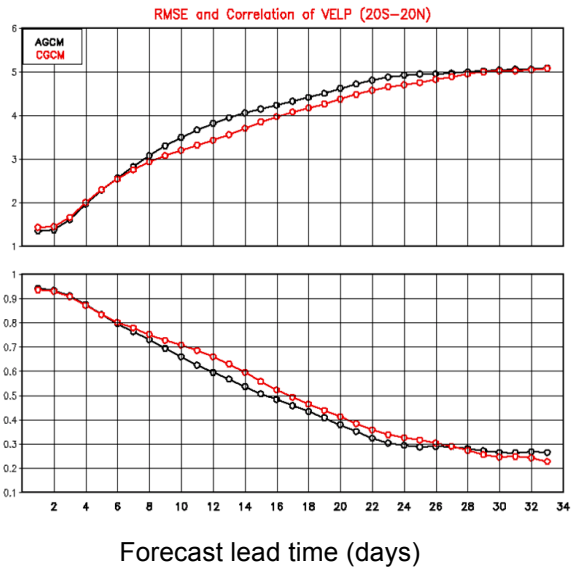

Figure 2: RMSE (top) and Correlation coefficients (bottom) between predicted and reanalysis velocity potential at 200mb (20S-20N) for the AOGCM (red) and the AGCM (black). The RMSE and correlations are shown as function of forecast lead-time in days.

A comparison of the AGCM and AOGCM results (Figure 2) shows that coupling tends to improve forecast skill. Interactive air-sea coupling is essential to maintaining the intensity of the MJO in the GEOS-5 coupled model. It is also clear that GEOS-5 exhibits different forecast skill depending on the phase of the MJO. It does poorly in developing the dry phase of the MJO over the Indian Ocean. Skill is enhanced during the wet phase (not shown).

The results show that the magnitudes of the surface latent heat fluxes in the AGCM are much weaker than those in the AOGCM. Also, the phasing of the AGCM response to the prescribed MJO SST anomalies and the associated surface flux anomalies are incorrectly simulated. This could be due to inadequacies in the model parameterizations. However, by forcing the atmospheric model with prescribed SST, it may be inherently difficult for the AGCM to simulate a realistic MJO.

This study suggests several avenues for improving MJO forecasts. They consist of a) improving the initial conditions especially the moisture fields (e.g. the wet and dry phases of the MJO over the Indian Ocean), b) using the coupled model to allow for air-sea interactions and realistic surface heat and moisture fluxes, and c) improving the model physics package, especially the convection parameterization and the links to the boundary layer.

We intend to repeat these experiments and conduct new ones with the latest version of the GEOS-5 model with a focus on the links between the MJO and ENSO. Higher resolution experiments employing the 1/2° MERRA for the initial conditions will be run to study tropical storms and their links to the MJO.

Evaluation of Constellation-based Satellite Microwave Rainfall Estimates

Xin Lin and Arthur Hou

Project Goals and Objectives: The goal of this project is to evaluate instantaneous rainfall estimates provided by the current generation of retrieval algorithms for passive microwave sensors using retrievals from the TRMM Precipitation Radar and merged surface radar/gauge measurements over the U.S. continent as references. Statistics of departures of these coincident retrievals from reference measurements are computed as a function of rain intensity over land and oceans. Results of this study provide important inputs for the planning of the Global Precipitation Measurement (GPM) mission.

Project Description: The Global Precipitation Measurement (GPM) mission, to be launched in 2013, is designed to provide unified global precipitation measurements from a constellation of microwave radiometers using an advanced radar/radiometer system on the GPM Core satellite as a calibration standard.

In order to improve constellation-based global precipitation estimates, the key is to gain a better understanding of the error characteristics of rainfall retrievals from current passive microwave (PMW) imagers and sounder data over land and ocean. We have performed a comprehensive analysis of rain detection and error characteristics of current satellite rainfall retrievals from microwave radiometers (both conical-scanning imagers and cross-track scanning sounder) through comparisons of coincident overpasses against TRMM Precipitation Radar data between 35°S and 35°N. In addition, the sampling and coverage of the future GPM satellite constellations are also thoroughly evaluated.

Results: The passive microwave sensors included in the study are three operational sounders (i.e., Advanced Microwave Sounding Unit-B instruments on NOAA-15, -16, and -17 satellites) and five imagers (the TRMM Microwave Imager, the Advanced Microwave Scanning Radiometer-EOS instrument on the Aqua satellite, and the Special Sensor Microwave/Imager instruments on DMSP F-13, F-14, and F-15 satellites). The comparisons against PR data are based on "coincident" observations defined as instantaneous retrievals (spatially averaged to 0.25° latitude and 0.25° longitude) within a 10-minute interval collected over a 20-month period from January 2005 to August 2006. Statistics of departures of these "coincident" retrievals from reference measurements as given by the TRMM PR or ground radar and gauges are computed as a function of rain intensity over land and oceans.

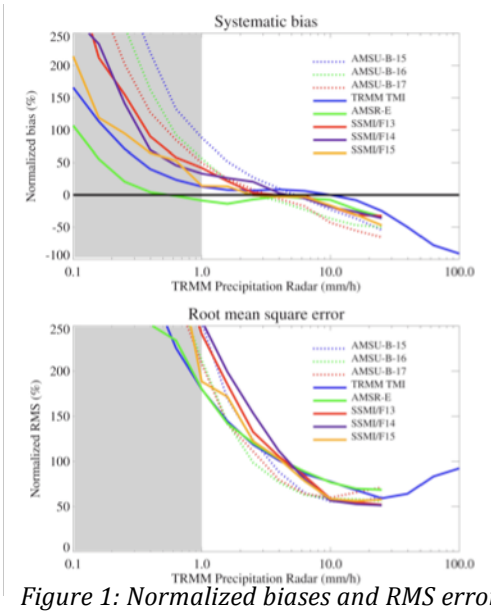

Figure 1: Normalized biases and RMS errors of rain retrievals (at 0.25° resolution) from PMW imager and sounder relative to TRMM PR data over the land from January 2005 to August 2006. The area below the rain intensity of 1.0 mm h^{-1} is lightly shaded.

Results show that, over land, AMSU-B sounder rain retrievals are comparable in quality to those from conical-scanning radiometers for instantaneous rain rates between 1.0 and 10.0 mm h^{-1} (see Figure 1). This result

holds true for comparisons using either TRMM PR estimates over tropical land areas or merged ground radar/gauge measurements over the continental U.S. as the reference.

Over tropical oceans, the standard deviation errors are comparable between imager and sounder retrievals for rain intensities above 5 mm h^{-1}, below which the imagers are noticeably better than the sounders, while systematic biases are small for both imagers and sounders (not shown).

Results of this study suggest that in planning future satellite missions for global precipitation measurement, cross-track scanning microwave humidity sounders on operational satellites may be used to augment conically scanning microwave radiometers to provide improved temporal sampling over land without degradation in the quality of precipitation estimates.

In conducting this analysis we noticed a significant change in frequencies of light, moderate, and heavy rain events between 2002 and 2008. Such a study is vital for a better understanding of the occurrence of extreme rain events in a changing climate, and will serve as an important test bed for evaluating MERRA and the NASA GSFC Global Cloud Model.

We are also investigating the impact of GPM satellite sampling at monthly (Figure 2) and diurnal time scales, and estimate the sampling capability of GPM constellation and individual satellites on hurricanes and mid-latitude storms. Observation System Simulation Experiments have been conducted to simulate the GPM mission sampling the MERRA analyses.

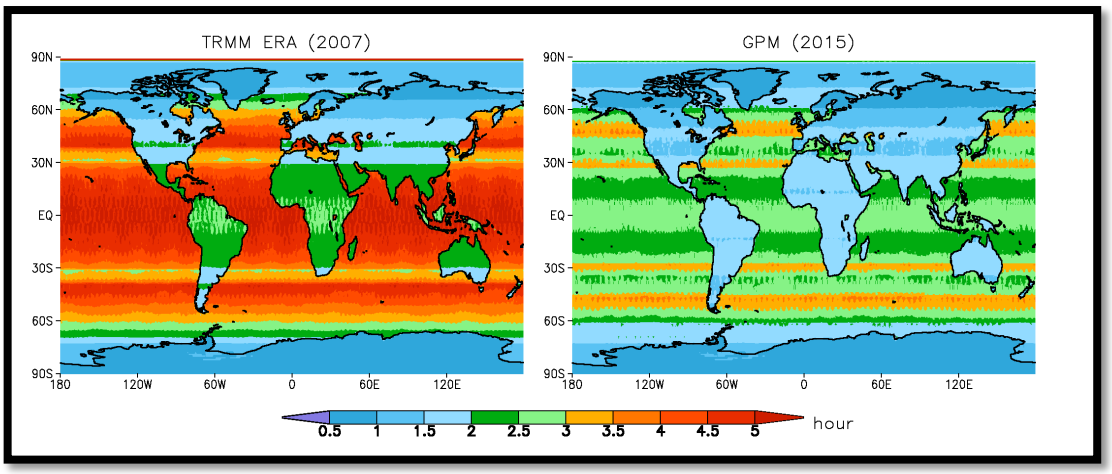

Figure 2: Comparison of mean revisit times by the GPM constellation in 2015 (right) with current capabilities (left).

Publication:

Lin, X., and A. Y. Hou, 2008: Evaluation of coincident passive microwave rainfall estimates using TRMM PR and ground measurements as references. *J. Appl. Meteorol. Climatol.,* **12**, 3170-3187.

The Influence of the 2006 Indonesian Biomass Burning Aerosols on Transport in the Tropical UTLS studied with the GEOS-5 AGCM

Lesley Ott and Steven Pawson, with Bryan Duncan (Code 613.3)

Project Goal: The goal of this project is to better understand the direct and semi-direct effects of biomass burning aerosols from Indonesian wildfires on dynamics and trace gas transport in the upper troposphere/lower stratosphere (UTLS).

Project Description: Aerosols strongly influence the dynamics and chemistry of the atmosphere in several ways. The direct aerosol effect refers to the scattering and absorption of solar radiation while the semi-direct effect refers to changes in clouds caused by alteration of the short-wave heating rate. The aerosol indirect effect, which refers to the influence of aerosols on cloud optical properties through microphysical processes, was not investigated but may be a topic of future research. Previous studies using offline chemical transport models have demonstrated that episodic wildfires in Indonesia, which typically occur between August and November, produce large radiative forcing perturbations at the surface. This project uses GEOS-5 to better understand how aerosols emitted by Indonesian wild fires impact dynamics in the UTLS through their direct impacts on radiative forcing. The GEOS-5 AGCM was run using observed SSTs from 2006, a year in which strong wildfires were observed. Two aerosol distributions, one that included the impact of these fires and one that did not, were taken from GOCART simulations and used as input to GEOS-5.

An ensemble methodology is used to separate the role of aerosol forcing from the potentially chaotic response of the model to perturbations. Five-member ensembles, with and without Indonesian aerosols, were produced by initializing simulations with meteorological fields taken from different days in April.

Results: The impact of Indonesian biomass burning aerosols was assessed by comparing ensemble averages of simulations that did and did not include these aerosols. The results demonstrate that aerosols interact with short wave radiation in the source region to produce a net warming throughout the troposphere with the strongest warming (~0.5 K day^{-1}) below 800 hPa. Considerable warming (~0.4 K day^{-1}) also occurs between 200 and 300 hPa. The effect on the long wave heating rate is more complex with the Indonesian aerosols causing a small degree of heating below 500 hPa and cooling above. This change is not due to direct interaction between long wave radiation and the aerosols, but results from increased low level cloudiness caused by aerosol heating. The inclusion of aerosols in these simulations also tends to increase precipitation in the Indonesian region.

Zonal mean temperature changes resulting from the simulation of Indonesian aerosols are generally small in the UTLS. In the lower stratosphere, aerosols produce a small warming (0.3 K) near the equator and cooling (-0.7 K) in the mid-latitudes of both hemispheres. Aerosols can strongly impact water vapor mixing ratios in the equatorial troposphere with increases greater than 20% in some areas below 300 hPa. Changes in water vapor in the UTLS are generally small with decreases of less than 4% throughout the tropics.

Heating associated with Indonesian biomass burning aerosols also influences tropospheric winds. The aerosols lead to a stronger and broader region of upwelling over Indonesia (Figure 1). This extends to the upper troposphere. Differences in the meridional velocity indicate that the increase

in upward motion is accompanied by an increase in divergence in the vicinity of the equatorial tropopause. The results of this increase in upward vertical transport are reflected in CO mixing ratios in the UTLS (Figure 2). All simulations use identical source distributions for CO, but CO distributions are altered by the aerosol-induced changes in the circulation. At 140 hPa, Indonesian aerosols increase CO mixing ratios by more than 150 ppbv near the source region, with increases of over 30 ppbv at 100 hPa.

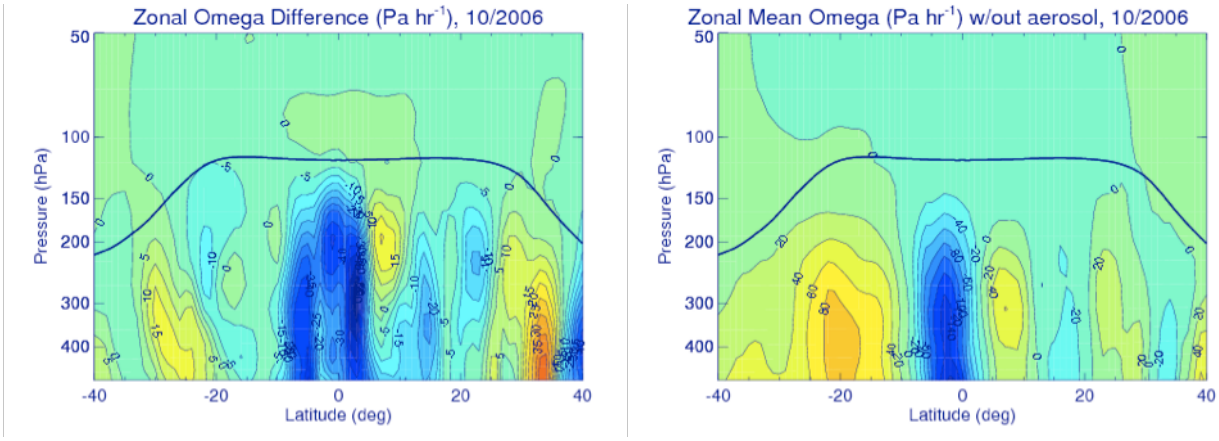

Figure 1: Ensemble-mean 60°-160°E mean vertical velocity differences for the five-member GEOS-5 ensembles with and without the Indonesian biomass-burning aerosols (left). Reference values for the ensemble without these aerosols (right). The thick black line indicates the tropopause.

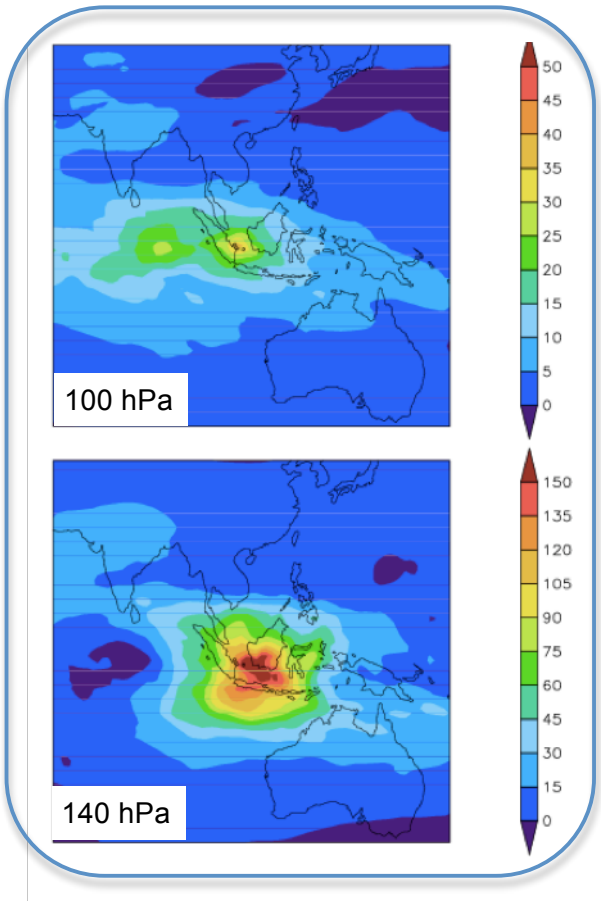

Figure 2: Difference in ensemble mean CO mixing ratio at 140 hPa (bottom) and 100 hPa (top) which results from including Indonesian biomass burning aerosols in the GEOS-5 simulations. CO biomass burning emissions are from the GFED2 inventory, which is based on MODIS burned area observations.

Calculations of the mass perturbation in CO induced by aerosol heating indicate that the presence of these aerosols increases CO mass throughout the tropical tropopause layer (TTL) by 25% in October and November. Mass perturbations of CO in the lower stratosphere lag those in the TTL by a month, but are nearly as large (~20%). Duncan et al. (2007; ACP) found that the 1997 Indonesian wildfires increased troposphere-to-stratosphere transport of trace gases by increasing ozone and decreasing the hydroxyl radical, thus increasing chemical lifetimes. Our results indicate that the impact of aerosols on UTLS dynamics may also play a role in increasing troposphere-to-stratosphere transport.

The Impact of Convective Parameter Sensitivity on Mass and Trace Gas Transport in the GEOS-5 AGCM

Lesley Ott, Julio Bacmeister and Steven Pawson

Project Goals: The goals of this project are to better understand the properties of convective transport of trace gases in GEOS-5 and to understand the impact of parameter settings in the model's moist physics code on simulated trace gas distributions and large-scale mass flux.

Project Description: Convection is an important process in determining trace gas distributions in the atmosphere. Ott et al. (2009; JAS) used a single-column version of GEOS-5 to demonstrate how convective mass flux varies with the choice of parameter settings. That study used statistical techniques to identify the five parameters whose settings exert the greatest influence on convective mass flux. We have used perturbations to these five parameters to produce an ensemble of 3D GEOS-5 simulations that represent the uncertainty introduced into trace gas distributions by convective parameter sensitivity.

The ensemble of simulations consists of eight members, including a control simulation with default parameter settings. Five members alter the value of a single parameter while holding the others constant. The two remaining simulations alter all five parameters simultaneously to produce representations of convection as strong (maximum convection) and as weak (minimum convection) as is reasonable. These simulations are performed in AMIP mode. The eight-member ensemble runs were integrated for one year. Additionally, the minimum and maximum convection simulations were integrated for five years to examine how the impact of parameter sensitivity varies from year to year.

Results: The ensemble mean and spread of simulated column CO are shown (Figure 1) for April, the peak in the southeast Asia biomass burning season, and October, the peak time for biomass burning in the Southern Hemisphere. Changes to the representation of convection introduced through perturbations to parameters tend to have the largest impact near source regions. In April, the largest spread is found near India and China while in October, the largest spread resides near the South American biomass burning maximum. A significant influence of convection is also evident in export pathways and ocean areas far removed from sources. Ensemble spreads in these regions can be as large as 30%.

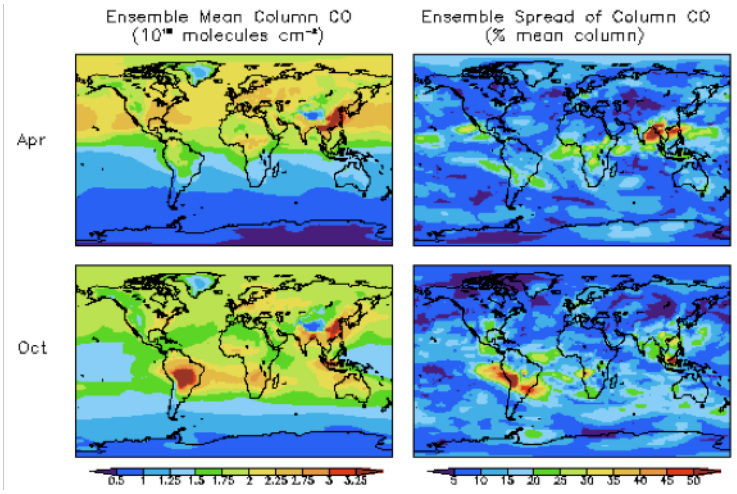

Figure 1: Mean column CO (10^{16} molecules per cm^2, left) and spread (%, right) from the eight-member ensemble of GEOS-5 simulations produced by altering parameters in the moist physics code. Top (bottom) panels show model results for April (October), the peak in biomass burning in Southeast Asia (South America and Africa).

An analysis of ensemble spread at NOAA GMD stations showed that the representation of convection also impacts simulated CO mixing ratios at these remote surface sites. At sites in the northern hemisphere high and mid-latitudes average annual ensemble spread was 16%, while at tropical and subtropical locations the variation was 13%. In the southern hemisphere high and mid-latitudes, the region with the least CO sources, variations were only 4%.

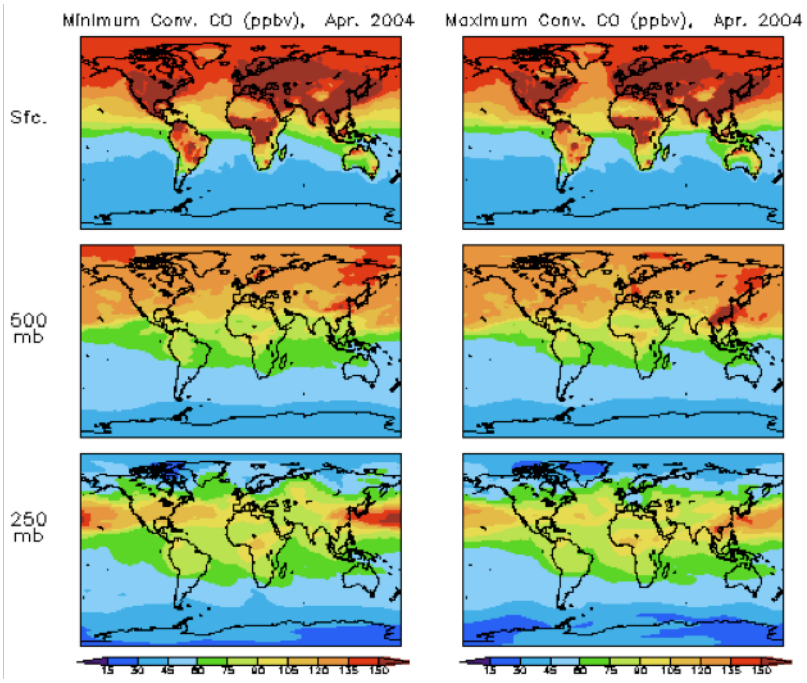

Figure 2: CO mixing ratios (ppbv) in April 2004 at the surface, 500, and 250 hPa for the minimum (left) and maximum (right) convection simulations.

The minimum and maximum convection simulations provide additional insight into the role of convective mass flux in determining trace gas distributions and mass transport. Figure 2 shows simulated CO mixing ratios in the lowest model layer, 500, and 250 hPa for both simulations. There is less CO near the surface in the maximum convection simulation, particularly in the North Atlantic and South America, which is consistent with stronger convection lofting more pollution in source regions. At 500 hPa, the largest differences between the simulations are found in Southeast Asia where more CO is evident in the maximum convection simulation. Interestingly, at 250 hPa the minimum convection simulation produces a stronger Asian pollution plume than does the maximum convection simulation.

An analysis of large-scale vertical mass flux shows that when convective mass flux is strongly reduced as in the minimum convection simulation, large-scale vertical velocity compensates to a large degree. Upward mass transport is increased throughout the troposphere, but this increase is most evident below 5 km. Because of this compensating effect of large-scale (resolved) transport, substantial alterations to convective mass flux may have a relatively small impact on trace gas distributions. In Figure 2, the minimum convection simulation produces a stronger Asian pollution plume at 250 hPa because of stronger large-scale vertical mass fluxes.

CO because it has a relatively short lifetime (~1-2 months), which allows for a short spin-up period. Future efforts will focus on examining the impact of convective parameter sensitivity on simulated CO_2 distributions and for other chemical species with longer and shorter lifetimes.

Publication:

Ott, L.E., J. Bacmeister, S. Pawson, K. Pickering, G. Stenchikov, M. Suarez, H. Huntrieser, M. Loewenstein, J. Lopez, and I. Xueref-Remy, Analysis of Convective Transport and Parameter Sensitivity in a Single Column Version of the Goddard Earth Observing System, Version 5, General Circulation Model. *J. Atmos. Sci.*, **66**, 627-646. doi:10.1175/2008JAS2694.1.

GEOS-5 Near Real-time Data Products

Gi-Kong Kim, Albert Ruddick and Austin Conaty

Project Goals: The GEOS-5 data assimilation system (DAS) products are generated to support remote sensing data retrieval and Earth system science research in the areas of climate and weather prediction, observing system modeling and design, and basic research in atmospheric processes. The objectives of this project are 1) to perform end-to-end testing of the GEOS-5 system under development, and 2) to maintain the near real time production as well as retro-processing of the GEOS-5 DAS products and 5-day forecasts.

Project Description: The GEOS-5 analysis products and forecasts are generated daily in near real time at the NCCS and distributed to the user community via the GES DISC. The current user community includes EOS instrument teams (MODIS/Land, CERES, MLS, TES, HIRDLS, and CALIPSO); other NASA Projects (POWER, FLASHFlux); University Research Groups (GEOS-CHEM at Harvard University, University of Maryland); other organizations/projects such as Lawrence Livermore National Laboratory and SPARC-IPY; and authorized individual researchers. GEOS-5 data production also provides real-time support to field experiments and short-duration NASA projects. The GMAO science monitoring team routinely performs quality assurance of the data products, providing valuable input into the planning of system quality improvements.

The system is upgraded periodically as the AGCM and GSI are modified to add new capabilities or improve performance. When a major system upgrade is made, the GMAO normally conducts DAS reprocessing over a limited time period to provide the EOS instrument teams with improved and consistent data products. As part of an operational readiness test, each new version of the system is configured as close as possible to the current operational version and is run in parallel with it. Sample data files are generated and provided to the GEOS data product users for testing of their algorithms and systems. The parallel production system is also used for external interface testing to verify the operational data flow from GMAO to the GEOS-5 data users.

Results: The GEOS-5 operational system upgrade from v5.0.1 to v5.1.0 was successfully implemented in December 2007. In close coordination with the EOS instrument teams, GEOS-5.1.0 reprocessing requirements and schedules were developed accommodating most of the user needs. The GEOS-5.1.0 reprocessing for the EOS instrument teams, covering October 2003 through December 2007, was completed in April 2008 as scheduled.

GMAO also implemented a real-time parallel test system to support the ARCTAS mission that lasted from March through July 2008. The parallel system was promoted to the operational GEOS-5.2.0 system in August 2008 after the real time support to the ARCTAS and the related CARB missions successfully concluded in July. The real-time mission support provided not only meteorological forecasts but also, for the first time, forecasts of chemical constituents. The GMAO also provided real time support to the HIPPO mission in January 2009. This mission support exercised an 'early-look' processing configuration in which a separate processing stream was run using input data available earlier than that normally used for the routine data production. This 'early-look' processing uses background information provided by the standard operational stream, which partially offset the quality reduction suffered by using fewer input observations.

GMAO started the delivery of special GEOS-5.2.0 data products to CERES team in October 2008. These products are generated using a controlled set of input observations to minimize the data shock due to a mid-stream introduction of a new observing system.

The near real time GEOS-5 data are currently generated on 1/2° × 2/3° horizontal grid and on 72 vertical levels. About 4 GB of data are delivered daily to the GES DISC for distribution to the users.

Relevant URL: http://gmao.gsfc.nasa.gov/operations/

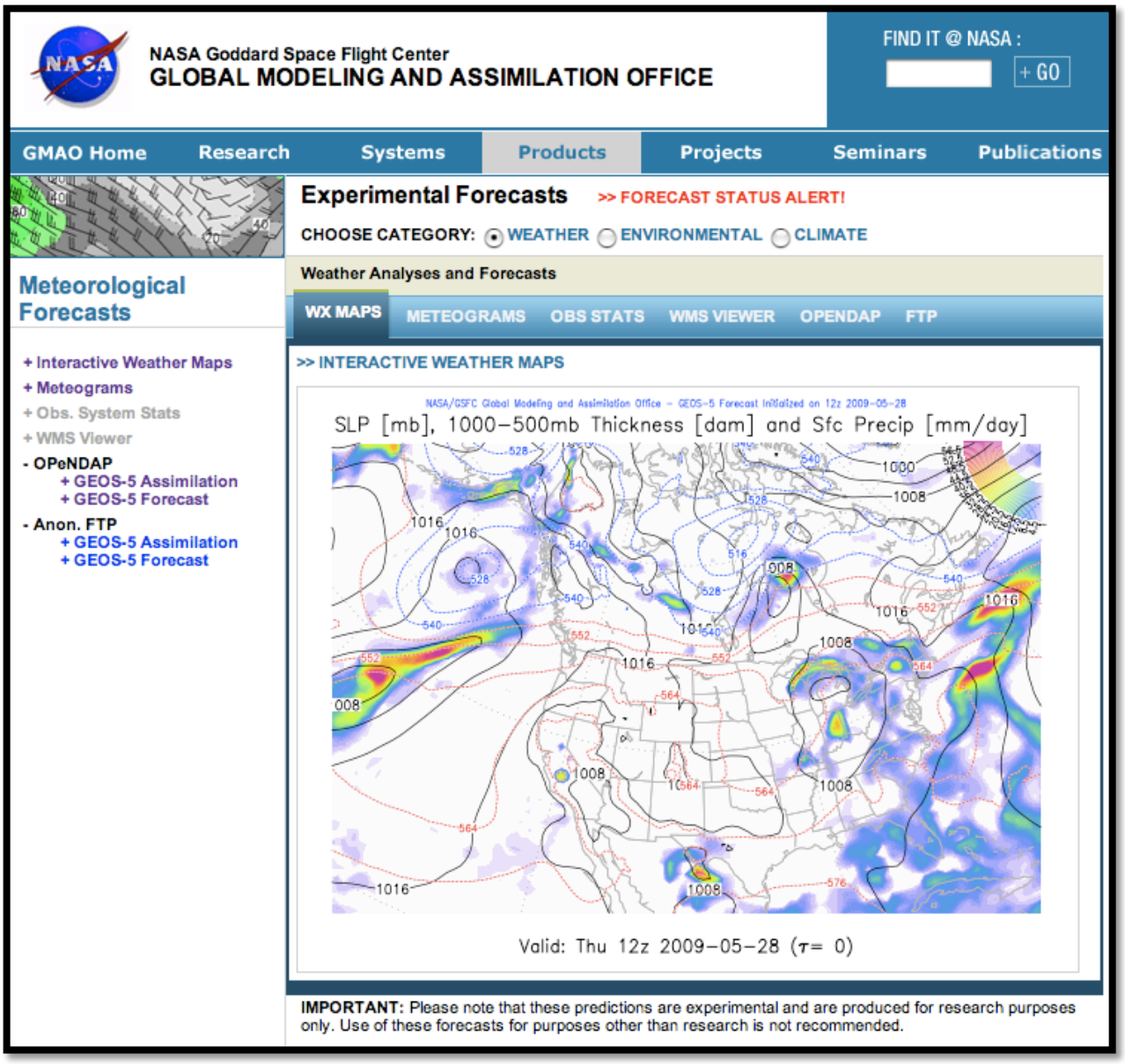

Sea level pressure [hPa in black], precipitation rate [mm/day shaded], and 1000-500 hPa thickness [dam in red and blue] from a GEOS-5 experimental forecast. Similar plots from other fields, including wind, temperature and moisture, are generated for different regions and levels every 3 hours through the 5-day forecast. *During mission support, flight-planning teams have found these types of plots quite useful. Analyses and experiemental forecasts are accessible online during missions. Other ancillary information, such as meteograms are also available.*